JOURNAL OF PETROLOGY | VOLUME 50 | NUMBER 5 | PAGES 933–966 | 2009 | doi:10.1093/petrology/egp027

Archean Accretion and Crustal Evolution of the Kalahari Craton—the Zircon Age and Hf Isotope Record of Granitic Rocks from Barberton/Swaziland to the Francistown Arc

ARMIN ZEH[1]*, AXEL GERDES[2] AND JACKSON M. BARTON, JR[3]

[1]GEOGRAPHISCHES INSTITUT, LEHRSTUHL FÜR GEODYNAMIK UND GEOMATERIALFORSCHUNG, AM HUBLAND, D-97074 WÜRZBURG, GERMANY

[2]INSTITUT FÜR GEOWISSENSCHAFTEN, ALTENHÖFER ALLEE 1, D-60438 FRANKFURT AM MAIN, GERMANY

[3]PO BOX 72196, PARKVIEW, 2122, SOUTH AFRICA

RECEIVED NOVEMBER 11, 2008; ACCEPTED APRIL 8, 2009
ADVANCE ACCESS PUBLICATION MAY 11, 2009

U–Pb and Lu–Hf isotope analyses, obtained by laser ablation-sector field-inductively coupled plasma-mass spectrometry on zircon grains from 37 granitoid samples indicate that the Kalahari Craton consists of at least five distinct terranes—Barberton South (BS), Barberton North (BN), Murchison–Northern Kaapvaal (MNK), Limpopo Central Zone (LCZ), and Francistown—which underwent different crustal evolutions, and were successively accreted at c. 3·23 Ga, 2·9 Ga and 2·65–2·7 Ga. The investigated granitoids were emplaced over a period of c. 1.5 billion years, and are exposed along a c. 1000 km long traverse from the Barberton Mountain Land/Swaziland to the Francistown arc complex, Botswana. The presented datasets reveal that most granitoids of the BS (3·45–3·10 Ga), MNK (2·93–2·67 Ga), Francistown (2·70–2·65 Ga) and LCZ terranes (3·2–2·03 Ga) show near-chondritic to subchondritic εHf_t *(BS = −1·7 to +0·5; MNK = −3·4 to +0·7; Francistown = −0·5 to +1·1; LCZ = −12·4 to −1·8), indicating that crustal recycling—perhaps by mixing of an older crust with a depleted mantle reservoir—played an important role during their formation and growth. Higher, superchondritic* εHf_t *values, as indicative for an important depleted mantle influence, were obtained only from some granitoids of the BN terrane (*$\varepsilon Hf_{3\cdot23Ga} = +2\cdot5 \pm 0\cdot8$*), the Gaborone Granite Suite (*$\varepsilon Hf_{2\cdot80Ga} = +2\cdot0 \pm 1\cdot6$*), and from a few detrital zircons from the Mahalapye complex of the Limpopo Belt. In addition, the datasets show that the internal Hf isotope variation of magmatic zircon domains from most granitoids is commonly less than ±1·5 ε-units, and only in rare cases up to ±3·1 ε-units. The rare significant* εHf_t *variations may be ascribed to incomplete mixing of different sources during magma crystallization. It is also shown that the combined approach of cathodoluminescence imaging with U–Pb and Lu–Hf isotope analysis provides a powerful tool to distinguish zircon domains formed and/or altered at different times.*

KEY WORDS: *Archean; Kalahari Craton; Kaapvaal Craton; Limpopo Belt; Lu–Hf isotopes; U–Pb dating; zircon*

INTRODUCTION

Numerous studies have demonstrated that the application of combined isotope systems provides a powerful tool to obtain information about the secular evolution of the crust–mantle system during the Earth's early history, comprising the Hadean to Archean eons (e.g. Patchett *et al.*, 1981; Stevenson & Pattchett, 1990; Vervoort *et al.*, 1996; Blichert-Toft & Albaréde, 1997, 2008; Amelin *et al.*, 1999, 2000; Vervoort & Blichert-Toft, 1999; Rino *et al.*, 2004; Condie *et al.*, 2005; Halpin *et al.*, 2005; Harrison *et al.*, 2005, 2008; Scherer *et al.*, 2007; Zeh *et al.*, 2007, 2008). Among these isotope systems, combined U–Pb and

*Corresponding author. +49-931-888-5415.
E-mail: armin.zeh@mail.uni-wuerzburg.de

Lu–Hf isotope data for single zircon grains have been proven to provide reliable and very detailed information about the timing of magma formation and metamorphic events, as well as about the magma source, such as a juvenile depleted mantle, a reworked older crust or a combination of both (e.g. Vervoort & Blichert-Toft, 1999; Griffin *et al.*, 2004; Condie *et al.*, 2005; Davis *et al.*, 2005; Harrison *et al.*, 2005, 2008; Gerdes & Zeh, 2006, 2009; Hawkesworth & Kemp, 2006; Wu *et al.*, 2006; Zeh *et al.*, 2007, 2008; Blichert-Toft & Albarède, 2008). Thus, such information, which now can be obtained very efficiently by laser ablation-sector field-inductively coupled plasma-mass spectrometry (LA-SF-ICP-MS) (Andersen *et al.*, 2002; Griffin *et al.*, 2004; Woodhead *et al.*, 2004; Iizuka & Hirata, 2005; Gerdes & Zeh, 2006, 2009; Pearson *et al.*, 2008; Kemp *et al.*, 2009), can help geoscientists to gain new and better insights into the complex formation mechanisms of Archean cratons. In particular, these data can help us to answer the questions of whether such cratons result from accretion of new, depleted mantle-derived material over a long period of time or from successive crustal recycling of older crust.

Combined U–Pb and Lu–Hf isotope studies carried out on zircon grains over the past 5 years have led to the conclusion that continental crust and a supplementary depleted mantle reservoir formed very early during the Earth's history. This conclusion is supported by up to 4·4 Ga zircon grains with quartz and feldspar inclusions from the Jack Hills (Harrison *et al.*, 2005, 2008; and data of Blichert-Toft & Albarède, 2008), and by Hadean to Archean detrital zircon grains (>2·5 Ga) with strongly negative epsilon hafnium values (εHf_t). Such zircon grains have been described from Archean rocks of the Yilgarn Craton, Australia (Amelin *et al.*, 1999; Griffin *et al.*, 2004; Harrison *et al.*, 2005, 2008; Blicher-Toft & Albarède, 2008); the Rayner Complex, Antarctica (Halpin *et al.*, 2005); the Superior and Rae provinces of Canada (Amelin *et al.*, 2000; Davis *et al.*, 2005; Hartlaub *et al.*, 2006); the North China Craton (Zheng *et al.*, 2004); and the Limpopo Belt of South Africa (Zeh *et al.*, 2008). Furthermore, the finding of a few Hadean to Archean age zircon grains with positive εHf_t points to the existence of a complementary depleted mantle reservoir coeval with the early crust. Such zircon grains are reported from the Jack Hills (Harrison *et al.*, 2005; Blichert-Toft & Albarède, 2008: $\varepsilon Hf_{4\cdot0-4\cdot4Ga} = 0\cdot0$ to $+3\cdot0$, rarely up to $+15$), from Paleoarchean rock from West Greenland (Vervoort *et al.*, 1996; Vervoort & Blichert-Toft, 1999; Amelin *et al.*, 2000: $\varepsilon Hf_{3\cdot6-3\cdot8Ga}$ up to $+3\cdot1$), and Paleo- to Mesoarchean rocks from the Superior province, Canada (Polat & Münker, 2004; Davis *et al.*, 2005: $\varepsilon Hf_{2\cdot7-3\cdot0Ga}$ up to $+5\cdot7$). However, it is worth noting that the Hf isotope data, in particular those from detrital zircon grains, tell us nothing about the amount of created continental crust nor about the size of the depleted mantle reservoir during the Hadean to Archean eons. In fact, it is unclear whether the Hf isotope data obtained from the Jack Hills zircon grains are representative for the worldwide crust–mantle composition during the Hadean–Archean or reflect only a local phenomenon restricted to a very tiny 'craton' or foundered oceanic plateau (Blichert-Toft & Albarède, 2008) and its underlying mantle reservoir. In general, this sampling problem is significant for all Archean gneiss terranes. At present, we do not really know whether the Lu–Hf isotope data as, for example, obtained from the Archean gneisses of the Greenland terranes are representative for crust–mantle evolution worldwide, or if different terranes sampled different mantle domains (contemporaneously or at different times), which did not communicate with each other and/or were affected by different degrees of crustal recycling during the Hadean to Archean. This lack of knowledge arises from the fact that the existing Lu–Hf database for Archean rocks is limited. At present, little is known about the Lu–Hf isotopic crust–mantle evolution of the Kalahari Craton, which was formed over a period of more than 1·5 billion years (from 3·6 to 2·0 Ga). The only data presented so far are from some komatiites and tonalite–trondhjemite–granodiorite (TTG) gneiss samples from the Barberton greenstone belt (Gruau *et al.*, 1990; Amelin *et al.*, 1999; Blichert-Toft & Arndt, 1999) and from the Limpopo Belt (Zeh *et al.*, 2007, 2008). These data, although valuable, allow only a limited interpretation of the crust–mantle evolution (both in space and time), and cannot help in answering a number of other important questions, relating to (1) the existence, origin and accretion of distinct terranes within the Kalahari Craton, (2) the secular crust–mantle evolution of the Kalahari domain (part of the Archean Earth's mantle from which all the terranes of the Kalahari Craton were derived), and (3) the temporal and spatial crust–mantle interactions that occurred between 3·6 and 2·0 Ga. Furthermore, the limited dataset prevents a detailed comparison with the crust–mantle evolution of other Archean gneiss terranes. In an effort to answer these questions, we present U–Pb and Lu–Hf zircon data for 37 mostly granitoid rocks, which were formed between 3·55 and 2·0 Ga. The samples were collected along a *c.* 1000 km long traverse from the Swaziland/Barberton Mountain Land to the Francistown arc complex (Botswana) to the north (Fig. 1). This traverse crosses many important suture zones, which might reflect Archean terrane boundaries (e.g. Anhaeusser, 2006).

GEOLOGICAL SETTING AND SAMPLES

Kalahari Craton

The Kalahari Craton consists of three major crustal domains, the Kaapvaal Craton to the south, the Zimbabwe Craton to the north and the Limpopo Belt

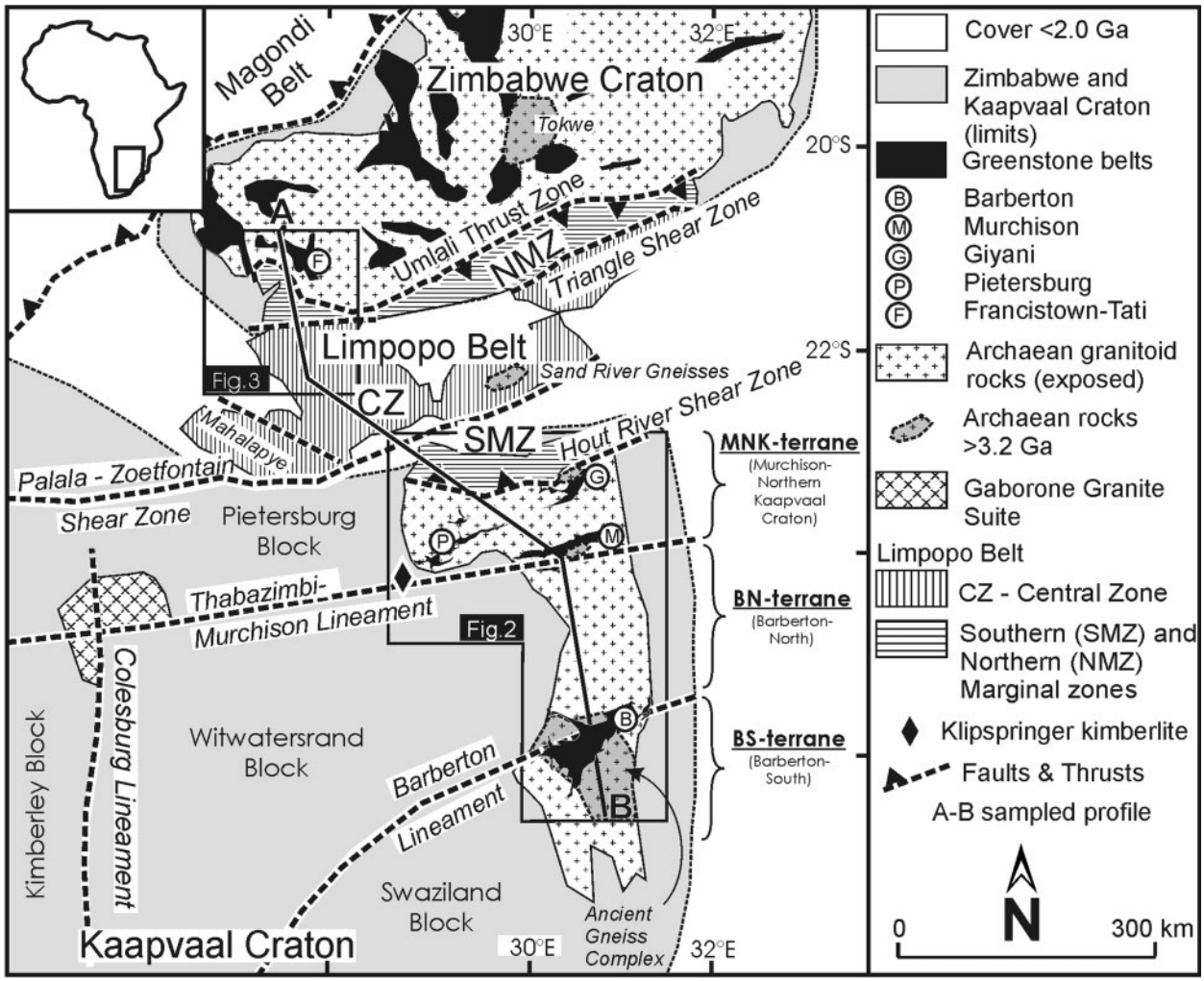

Fig. 1. Simplified geological map of the Kalahari Craton of southern Africa showing the location of the Kaapvaal Craton, Limpopo Belt and Zimbabwe Craton.

between them (Fig. 1). Each of these three domains represents a composite of terranes, which experienced a long-lasting Archean history (see summaries by Dirks & Jelsma, 2002; Barton *et al.*, 2006; Robb *et al.*, 2006), and is separated from the adjacent domain by important crustal shear zones: the Sashwe–Umlali Thrust Zone and the Palala–Zoetfontain (+Hout River) shear zones (Figs 1–3). A common feature of all three domains is that they contain Paleoarchean crust older than 3·2 Ga (Figs 1 and 2), as represented by the Tokwe nucleus of the Zimbawe Craton (3·57–3·30 Ga: Wilson *et al.*, 1995; Jelsma *et al.*, 1996; Horstwood *et al.*, 1999), the Sand River gneisses of the Limpopo Belt (3·30–3·27 Ga, Kröner *et al.*, 1999; Zeh *et al.*, 2007), the Barberton greenstone belt area of the eastern Kaapvaal Craton (3·7–3·23 Ga: e.g. Compston & Kröner, 1988; Armstrong *et al.*, 1990; Kamo & Davis, 1994; Kröner & Tegtmeyer, 1994; Schoene *et al.*, 2008), and small areas of the northern Kaapvaal Craton, comprising the Goudplaats–Hout River gneisses (3·27–3·33 Ga: Brandl & Kröner, 1993; Kröner *et al.*, 2000) and the TTGs of the French Bob Mine (Poujol *et al.*, 1996). Furthermore, each of the three domains is underlain by a buoyant subcontinental lithospheric mantle (up to 250 km thick), as suggested by seismic data (James *et al.*, 2001; James & Fouch, 2002) and by kimberlite-borne xenoliths, garnet and diamond inclusions (e.g. Pearson, 1999; Griffin *et al.*, 2003; Richardson *et al.*, 2004; Shirey *et al.*, 2004). This subcontinental lithosphere mantle formed by multiple processes, which predominantly occurred at 3·2–3·3 Ga(?), 2·9 and 2·0 Ga (e.g. Pearson, 1999; Richardson *et al.*, 2004).

Kaapvaal Craton

Based on a large number of age data and the distribution of ultrabasic to basic rock units (greenstone belts), it is suggested that the Kaapvaal Craton results from the amalgamation of at least three larger terranes, which mainly

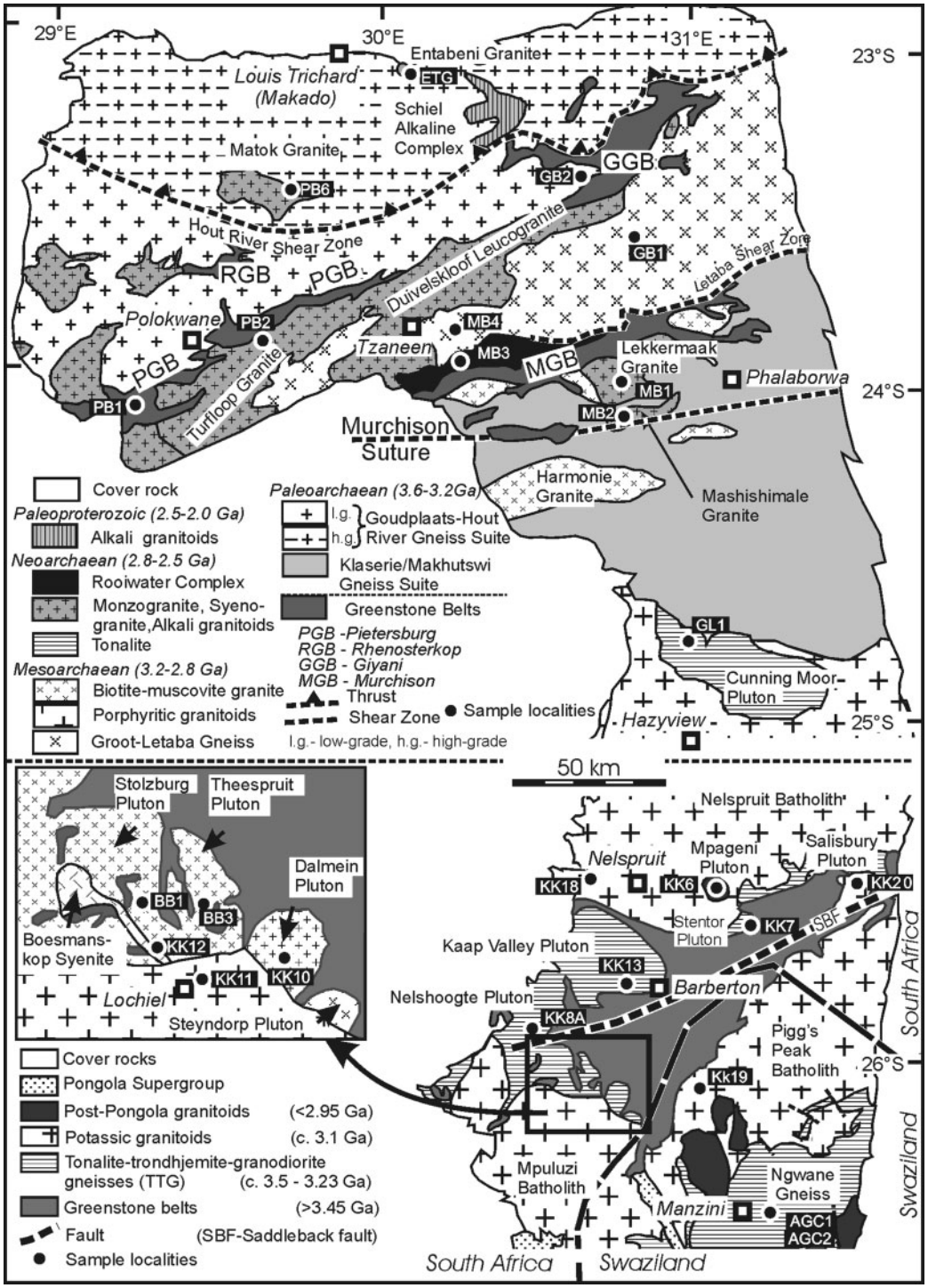

Fig. 2. Geological map of the eastern Kaapvaal Craton indicating sample localities (modified after Brandl *et al.*, 2006).

formed during the Archean (3·7–2·8 Ga), and collided at about 3·23 and 2·9 Ga (Poujol *et al.*, 2003; Anhaeusser, 2006; Robb *et al.*, 2006). Anhaeusser (2006) suggested that the terrane accretion occurred along two prominent ENE–WSW-trending suture zones, the Barberton Lineament and the Murchison–Thabazimbi suture zone (Figs 1 and 2). These two suture zones are highlighted by mafic to ultramafic lithologies (serpentinites, komatiites to komatiitic basalts), which are abundantly exposed in the Barberton greenstone belt and in the Murchison

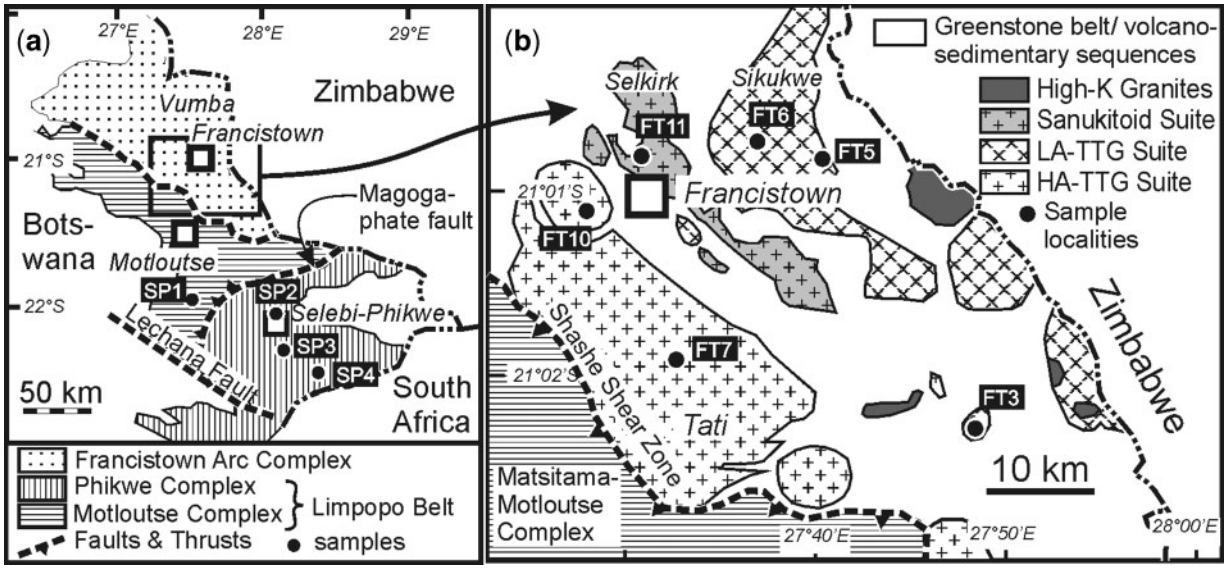

Fig. 3. Geological maps with sample localities for the western part of the Limpopo Belt (a) and the Francistown arc complex (b) (modified after McCourt *et al.*, 2004; Zhai *et al.*, 2006).

greenstone belt (Murchison suture after Anhaeusser, 2006). Recently, the *c.* 3·49 Ga komatiites of the Barberton greenstone belt have been interpreted to represent relics of boninite-like fore-arc lavas, which were obducted during collision between a northern and a southern terrane (Parman *et al.*, 1997, 2004). Earlier models, however, suggested that the Barberton ultramafic rocks were formed either in an oceanic extensional or oceanic plateau setting (de Wit *et al.*, 1987; de Wit *et al.*, 1992; de Ronde & de Wit, 1994; Cloete, 1999).

In this study, the terranes of the Kaapvaal Craton separated by the ENE–WSW-trending lineaments are designated as the Barberton South (BS), Barberton North (BN), and Murchison–Northern Kaapvaal Craton (MNK) terranes (Fig. 1). These three terranes form part of the previously defined Swaziland block, Witwatersrand block and Pietersburg block, respectively (Eglington & Armstrong, 2004) (Fig. 1). The BS terrane, which comprises the area south of the Barberton greenstone belt and the Swaziland Ancient gneiss complex (AGC), contains the oldest rocks (mostly TTGs) of the Kaapvaal Craton. These TTGs are locally associated with minor mafic and ultramafic lithologies (Fig. 2), and were emplaced predominantly between 3·55 and 3·45 Ga (e.g. the Steyndorp pluton, Stolzburg pluton, Ngwane gneiss and felsic metavolcanic rocks; see Armstrong *et al.*, 1990; Kamo & Davis, 1994; Kröner & Tegtmeyer, 1994; Kröner *et al.*, 1996; Schoene *et al.*, 2008). Minor U–Pb zircon ages as old as 3·70 Ga, and Nd model ages between 3·70 and 3·99 Ga indicate that the BS terrane also contains relics of much older crust (Compston & Kröner, 1988; Kröner & Tegtmeyer, 1994). Lu–Hf isotope data for a few magmatic zircon grains from the Steyndorp and Stolzburg tonalite/tromdjemites show a scatter of $\varepsilon Hf_{3\cdot45-3\cdot55Ga}$ between +2·0 and −0·4 [Amelin *et al.* (2000); data recalculated using the decay constant of Scherer *et al.* (2001) and CHUR parameters of Bouvier *et al.* (2008)]. These data are nearly identical to those for tholeiitic basalts ($\varepsilon Hf_{3\cdot45Ga} = +2\cdot3$ to −0·5) from the adjacent Barberton greenstone belt, but lower than the $\varepsilon Hf_{3\cdot45Ga}$ values obtained for most Barberton komatiites (+2·3 to +7·0) (Blichert-Toft & Arndt, 1999). Following the emplacement of the 3·45–3·55 Ga TTG suite, the BS terrane was subsequently affected by numerous magmatic events that, from their timing, coincide well with those in the BN terrane but also in other parts of the Kalahari Craton (see Table 1). These magmatic events took place at 3·21–3·22 Ga (Dalmein monzonite, small porphyry bodies, and younger TTGs; Kröner *et al.*, 1989; de Ronde *et al.*, 1991; Kamo & Davis, 1994; Kröner & Tegtmeyer, 1994), at about 3·11 Ga (intrusion of large potassic granite batholiths; e.g. Pigg's Peak and Mpuluzi batholites, and the Boesmanskop syenite body; Kamo & Davis, 1994), at 3·07–2·80 Ga (S-type, low-Ca granites; Sinceni, Mooihoek, Mhlosheni and Godlwayo plutons; Maphalala & Kröner, 1993; Meyer *et al.*, 1994), and finally at 2·78–2·69 Ga (intrusion of highly differentiated high-Ca, alkali granite plutons with I-type characteristics; Mbabane, Ngwempisi and Sicunusa granites; Layer *et al.*, 1992; Maphalala & Kröner, 1993; Meyer *et al.*, 1994).

In contrast to the BS terrane, the TTGs of the BN terrane (between the Barberton Lineament and the Murchison Lineament), are mostly younger than 3·23 Ga. The only exception, so far reported, is a U–Pb zircon age

Table 1: Compilation of magmatic events in geological units investigated during this study (in Ga)

Kaapvaal Craton					Limpopo Belt		Zimbabwe Cr.
BS	BN	MNK Murchison area	MNK Pietersburg/Giyani area	Gaborone	SMZ	CZ	Francistown area
3·6–3·7*						3·9–3·4*†	
3·50–3·45							
	3·30*	3·36*	3·33			3·33–3·28†	
3·21	3·23	3·23	3·20				
3·11	3·11						
3·07		3·09–3·07					
to		2·97–2·95	2·95–2·87				
2·82		2·90–2·82					
2·74–2·70	2·74	2·73–2·69	2·78–2·67	2·78	2·69–2·62	2·73–2·60	2·71–2·65
					2·02	2·06–2·02	

*Detrital or xenocyst zircon grains or domains.
†Observed only in the eastern part of the Limpopo Central Zone (between Venetia and Musina).
BS, Barberton South terrane, BN, Barberton North terrane, MNK, Murchison–Northern Kaapvaal Craton terrane; SMZ, Southern Marginal Zone; CZ, Central Zone (for data sources see text).

of 3·30 Ga, obtained from a tonalitic gneiss xenolith within the Nelspruit batholith (Kamo & Davis, 1994). The oldest TTGs of the BN terrane are exposed on the northern flank of the Barberton greenstone belt and comprise the Kaap Valley, Nelshoogte, and Stentor plutons (Fig. 2), which were all emplaced at about 3·23 Ga (Armstrong *et al.*, 1990; Kamo & Davis, 1994; Kröner & Tegtmeyer, 1994). In contrast, granitoid rocks near the Murchison suture (Fig. 2) are mostly younger than 3·12 Ga [e.g. the Makhutswi gneisses (3·12 Ga), Harmonie granite (3·09 Ga) (Brandl & Kröner, 1993; Poujol & Robb, 1999; Poujol, 2001)], and overlap in age with the Nelspruit batholith (and associated smaller granites), which intruded the central part of the BN terrane at about 3·11 Ga (Kamo & Davis, 1994); that is, contemporaneous with the batholiths of the BS terrane (see above). Finally, the BN terrane was intruded by the Mpageni alkali granite at 2·74 Ga (Kamo & Davies, 1994), which shows the same geochemical characteristics as the late alkali granites of the BS terrane (Meyer *et al.*, 1994). A young Neoarchean age of $2{\cdot}78 \pm 0{\cdot}53$ Ga (Rb–Sr) has been reported for the Cunning Moor tonalite, which intruded the boundary between the Nelspruit batholith and the Makhutswi–Klaserie gneisses (Barton *et al.*, 1983a).

In contrast to the BS and BN terranes, the MNK terrane [part of the northern geographical domain of Poujol *et al.* (2003), or the Pietersburg block; see Fig. 1] contains abundant granitoids that were emplaced between 2·9 and 2·67 Ga, and comprises several greenstone belts (Murchison, Giyani, Pietersburg, Rhenosterkop; see Fig. 2); their origins, spatial and temporal relationships are still under debate (see summary by Brandl *et al.*, 2006). The MNK terrane also contains a few granite gneiss domains as old as 3·33 Ga (Goudplaats–Hout River gneiss; Brandl & Kröner, 1993), and 3·20 Ga TTGs and meta-andesites. The latter are predominantly described from the Giyani (Brandl & Kröner, 1993; Kröner *et al.*, 2000) and rarely from the Murchison greenstone belt area (Poujol *et al.*, 1996). Vearncombe (1991) postulated that the Murchison greenstone belt represents a volcanic arc, which, if this proposal is correct, was active between 3·09 and 2·97 Ga, as suggested by U–Pb zircon ages obtained from associated felsic volcanic rocks and from surrounding granitoids, such as the Harmony Granite and Makhutswi gneisses (Brandl *et al.*, 1996; Poujol *et al.*, 1996). The TTGs at French Bob's mine (south of the Murchison greenstone belt), which yield a U–Pb zircon age of 3·23 Ga, indicate that older crust was present in the Murchison area prior to volcanic arc formation. In contrast to the Murchison greenstone belt, the formation of the Giyani greenstone belt obviously occurred earlier, as suggested by the 3·20 Ga U–Pb zircon ages of associated meta-andesites (Kröner *et al.*, 2000). This age is also much older than those obtained from the felsic rocks of the Pietersburg greenstone belt (2·96–2·94 Ga), as obtained from monzonites and metaquartz-porphyries (de Wit *et al.*, 1993; Kröner *et al.*, 2000). Following the period of greenstone belt formation the MNK terrane was intruded by numerous, post-tectonic granitoids in the Pietersburg and Murchison areas at 2·85–2·82 Ga, for example, the Melkboomfontein and Willie granites (Kröner *et al.*, 2000; Poujol & Robb, 1999), and by a felsic porphyry in the Giyani belt at 2·88 Ga

(Kröner *et al.*, 2000). Younger intrusions in the Pietersburg area are represented by the Turfloop granite (2·78–2·67 Ga: Henderson *et al.*, 2000; Kröner *et al.*, 2000), and in the Murchison area by a hornblende-tonalite of the Rooiwater layered intrusion (2·74 Ga) and the peraluminous Mashishimale granite (2·70 Ga) (Poujol *et al.*, 1996; Poujol, 2001). Finally, it should be noted that the youngest granites of the MNK terrane were emplaced nearly coeval with the Gaborone Granite Suite (2·78 Ga; Moore *et al.*, 1993; Grobler & Walraven, 1993), which is located at the northeastern edge of the Witwatersrand block, where the Thabazimbi–Murchison lineament is cross-cut by the Colesburg lineament (Fig. 1). Furthermore, their emplacement is nearly coeval with mantle processes beneath the Murchison–Thabazimbi lineament, as suggested by a Re–Os isochron age of $2{\cdot}55 \pm 0{\cdot}15$ Ga obtained from sulphide inclusion in diamonds from the Jurassic Klipspringer kimberlite pipe (Westerlund *et al.*, 2004).

Based on lithological, structural, and geochronological datasets, Poujol *et al.* (2003) suggested that the formation of the Kaapvaal Craton took place in four major steps. (1) During its early evolution (3·6–3·2 Ga) small protocontinental blocks underwent magmatic accretion and tectonic amalgamation (also see Lowe, 1994). That led to the formation of the central part of the Kaapvaal Craton, comprising the rocks around the Barberton greenstone belt (BS and BN terranes of this study). (2) At about 3·1–3·0 Ga, the central part of the Kaapvaal Craton was affected by a period of cratonic magmatism (reflected by the emplacement of the Nelspruit, Mpuluzi, and Pigg's Peak batholiths—parts of the BS and BN terranes), whereas the northern margin was rimmed by a crescent-shaped juvenile arc. (3) This juvenile magmatic arc (including the granite–greenstone belts of the MNK terrane) successively accreted onto the southern block between 3·0 and 2·8 Ga, as supported by the emplacement ages of the granitoids of the MNK terrane. (4) Finally, the accreted Kaapvaal Craton was affected by numerous post-tectonic granites between 2·78 and 2·69 Ga (BS, BN and MNK terranes); their emplacement was accompanied by craton-wide episodic extension and rifting. This rifting caused the intrusion of the Gaborone Granite Suite (Moore *et al.*, 1993), and the extensive Ventersdorp volcanism that occurred at 2·71 Ga (Armstrong *et al.*, 1991).

At present, all crustal evolution models for the Kaapvaal Craton are poorly constrained by isotope data, in particular for the Lu–Hf isotope system. The only Lu–Hf data published so far stem from a few samples from the Barberton greenstone belt (Amelin *et al.*, 1999; Blichert-Toft & Arndt, 1999). To provide new constraints on the complex crust–mantle evolution of the Kaapvaal Craton crust we present new Lu–Hf zircon data for 23 granitoids from the BS ($n = 8$), BN ($n = 7$) and MNK ($n = 8$) terranes. These samples encompass an age range from 3·55 to 2·67 Ga. In addition, we present results from two samples of the Gaborone Granite Suite (Tables 2 and 3, and Fig. 2).

Limpopo Belt

The Limpopo Belt (Fig. 1) is a high-grade metamorphic province, located between the Zimbabwe and Kaapvaal cratons, and comprises Archean to Paleoproterozoic components (e.g. Roering *et al.*, 1992; Berger *et al.*, 1995; Kamber *et al.*, 1995a, 1995*b*; Rollinson & Blenkinsop, 1995; Berger & Rollinson, 1997; Holzer *et al.*, 1998, 1999; Barton *et al.*, 2006). Lithologically and structurally, it is subdivided into three distinct domains, separated by major shear zones (e.g. McCourt & Vearncombe, 1987, 1992; Holzer *et al.*, 1999; Schaller *et al.*, 1999). The Limpopo Central Zone (LCZ) is structurally bounded by the >10 km wide Palala–Zoetfontain and Triangle shear zones against the Southern and Northern Marginal zones, respectively. These steep-dipping shear zones were formed and/or activated under high-grade metamorphic conditions at about 2·0 Ga (Holzer *et al.*, 1998, 1999; Chavagnac *et al.*, 2001; Kreissig *et al.*, 2001). The Southern Marginal Zone (SMZ) consists of high-grade, intensely deformed and metamorphosed TTGs with minor greenstones, and is interpreted as a reworked counterpart of the northern Kaapvaal Craton (e.g. Coward *et al.*, 1976; van Reenen *et al.*, 1987, 1992; Kreissig *et al.*, 2000), whereas the Northern Marginal Zone (NMZ) is dominated by enderbite and charnoenderbitic orthogneisses with some greenstones and granitoid rocks (e.g. Mason, 1973; Berger *et al.*, 1995; Kamber & Biino, 1995; Berger & Rollinson, 1997; Jelsma & Dirks, 2002). The rocks of both marginal zones were thrust onto their adjacent cratons along >10 km wide, steeply dipping shear zones, the Hout River and Umlali shear (thrust) zones, respectively (Fig. 1). According to Kreissig *et al.* (2001), magmatic intrusion and metamorphism of the SMZ occurred between 2·69 and 2·62 Ga, coeval or slightly younger than the magmatic–metamorphic evolution of the NMZ between 2·72 and 2·58 or 2·62 Ga (Berger *et al.*, 1995; Kamber & Biino, 1995; Mkweli *et al.*, 1995). High-grade metamorphism and thrusting of the SMZ onto the northern Kaapvaal Craton is postdated by the intrusion of the Matok granite at 2·67 Ga (Barton *et al.*, 1992). Finally, the SMZ was intruded by the Paleoproterozoic Entabeni granite at 2·02 Ga (Dorland *et al.*, 2006).

In contrast to the SMZ and NMZ, the LCZ is more complex. Field relationships in combination with petrological and geochronological data provide evidence that at least some parts of the LCZ were affected by Paleoarchean (3·24 Ga) and Neoarchean (2·61–2·65 Ga) tectono-metamorphic events (Kröner *et al.*, 1999; Millonig *et al.*, 2008; Van Reenen *et al.*, 2008; Gerdes & Zeh, 2009), and that all parts underwent a medium- to high-grade tectono-metamorphic overprint at *c.* 2·02 Ga (e.g. Jaeckel

Table 2: Co-ordinates of sample localities

Sample	Local name	Locality	Longitude	Latitude
Barberton South (BS) terrane				
Swaziland				
AGC1	Ngwane gneiss	E Manzini	31°27′95·2″E	26°29′83·1″S
AGC2	Ngwane gneiss	E Manzini	31°30′89·4″E	26°30′63·7″S
KK19	Pigg's Peak pluton	near Komatii river reservoir	31°10′33·7″E	26°07′21·5″S
S Barberton Mountain Land				
BB2	Stolzburg pluton	E Badplaas	30°45′22·3″E	26°01′12·5″S
BB3	Theespruit pluton	E Badplaas	30°48′35·8″E	26°01′25·8″S
KK10	Dalmain pluton	E Badplaas	30°37′20·2″E	26°05′20·8″S
KK11	Mpuluzi batholith	near Lochiel	30°50′68·3″E	26°08′75·8″S
KK12	Boesmanskop syenite	E Badplaas	30°44′08·0″E	26°04′42·6″S
Barberton North (BN) terrane				
KK7	Stentor pluton	road near Low's Creek	31°18′42·5″E	25°36′95·0″S
KK89	Nelshoogte pluton	N Badplaas (Komatii bridge)	30°37′30·8″E	25°53′55·5″S
KK13	Kaap Valley pluton	NW Barberton	30°59′05·5″E	25°44′37·6″S
KK18	Nelspruit pluton	E Nelspruit	30°52′98·2″E	25°25′92·5″S
KK20	Salisbury granite	road S Hectorspruit	31°39′96·7″E	25°30′04·2″S
KK06	Mpageni granite	road Nelspruit–Komatiiport	31°12′67·6″E	25°30′79·8″S
GL1	Cunningmore pluton	N Bosbokrand	31°04′50·0″E	24°49′90·5″S
Murchison–Northern Kaapvaal (MNK) terrane				
Murchison area				
MB1	Lekkersmaak granite	road Phalabwora–Gravelotte	30°51′68·6″E	23°55′12·5″S
MB2	Mashishimale granite	road Gravelotte–Mica	30°48′69·0″E	24°04′10·5″S
MB3	Rooiwater complex	SE Tzaneen	30°15′21·7″E	23°59′19·5″S
MB4	Groot Letaba gneiss	*c*. 10 km E Tzaneen	30°14′20·0″E	23°48′18·3″S
Giyani area				
GB1	Groot Letaba gneiss	20 km S Gyani (road)	30°42′95·8″E	23°29′11·7″S
GB2	Meriri gneiss	road Giyani–Polokwane	30°34′52·9″E	23°22′28·0″S
Polokwane area				
PB1	Uitloop granite	N1, *c*. 20 km SW Polokwane	29°10′32·3″E	24°05′68·5″S
PB2	Turfloop granite	road E Polokwane–Tzaneen	29°49′82·2″E	23°53′43·7″S
Limpopo Belt				
Southern Marginal Zone				
PB6	Matok pluton	road Polokwane–Makado	29°42′72·1″E	23°30′44·3″S
ETG	Etabeni granite	E Makado	30°13′93·7″E	23°02′83·0″S
Moutloutse Complex				
SP1		road Palapye–Francistown	27°14′73·6″E	22°14′94·9″S
Mahalapye terrane				
Mo5a		W Radisele	26°53′18·0″E	22°46′72·5″S
Phikwe terrane				
SP2	Selebi-Phikwe granite	N Selebi-Phikwe	27°49′60·4″E	21°57′65·6″S
SP3		road Selebi Phikwe–Sefophe	27°53′86·5″E	22°04′58·8″S
SP4		N Tsesebwje	28°21′39·6″E	22°23′77·2″S
Francistown arc complex				
FT3	Hill View tonalite	30 km SW Francistown	27°47′99·3″E	21°21′80·3″S
FT5	Sikukwe TTG Suite	10 km E Francistown	27°41′41·9″E	21°10′39·8″S
FT6	Sikukwe TTG Suite	11 km E Francistown	27°37′52·6″E	21°08′88·8″S
FT7	Tati TTG suite	Wulff Hill	27°34′65·0″E	21°18′03·5″S
FT10	Airport granite	near Airport Francistown	27°29′04·3″E	21°11′46·6″S
FT11	Selkirk Sanukitoid Suite	Nyangabwe hill N Francistown	27°30′61·7″E	21°09′11·3″S
Gaborone Granite Suite				
GA		10 km S Gaborone	25°50′45·1″E	24°43′44·4″S
KA		15 km E Kanye	25°42′72·1″E	25°05′92·2″S

Table 3: Compilation of U–Pb and Lu–Hf isotope results obtained during this and previous studies

Sample	Age (Ma)[1]	Error 2σ	Type	c/s/z[2]	Core (Ga)[3]	Over-growths (Ga)[4]	$^{176}Hf/^{177}Hf_{int}$[5] (average)	±2σ mean (×10^{-5})	εHf_{int}[6] (av.)	±2σ mean	No.[7]	Age[8] pub. (Ma)	Error	Ref.
Barberton South (BS) terrane														
AGC1	3245	8	conc.	09/15/13	3·54	—	0·28066	3	−0·4	1·1	15/17	—	—	—
AGC2	3238	8	conc.	08/23/12	3·44	—	0·28064	4	−1·7	1·1	19/23	—	—	—
KK19	3099	8	conc.	10/13/11	—	—	0·28078	4	−0·1	1·5	14/14	3074	4	(1)
BB2	3440	8	conc.	06/15/13	—	—	0·28056	4	0·3	1·6	15	3431	11	(2)
BB3	3451	7	conc.	13/15/14	3·53	—	0·28057	2	0·7	0·6	14/15	3443	3	(3)
KK10	3192	27	u.i.	05/14/10	—	—	0·28070	3	−0·7	1·4	14	3216	2	(3)
KK11	3082	6	u.i.	07/12/11	—	—	0·28075	5	−1·7	2·2	12	3105	3	(3)
KK12	3097	11	u.i.	12/15/10	—	—	0·28078	7	−0·4	2·6	12	3107	4	(3)
Barberton North (BN) terrane														
KK7	3218	9	conc.	04/07/07	—	—	0·28073	3	0·9	1·0	7	3250	30	(4)
KK89	3238	8	conc.	06/16/15	—	—	0·28073	2	1·4	0·8	16	3236	1	(5)
KK13	3231	9	conc.	12/14/14	—	—	0·28076	2	2·5	0·8	15	3229	5	(4)
KK18	3111	24	u.i.	07/17/11	3·21–3·24	—	0·28075	3	−1·0	1·0	13/17	3106	4	(3)
KK20	3100	14	u.i.	09/16/15	—	—	0·28076	3	−0·8	1·1	15	3105	10	(3)
KK06	2698	7	conc.	12/15/10	—	—	0·28088	4	−6·1	1·2	15	2740	15	(3)
GL1	3049	8	conc.	05/15/14	3·27	2·70–2·74	0·28080	3	−0·6	1·0	10/14	2784	53	(16)
Murchison–Northern Kaapvaal (MNK) terrane														
MB1	2795	8	conc.	09/14/14	2·99–3·11	—	0·28096	4	−0·7	1·3	14/15	2690	65	(6)
MB2	2671	8	conc.	09/13/10	—	—	0·28097	5	−3·5	1·7	15	2698	21	(7)
MB3	2611	10	conc.	05/14/16	—	—	0·28109	4	−0·6	1·3	15	2740	4	(8)
MB4	2839	8	conc.	09/12/14	2·95–3·21	—	0·28096	4	0·4	1·5	15	—	—	—
GB1	2784	8	conc.	14/17/13	—	—	0·28100	5	0·3	1·8	16	—	—	—
GB2	2931	8	u.i.	10/14/14	3·14–3·22	—	0·28092	4	0·7	1·5	11/15	—	—	—
PB1	2679	8	conc.	07/19/13	—	—	0·28099	5	−2·6	1·9	18	2674	16	(9)
PB2	2782	13	u.i.	13/16/10	—	—	0·28099	6	−0·2	2·1	15	2777	10	(10)
Limpopo Belt														
PB6	2679	7	conc.	14/19/12	—	—	0·28095	3	−3·9	1·1	19	2667	—	(11)
ETG	2023	6	conc.	10/15/11	—	—	0·28114	4	−12·5	1·4	14	2021	5	(12)
SP1	2645	22	u.i.	03/25/15	2·86	2·056 ± 12	0·28101	5	−2·7	2·1	21/28	—	—	—
Mo5a	2040	18	u.i.	08/10/08	—	—	0·28138	3	−3·6	1·3	16	—	—	—
SP2	2658	9	u.i.	07/16/08	2·87	—	0·28098	13	−3·7	1·6	9/14	2742–2643		(13)
SP3	2612	12	u.i.	04/18/13	>2·62*	—	0·28106	3	−1·6	1·0	15/17	—	—	—
SP4	2610	7	conc.	08/20/15	—	2·0(?)*	0·28104	5	−2·5	1·9	16/20	—	—	—
Francistown arc complex														
FT3	2649	9	conc.	07/17/08	—	—	0·28108	3	0·1	0·9	14	—	—	—
FT5	2700	8	u.i.	07/14/13	—	—	0·28106	3	0·7	1·1	13	—	—	—
FT6	2662	6	u.i.	11/17/13	—	—	0·28110	6	1·1	1·1	13/15	—	—	—
FT7	2734	39	u.i.	11/11/06	—	—	0·28103	5	0·2	1·9	9	—	—	—
FT10	2648	12	u.i.	09/13/11	—	—	0·28108	5	−0·1	1·6	13	—	—	—
FT11	2707	7	conc.	11/16/09	—	—	0·28104	5	−0·1	1·7	14	—	—	—
Gaborone Granite Suite														
GA	2784	9	conc.	09/13/12	—	—	0·28105	4	2·1	1·6	14	2785	2	(14)
KA	2777	7	conc.	09/15/14	—	—	0·28103	9	1·3	3·1	15	2782	5	(15)
Limpopo Belt, Central Zone; data from Zeh et al. *(2007)*														
SR	3283	8					0·28065	5	−0·5	0·9	8	Sand River gneiss		
Bu	2612	7					0·28102	4	−3·1	1·2	19	Bulai pluton		
Sin	2646	12					0·28097	5	−4·5	1·6	39	Singelele gneiss		
Reg	2649	9					0·28096	4	−4·5	1·3	11	Regina gneiss		
ZAG	2613	9					0·28107	4	−1·3	1·4	23	Zanzibar gneiss		
ZAL	2613	9					0·28108	5	−1·0	1·6	15	Zanzibar gneiss		
Mo1	2026	10					0·28119	7	−10·6	2·5	10	Mokgware granite		
Ma1h	2061	6					0·28145	2	−0·8	0·6	15	Lose quarry metadiorite		

[1]Intrusion age. Type: conc., concordia age; u.i., upper intercept age (see Table S1). [2]c/s/z: c, number of zircon analyses used for age calculation; s, number of spot analyses per sample(s); z, number of analysed zircon grains per sample. [3]Xenocryst zircon cores; *age assumed based on Hf isotope data. [4]Metamorphic zircon overgrowths. [5]Average $^{176}Hf/^{177}Hf_{int}$ calculated by applying the intrusion age to all analyses. [6]Average εHf_{int} calculated by applying the intrusion age to all analyses. [7]Number of zircon spots used for $^{176}Hf/^{177}Hf_{int}$ and εHf_{int} calculation/analysed per sample. [8]Published U–Pb zircon age for the respective plutons (except sample GL1: Rb–Sr whole-rock age). References: (1) Maphalala & Kröner (1993); (2) Dziggel *et al*. (2002); (3) Kamo & Davis (1994); (4) Tegtmeyer & Kröner (1987); (5) de Ronde & Kamo (2000); (6) Walraven (1989); (7) Poujol (2001); (8) Poujol *et al*. (1996); (9) Henderson *et al*. (2000); (10) Kröner *et al*. (2000); (11) Barton *et al*. (1992); (12) Dorland *et al*. (2006); (13) McCourt & Armstrong (1998); (14) Moore *et al*. (1993); (15) Grobler & Walraven (1993); (16) Rb–Sr age of Barton *et al*. (1983*a*).

et al., 1997; Holzer *et al.*, 1998, 1999; Barton *et al.*, 2003, 2006; Buick *et al.*, 2003; Zeh *et al.*, 2004, 2005*a*, 2005*b*; Van Reenen *et al.*, 2004; Boshoff *et al.*, 2006; Gerdes & Zeh, 2009). Barton *et al.* (2006) subdivided the Central Zone into three terranes: (1) the Mahalapye terrane, which is dominated by *c.* 2·06 to *c.* 2·02 Ga granites with minor high-grade meta-sedimentary rocks (Hisada & Miyano, 1996; McCourt & Armstrong, 1998; Holzer *et al.*, 1999; Chavagnac *et al.*, 2001; Zeh *et al.*, 2007); (2) the Phikwe terrane, which contains abundant hornblende-bearing, tonalitic and trondjemitic gneisses emplaced at 2·74–2·60 Ga [concordant U–Pb sensitive high-resolution ion microprobe (SHRIMP) data of McCourt & Armstrong (1998)]; (3) the Beit Bridge terrane. The Beit Bridge terrane hosts the *c.* 3·2–3·3 Ga Sand River TTG Suite and Messina layered intrusion (Barton, 1983; Barton & Sergeev, 1997; Kröner *et al.*, 1999) and numerous Neoarchean granitic to granodioritic orthogneisses with ages between 2·73 and 2·60 Ga, such as the Alldays, Singelele, Bulai, Zoetfontain, and Regina gneisses (e.g. Jaeckel *et al.*, 1997; Kröner *et al.*, 1998, 1999; Zeh *et al.*, 2007). Lu–Hf isotope zircon data from granitoid rocks of the Beit Bridge terrane yield mostly near-chondritic to subchondritic εHf_t: Sand River Gneisses ($\varepsilon Hf_{3\cdot28Ga} = +0\cdot9$ to $-2\cdot0$), Neoarchean granitoids ($\varepsilon Hf_{2\cdot65-2\cdot60Ga} = +0\cdot7$ to $-7\cdot1$). The same holds true for Paleoproterozoic metadiorites and granitoid rocks of the Mahalapye complex; for example, Lose quarry diorite ($\varepsilon Hf_{2\cdot06Ga} = -0\cdot3$ to $-1\cdot2$) and Mokgware granite ($\varepsilon Hf_{2\cdot026Ga} = -8\cdot6$ to $-12\cdot7$). Significantly positive εHf_t values up to $+7\cdot1$ were obtained only from a few 2·71 Ga xenocryst zircon cores of a migmatic leucosome from the Lose quarry (Zeh *et al.*, 2007). The existing Lu–Hf isotope data are interpreted to reflect mixing of older crust with depleted(?) mantle-derived material at 3·3 Ga, 2·6–2·7 Ga and at 2·0 Ga, and remelting of a Neoarchean juvenile crust at 2·0 Ga (Zeh *et al.*, 2007). U–Pb and Lu–Hf isotope data for detrital zircon grains from metasediments of the Beit Bridge terrane indicate that the Limpopo Belt and its hinterland formed as a result of continuous recycling of a very old Hadean protocrust between 3·9 and 3·3 Ga (Zeh *et al.*, 2008). This interpretation is supported by an εHf_t increase from $-6\cdot3$ to $-0\cdot2$ between 3·9 and 3·3 Ga.

Pb isotope data provide evidence that the rocks of the LCZ were, like those of the Zimbabwe Craton and NMZ, derived from a source with a long-lived, high μ value ($^{238}U/^{204}Pb > 11–12$), whereas the rocks of the SMZ and the northern Kaapvaal Craton were derived from a source with lower μ values close to Bulk Earth (Barton *et al.*, 1983*b*; Taylor *et al.*, 1991; Barton, 1996; Berger & Rollinson, 1997; Kreissig *et al.*, 2000). Hence, the rocks of the Zimbabwe Craton, NMZ, and LCZ may stem from the same mantle source, but they cannot be genetically related in an easy way to those of the Kaapvaal Craton and SMZ (Barton *et al.*, 2006).

The westernmost part of the LCZ is made up of metasediments and granitic rocks of the Motloutse Complex (Fig. 3a), which is separated from the Phikwe terrane by the Magogaphate shear zone (Aldiss, 1991; Key *et al.*, 1994; McCourt *et al.*, 2004). According to McCourt *et al.* (2004), the Motloutse terrane contains detrital material as old as 3·4 Ga (e.g. Dilolwane quartzite), but mostly not older than 2·7 Ga (Matsitama quartzite), and was accreted to the southwestern margin of the proto Zimbabwe Craton along the Sashwe shear zone at about 2·66–2·50 Ga. So far, there are no Hf isotopic data from the Motloutse terrane and only a few rocks of the Phikwe terrane (Zanzibar gneisses, Zeh *et al.*, 2007). To obtain deeper insight in the crustal evolution of these terranes we present new data for four granitoids from this area (see Fig. 3a; Tables 2 and 3).

Zimbabwe Craton

Wilson *et al.* (1978) divided the Zimbabwe Craton into four domains, largely based on Rb–Sr isotope data: three generations of granite–greenstone terranes emplaced at *c.* 3·5 Ga, 2·9 Ga and 2·7 Ga, and the later Chilimanzi–Razi granite suite emplaced at 2·6–2·5 Ga. This division was later supported by U–Pb and Sm–Nd dating (Jelsma & Dirks, 2002). It is postulated that the formation of the variable age granite–greenstone terranes started with the effusion and intrusion of mafic magmas, forming the greenstone belts, followed by the intrusion of plutonic bodies including TTGs, Na-granites and sanukitoids, and ceased with the intrusion of K-rich granites. Furthermore, there is some evidence for very old Early Archean crustal components in the Zimbabwe Craton, as represented by detrital zircon grains as old as 3·8 Ga (Dodson *et al.*, 1988). Re–Os isotope data by Nägler *et al.* (1997) additionally suggest that the lithospheric mantle underneath the Zimbabwe Craton was separated from the convective asthenospheric mantle at $\geq 3\cdot8$ Ga.

In this study, we consider only a small area of the Zimbabwe Carton, which is exposed in NE Botswana. This area is made up by the Francistown arc complex (McCourt *et al.*, 2004), which is composed of three greenstone belts (Francistown–Tati, Vumba, and Maitengwe). These greenstone belts experienced low- to medium-grade metamorphic overprints, and are surrounded and locally intruded by large granitoid bodies (e.g. Key, 1976; Carney *et al.*, 1994; Ranganai *et al.*, 2002). Toward the south, the Francistown arc complex is separated from the medium- to high-grade gneisses of the Motloutse terrane (part of the Limpopo Belt) by the NW–SE-trending Sashwe thrust zone (Fig. 3b).

Precise geochronological data exist only from the northwestern part of the Francistown arc complex, comprising the Vumba belt and Motsetse area. Granitoid gneisses from this area yielded SHRIMP U–Pb zircon ages between 2647 ± 4 and 2710 ± 19 Ma (Bagai *et al.*, 2002).

In contrast, Rb–Sr and Sm–Nd data obtained from the Francistown–Tati complex show a wide scatter between 1986 ± 780 and 3291 ± 1600 Ma (Zhai *et al.*, 2006), and Nd model ages mostly cluster around 2·6–2·9 Ga. The Nd model ages hint that the granitoid rocks of the Francistown–Tati area—comprising TTGs, sanukitoids and high-K granites—were emplaced contemporaneously with those of the Vumba belt (Zhai *et al.*, 2006). Based on the available Rb–Sr and Sm–Nd isotope data, Zhai *et al.* (2006) suggested that the Francistown TTG suite was formed by partial melting of a relatively young oceanic plate during its subduction, and that the parental melts underwent fractionation coupled with crustal assimilation (up to 14%) during their emplacement. The sanukitoids of the same area (see Fig. 3b) are suggested to result from partial melting of the mantle wedge above the subduction zone, and the high-K granite magmas by partial melting of previously emplaced TTG suites and/or lower crust of the overriding plate. Jelsma & Dirks (2002) suggested that the Francistown arc formed by SE-directed subduction, whereas McCourt *et al.* (2004) suggested a NE-directed subduction zone below the older Zimbabwe protocontinent at *c.* 2·65 Ga, with the Limpopo Belt (Motloutse complex) as the lower plate. So far, all crust–mantle evolution models proposed for the Francistown–Tati greenstone belt remain speculative, mainly becasue of the lack of precise age data. To provide new constraints we present new U–Pb and Lu–Hf isotope data for six granitoid samples from this area (see Tables 2 and 3, and Fig. 3b).

ANALYTICAL TECHNIQUES

Sample preparation

Zircon grains were separated from 1–5 kg rock samples by means of standard crushing techniques, a Wifley Table and heavy liquids. Subsequently, zircon grains from the respective samples were selected by hand-picking under a binocular microscope, mounted in epoxy resin (up to seven samples per 1 inch block), and ground down to expose their centres. After polishing, but prior to isotope analysis, all grains were imaged by scanning electron microscopy (SEM) using a Jeol JSM-6490 instrument with Gatan MiniCL at Goethe University Frankfurt (GUF) to obtain information about their internal structure. Based on the cathodoluminescence (CL) images, between seven and 28 U–Pb and Lu–Hf analyses were obtained from selected domains in each zircon sample (see Table 2, and supplementary material S1 and S2 available from http://petrology.oxfordjournals.org/). First, U–Pb analyses were carried out, and during a later session Lu–Hf isotope analyses were obtained from the same domains, either by setting the Lu–Hf spot directly 'on top' of the U–Pb spot, or immediately beside but within the same zone as determined by CL (see Fig. 4 and Gerdes & Zeh, 2009).

LA-SF-ICP-MS U–Th–Pb dating

Uranium, thorium and lead isotopes were analyzed by SF-ICP-MS using a Thermo-Finnigan Element 2 system coupled to a New Wave Research UP-213 laser system with a teardrop low-volume cell at GUF, following the methods of Gerdes & Zeh (2006, 2009) and Frei & Gerdes (2009). Laser spot sizes varied from 20 to 30 μm with a typical penetration depth of ~15–20 μm. A common-Pb correction based on the interference- and background-corrected ^{204}Pb signal and a model Pb composition (Stacey & Kramers, 1975) was carried out, where necessary. The necessity for the correction was usually based on the ^{206}Pb/^{204}Pb value (<10 000). However, in case the interference-corrected ^{204}Pb could not be precisely detected [e.g. <30 counts per second (c.p.s.)], this was

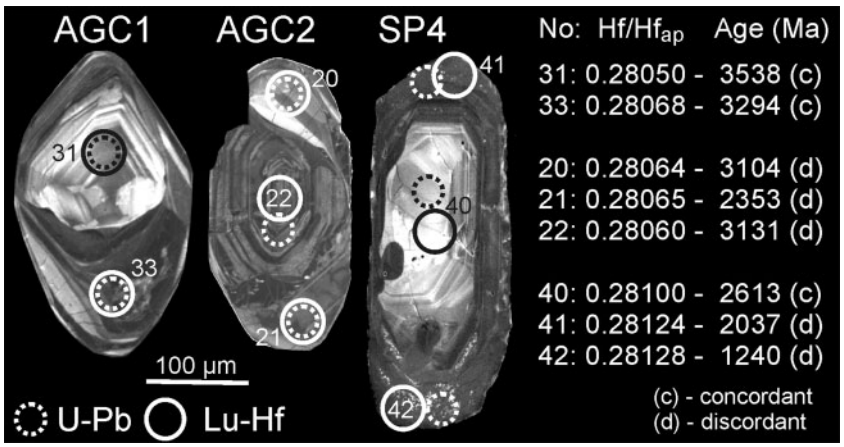

Fig. 4. Cathodoluminescence images of zoned zircon grains from three samples. Circles with numbers mark the location of the laser spots from which the U–Pb and Lu–Hf isotope data were obtained. Hf/Hf$_{ap}$, initial ^{176}Hf/^{177}Hf calculated by using the apparent ^{206}Pb/^{207}Pb age (for further explanation see text).

applied only when the corrected $^{207}Pb/^{206}Pb$ was outside the internal errors of the measured ratios and yielded more concordant results. The interference of ^{204}Hg (mean = 109 ± 15 c.p.s.) on mass 204 was estimated using a $^{204}Hg/^{202}Hg$ value of 0·2299 and the measured ^{202}Hg. All data were normalized relative to the GJ-1 reference. The total offset of the measured drift-corrected $^{206}Pb/^{238}U$ ratio from the 'true' isotope dilution thermal ionization mass spectrometry (ID TIMS) value of the analyzed GJ-1 grain varied between 5 and 13% for the different sections of the analytical sessions (see supplementary material, Table S1 and Fig. S1). Reported uncertainties (2σ) of the $^{206}Pb/^{238}U$ values were propagated by quadratic addition of the external reproducibility (2 SD) obtained from the standard zircon GJ-1 ($n = 13$; 2 SD ~1·3%, see Table S1 and Fig. S1) during each analytical sequence and the within-run precision of each analysis (2 SE). It should be noted that a complete sequence (protocol) comprises 68 measurements: 13 standards and 55 unknowns. For $^{207}Pb/^{206}Pb$ we used a ^{207}Pb signal-dependent uncertainty propagation (Gerdes & Zeh, 2009). For the Neoproterozoic GJ-1 zircon the reproducibility was 1·0 and 1·1% (2 SD), respectively (Fig. S1). Concordia diagrams (2σ error ellipses) (Fig. 5), concordia ages and upper intercept ages (95% confidence level) (Table S1) were calculated using Isoplot/Ex 2.49 (Ludwig, 2001).

LA-MC-ICP-MS Lu–Hf isotope analyses

Hafnium isotope measurements were performed by multi-collector (MS)-ICP-MS using a Thermo-Finnigan Neptune system at GUF coupled to the New Wave Research UP-213 laser system with a teardrop-shaped, low-volume laser cell, following the method of Gerdes & Zeh (2006, 2009). Wherever possible the 'Lu–Hf laser spot' of 40 μm diameter was drilled 'on top' of the 30 μm 'U–Pb laser spot'. Multiple analyses of Lu- and Yb-doped JMC 475 solutions show that results with a similar precision and accuracy can also be achieved if Yb/Hf and Lu/Hf is 5–10 times higher than in most magmatic zircons. All data were adjusted relative to the JMC 475 $^{176}Hf/^{177}Hf$ ratio of 0·282160 and quoted uncertainties are quadratic additions of the within-run precision and the reproducibility of the 40 ppb JMC 475 solution (2SD = 0·0033%, $n = 10$ per day).

For calculation of the epsilon Hf (εHf_t) value, the chondritic uniform reservoir (CHUR) was used as recommended by Bouvier *et al.* (2008; $^{176}Lu/^{177}Hf$ and $^{176}Hf/^{177}Hf$ of 0·0336 and 0·282785, respectively), and a decay constant of $1{\cdot}867 \times 10^{-11}$ (Scherer *et al.*, 2001; Söderlund *et al.*, 2004). Initial $^{176}Hf/^{177}Hf_t$ and εHf_t for all analysed zircon domains were calculated using the apparent Pb–Pb ages obtained for the respective domains [$^{176}Hf/^{177}Hf_{ap}$ and εHf_{ap}] (Figs 5–8), and for all cogenetic zircon domains by using the intrusion ages of the respective granitoids [$^{176}Hf/^{177}Hf_{int}$ and εHf_{int}] (Figs 9–12). Average values of $^{176}Hf/^{177}Hf_{int}$ and εHf_{int}, and related errors (±2 SD), for the respective granitoids are shown in Table 3. Further explanation has been given in the caption of Tables S1 and S2 (supplementary material).

RESULTS

CL images, and U–Pb and Lu–Hf isotope patterns

The results of the U–Pb and Lu–Hf analyses are shown in Table 3 and Figs 4–8, and in Tables S1 and S2 (supplementary material). For data interpretation we use the combined set of CL images and the U–Pb and Lu–Hf isotope data. The CL images of many zircon grains show typical oscillatory magmatic zoning patterns. However, there are also grains where the primary magmatic zoning patterns are partially or even completely 'erased'. Furthermore, there are some zircon grains that reveal complex core–rim structures, as illustrated by the three grains in Fig. 4. Based on CL images alone it cannot be resolved whether these core–rim relationships reflect crystallization during distinct magmatic and/or metamorphic events, or result from a change in physico-chemical conditions during a unique magma crystallization event. Such discriminations, however, are possible by the additional use of combined U–Pb and Lu–Hf isotope datasets (see Zeh *et al.*, 2007; Gerdes & Zeh, 2009).

For most samples, the combined U–Pb and Lu–Hf datasets reveal simple patterns when plotted in $^{176}Hf/^{177}Hf_{ap}$ vs apparent Pb–Pb age diagrams (see Figs 6–8). In general, four scenarios can be distinguished (Fig. 5). In the first case (case 1, the most simple) all analysed zircon domains yield within error identical $^{206}Pb/^{207}Pb$ and initial $^{176}Hf/^{177}Hf_{ap}$ (Fig. 5a and b). This indicates that all these domains were formed during a single crystallization event, and that their primary Pb–Pb age and Hf-isotope information are still preserved. This case, however, is rare and was observed only for zircon populations from a few samples; for example, KK13 (Kaap Valley granite), PB6 (Matok granite), ETG (Entabeni granite), FT11 (Selkirk sanukitoid) (see Figs 6i and 8f, i). As shown in Table 3, the $^{176}Hf/^{177}Hf_{int}$ values obtained from the respective granitoid samples scatter between ±0·00002 and ± 0·00004 (2 SD) around the mean value. This corresponds to ± 0·7 to ±1·4 epsilon units (εHf_{int}), respectively.

In the second case (case 2), all analysed zircon domains yield within error identical initial $^{176}Hf/^{177}Hf_{ap}$ but show large variations of their corresponding $^{206}Pb/^{207}Pb$ ages (Fig. 5c and d). This indicates that all these zircon grains formed at the same time (most probably during magma crystallization), but that several zircon domains were subsequently affected by multiple Pb loss via alteration. That caused resetting of the U–Pb system but left the zircon Hf isotope system unaffected (also see Amelin *et al.*, 2000;

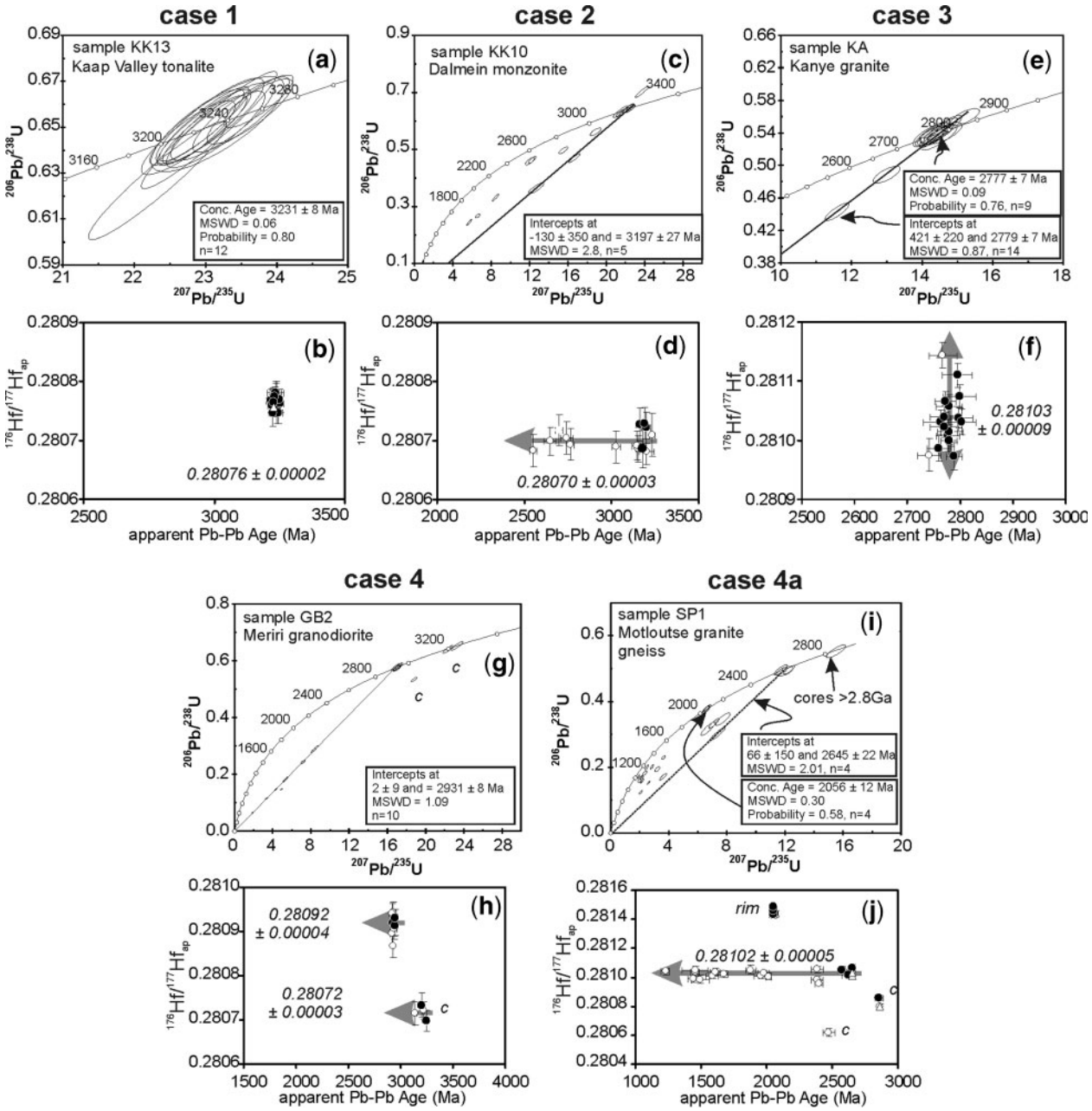

Fig. 5. Four cases for the interpretation of combined U–Pb and Lu–Hf datasets from zircon spot analyses, reflected in concordia diagrams (a, c, e, g, i) and related $^{176}Hf/^{177}Hf_{ap}$ vs apparent Pb–Pb age diagrams (b, d, f, h, j). Case l: all Pb–Pb ages and $^{176}Hf/^{177}Hf_{ap}$ are identical; case 2: the Pb–Pb ages are variable but all $^{176}Hf/^{177}Hf_{ap}$ are identical; case 3: all Pb–Pb ages are identical but the $^{176}Hf/^{177}Hf_{ap}$ are variable; case 4: zircon analyses of distinct domains show different $^{176}Hf/^{177}Hf_{ap}$ and different Pb–Pb ages (for detailed explanation see text).

Zeh *et al.*, 2007; Gerdes & Zeh, 2009). This effect is reflected by a horizontal array in the $^{176}Hf/^{177}Hf_{ap}$ vs apparent Pb–Pb age diagram (Fig. 5d), and was observed for several samples, such as KKl0 (Dalmein monzonite), KKll (Mpuluzi granite), KK89 (Nelshoogte granite), KK7 (Stentor granite), etc. (Figs 6–8). In general, zircon analyses of these samples show a similar scatter of their $^{176}Hf/^{177}Hf_{int}$ to zircon from case-1 rocks (±0·00002 and ±0·00004; 2 SD; see Table 3).

In the third case (case 3), nearly all zircon domains yield identical Pb–Pb ages, but show an enhanced scatter of their initial $^{176}Hf/^{177}Hf_{ap}$ (Fig. 5e and f). This suggests that zircon crystallized within a short time interval from a magma, which obviously had a heterogeneous (not

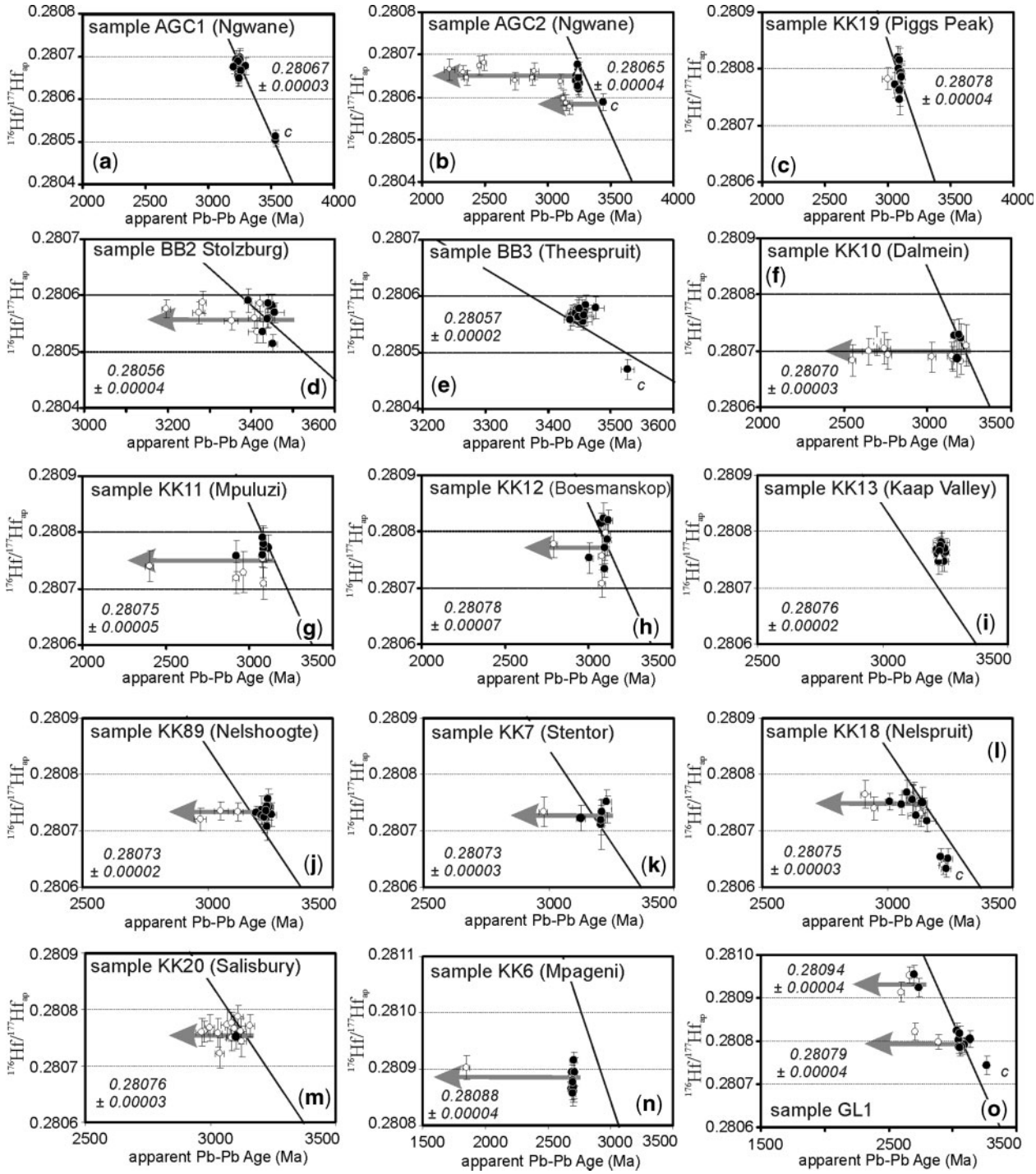

Fig. 6. $^{176}Hf/^{177}Hf_{ap}$ vs apparent Pb–Pb age diagrams showing the combined U–Pb and Lu–Hf isotope data obtained from samples of the BS terrane (a–h) and BN terrane (i–o). •, concordant analyses (95–105%); {cir}, discordant analyses. Error bars are ±2 SD; c, zircon core analyses; italic numbers indicate average $^{176}Hf/^{177}Hf_{ap}$ (±2 SD) obtained from all analyses of the respective samples (exclusive unambiguous core and rim analyses). Grey arrow, locus of the average $^{176}Hf/^{177}Hf_{ap}$. Black line, CHUR.

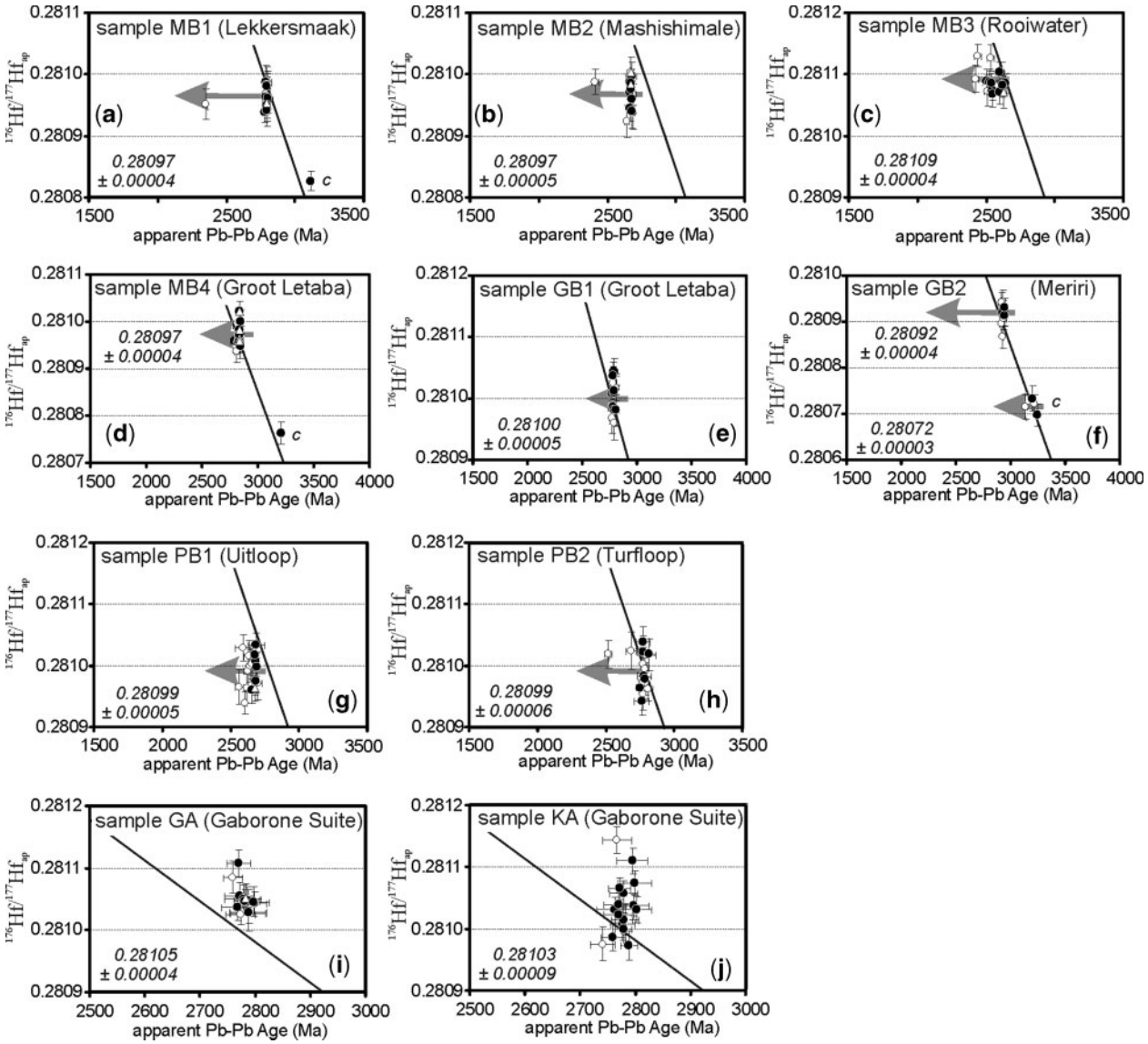

Fig. 7. $^{176}Hf/^{177}Hf_{ap}$ vs apparent Pb–Pb age diagrams showing the combined U–Pb and Lu–Hf isotope data obtained for samples from the MNK terrane (a–h) and from the Gaborone Granite Suite (i, j) (for further explanation see the caption of Fig. 6 and the main text).

equilibrated) hafnium isotopic composition. This, in particular, seems to be the case for sample KA (Gaborone Suite), where the $^{176}Hf/^{177}Hf_{int}$ shows a scatter of ±0·00009 (2 SD; equal to ±3·1 epsilon units; Table 3). At this point it is important to emphasize that this scatter does not result from post-zircon growth alteration or from analytical problems. Post-zircon growth alteration of the initial $^{176}Hf/^{177}Hf_{int}$ is unlikely, because nearly all analysed zircon domains of sample KA yielded concordant ages (Fig. 5e), indicating that the U–Pb system, which is easier to disturb than the $^{176}Hf/^{177}Hf_{int}$, is still intact. Second, there is no correlation between extreme $^{176}Hf/^{177}Hf_{int}$ and very low $^{206}Pb/^{204}Pb$ ratios (Table S1), indicative of 'present-day' alteration. Third, there are several studies which show that magmatic and metamorphic zircon domains maintain their primary $^{176}Hf/^{177}Hf_{int}$ even during (polymetamorphic) high-grade metamorphic conditions (e.g. Zeh *et al.*, 2007; Gerdes & Zeh, 2009). Analytical artefacts, in particular, problems with the ^{176}Yb interference correction, can also be ruled out. In fact, the $^{176}Yb/^{177}Hf$ obtained from the zircon domains of sample KA (0·021–0·053) is similar to or even lower than those of other samples, which show much smaller scatter of their εHf_{int} (e.g. sample Ga or FT11) and were measured during the same analytical session, with the same signal intensity (voltage). Last but not least, the $^{176}Hf/^{177}Hf_{int}$ obtained from cores and rims of single zircon grains of sample KA vary between 0·8 and 1·5 epsilon units (see Table S2); that is,

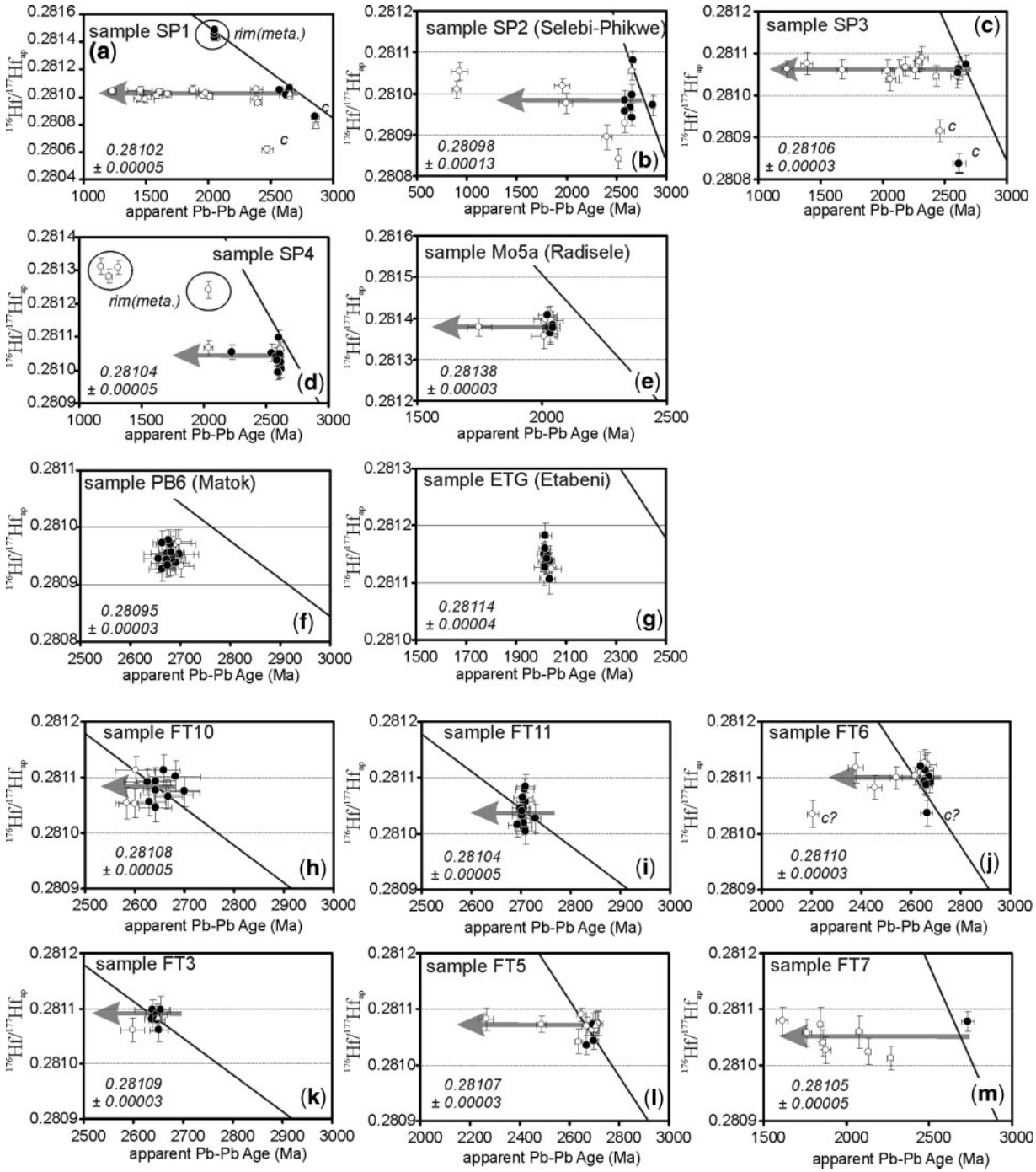

Fig. 8. $^{176}Hf/^{177}Hf_{ap}$ vs apparent Pb–Pb age diagrams showing the combined U–Pb and Lu–Hf isotope results obtained from samples of the Limpopo Belt (a–g) and from the Francistown arc complex (h–m). rim(meta.), metamorphic zircon overgrowth (for further explanation see the caption of Fig. 6 and the main text).

much lower than the scatter obtained from all the zircon grains from sample KA.

In the fourth case (case 4), zircon populations show a complex hafnium–age relationship, with distinct initial $^{176}Hf/^{177}Hf_{ap}$ and Pb–Pb ages obtained from different zircon domains (e.g. cores and rims), which are distinguishable in CL images (Figs 4 and 5g–j). In general, the initial $^{176}Hf/^{177}Hf_{ap}$ of the older domains (e.g. xenocryst cores) are lower than that of the younger domains (e.g. magmatic or metamorphic overgrowths). These variations

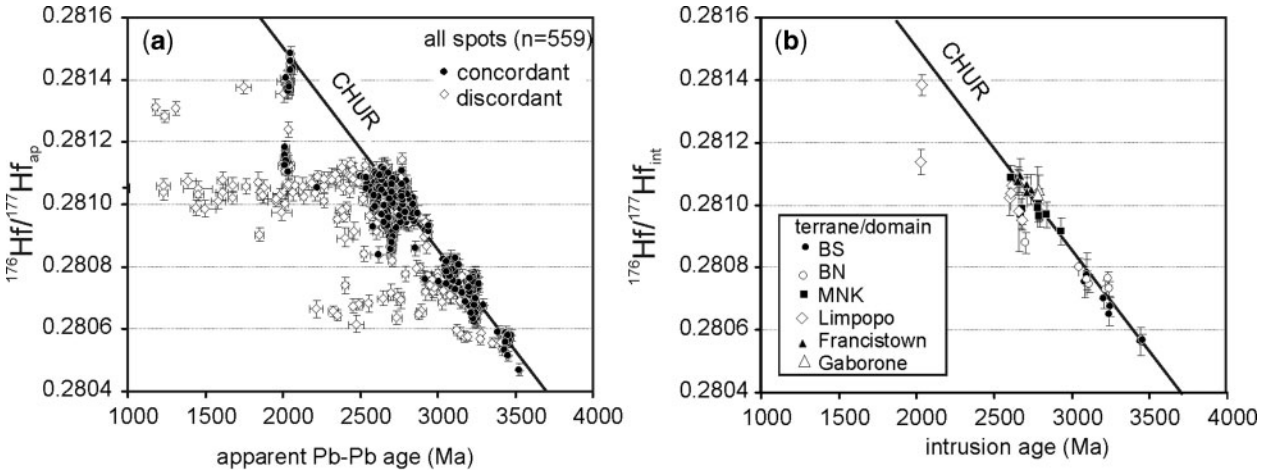

Fig. 9. (a) $^{176}Hf/^{177}Hf_{ap}$ vs apparent Pb–Pb age diagram showing the results of all U–Pb and Lu–Hf isotope spot analyses, and (b) $^{176}Hf/^{177}Hf_{int}$ vs intrusion age diagram showing the average $^{176}Hf/^{177}Hf_{int}$ for each sample (error bars ±2 SD). CHUR, evolution of the chondritic uniform reservoir; data from Bouvier *et al.* (2008) (for further explanation see text).

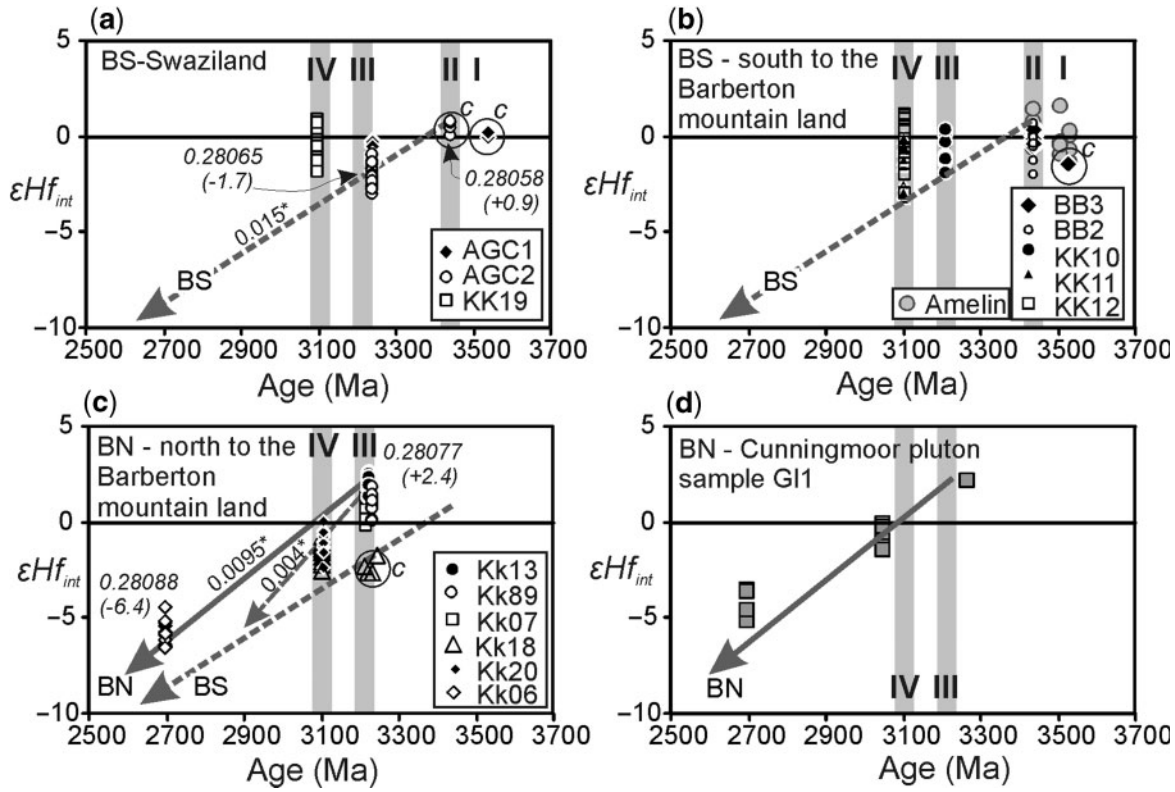

Fig. 10. εHf_{int} vs age diagrams showing the results obtained for samples from the BS terrane (a, b) and BN terrane (c, d). Grey vertical bars numbered I–IV mark different intrusion events (see text); c, xenocryst zircon cores; arrows labelled BS and BN reflect the crustal evolution trends of the respective terranes. (*) $^{176}Lu/^{177}Hf_{today}$ derived by using average $^{176}Hf/^{177}Hf_{int}$ data obtained from variable age rocks from the distinct terranes. Italic numbers indicate $^{176}Hf/^{177}Hf_{int}$ and corresponding εHf_{int} (in parentheses) (for further explanation see text).

indicate that zircon growth in these rocks took place during distinct magmatic and/or metamorphic events [for a more detailed explanation of complex $^{176}Hf/^{177}Hf_{ap}$–$^{206}Pb/^{207}Pb$ age relationships see Zeh *et al.* (2007) and Gerdes & Zeh (2009)]. Such variations are reflected by the zircon populations of samples AGC1 (Ngwane gneiss), BB3 (Theespruit granite), KK18 (Nelspruit granite), GB2 (Meriri granite gneiss) and SP4 (Phikwe terrane granite) (Figs 6e, l, 7f

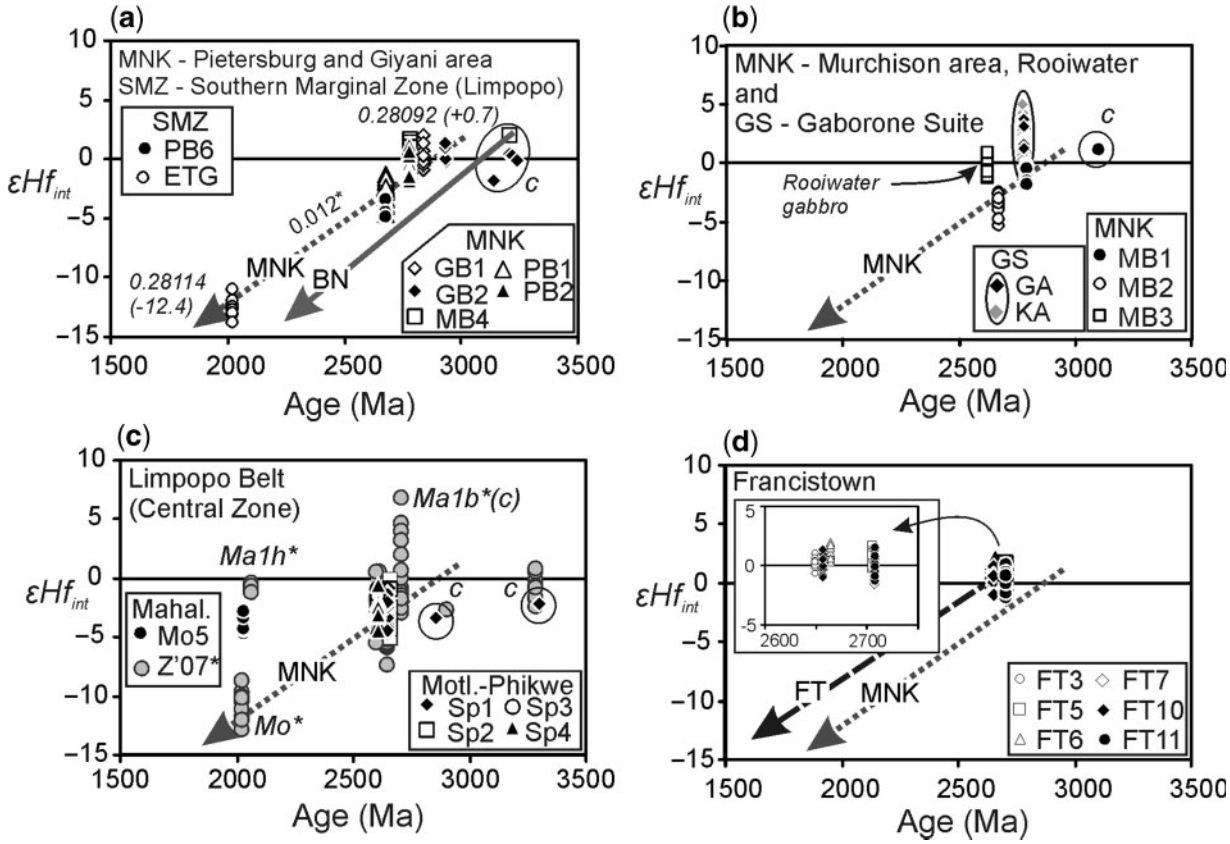

Fig. 11. εHf_{int} vs age diagrams showing the results obtained from samples of the MNK terrane (a, b), the Limpopo Belt (a, c), the Gaborone Granite Suite (b), and from the Francistown arc complex (d). Arrows labelled BN, MNK and FT indicate the crustal evolution trends of the respective terranes. c, xenocryst zircon cores; (*) $^{176}Lu/^{177}Hf_{today}$ derived by using average $^{176}Hf/^{177}Hf_{int}$ data obtained from variable age rocks of the distinct terranes; Z'07, data from Zeh *et al.* (2007); Mahal., data from the Mahalapye complex; Motl.-Phikwe, data from the Motloutse and Phikwe terrane (magmatic zircon domains only (for further explanation see caption of Fig. 10 and main text).

and 8d). In some samples two distinct horizontal arrays can be observed in the $^{176}Hf/^{177}Hf_{ap}$ vs apparent Pb–Pb age diagram (Figs 5h and 6o). This indicates that zircon cores and younger overgrowths were both affected by Pb loss, whereas their Hf isotope composition has not been modified. Such double arrays are seen for sample AGC2 (Ngwane gneiss) and GL1 (Cunning Moor pluton) (Fig. 6b and o). The zircon population of the Cunning Moor pluton is even more complex because it additionally contains a xenocryst core. Similarly complex patterns are also revealed by sample SP1 (Motloutse granite gneiss), where 2·6 Ga magmatic zircon domains contain xenocryst cores (>2·8 Ga), and locally show metamorphic overgrowths formed at 2·06 Ga (Fig. 8a).

Geochronological results

For many granitoid rocks from the Kaapvaal Craton, the emplacement age has already been obtained during previous geochronological studies [for summary see Poujol *et al.* (2003)]. In most cases, these age data are, within error, identical to those obtained by LA-SF-ICP-MS during this study (for comparison see Table 3). This is the case for the samples GA and KA (2784–2777 ± 9–7 Ma: Gaborone Suite), SP2 (2658 ± 9 Ma: Selebi–Phikwe granite), ETG (2023 ± 6 Ma: Etabeni granite), PB2 (2782 ± 13 Ma: Turfloop granite), MB2 (2671 ± 8 Ma: Mashishimale granite), KK20 (3100 ± 14 Ma: Salisbury granite), KK18 (3111 ± 24 Ma: Nelspruit batholith), KK13 (3231 ± 9 Ma: Kaap Valley pluton), KK89 (3238 ± 8: Nelshoogte pluton), KK7 (3218 ± 9 Ma: Stentor pluton), KK12 (3097 ± 11 Ma: Boesmanskop syenite), KK10 (3192 ± 27 Ma: Dalmein pluton), BB3 (3451 ± 7 Ma: Theespruit pluton), and BB2 (3440 ± 8 Ma: Stolzburg pluton). For four samples, ages were obtained that differ slightly from those obtained during previous studies (less than 2% age difference): samples PB6 (2679 ± 7 Ma: Matok granite), KK06 (2698 ± 7 Ma, Mpageni granite), KK11 (3082 ± 6 Ma; Mpuluzi batholith), and KK19 (3099 ± 8 Ma: Pigg's Peak batholith), and for three granitoids the age data obtained during this study differ significantly from published

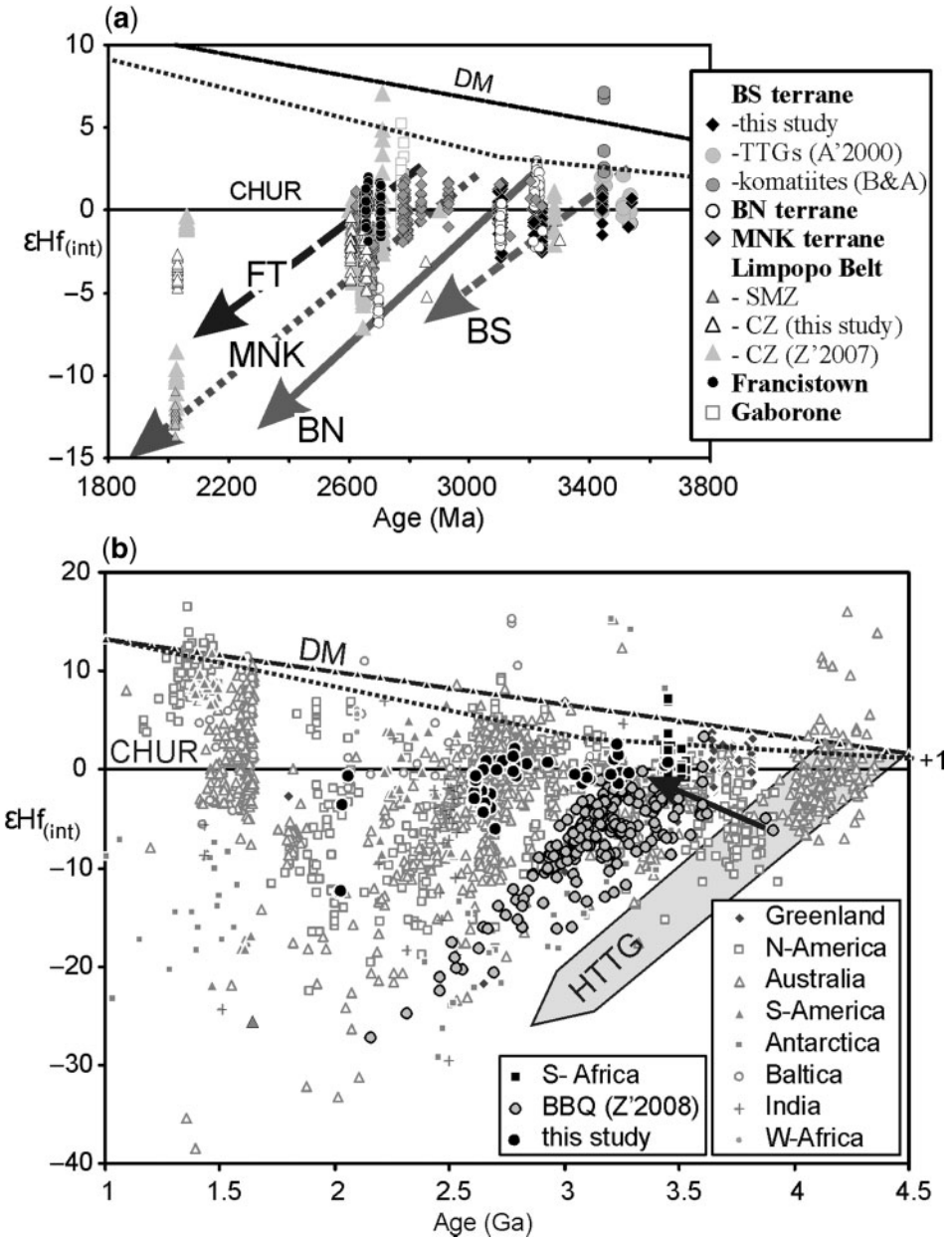

Fig. 12. (a) εHf_{int} vs age diagram showing all the Lu–Hf isotope data for the Kalahari Craton obtained during this study, by Amelin *et al.* (2000; A'2000), Blichert-Toft & Arndt 1999 (B&A), and Zeh *et al.* (2007; Z'2007). Arrows labelled BS, BN, MNK and FT mark the evolution trends of the respective terranes. The dotted line marks a two-stage depleted mantle evolution model (for further explanation see text). (b) εHf_{int} vs age diagram showing worldwide Hadean to Proterozoic Hf isotope data (small grey symbols) and those obtained for magmatic rocks from the Kalahari Craton (black circles, average εHf_{int} from this study and Zeh *et al.*, 2007). Data for TTGs and komatiites from the Barberton greenstone belt are also plotted (black squares: Blichert-Toft & Arndt, 1999; Amelin *et al.*, 2000), and data for detrital zircon grains from a metasediment from the Limpopo Belt (grey circles: Zeh *et al.*, 2008; Z'2008). Data sources for worldwide compilations: Patchett *et al.* (1981); Pettingill & Patchett (1981); Stevenson & Patchett (1990); Vervoort *et al.* (1996); Amelin *et al.* (1999, 2000); Vervoort & Blichert-Toft (1999); Griffin *et al.* (2004); Polat & Münker (2004); Condie *et al.* (2005); Davis *et al.* (2005); Halpin *et al.* (2005); Harrison *et al.* (2005); Hartlaub *et al.* (2006); Blichert-Toft & Albarède (2008); Kemp *et al.* (2009). The depleted mantle evolution trend (DM) was constructed using the modern-day values of mid-ocean ridge basalts (MORB) of Chauvel & Blichert-Toft (2001) ($^{176}Hf/^{177}Hf = 0{\cdot}28325$ and $^{176}Lu/^{177}Hf = 0{\cdot}0384$), and for calculation of εHf_t we used the chondritic uniform reservoir (CHUR) data of Bouvier *et al.* (2008) ($^{176}Hf/^{177}Hf = 0{\cdot}282785$ and $^{176}Lu/^{177}Hf = 0{\cdot}0336$) and the decay constant of $1{\cdot}867 \times 10^{-11}$ (Scherer *et al.*, 2001). Large grey arrow labelled HTTG defines the evolution of Hadean TTG rocks, and the black arrow marks the rejuvenation trend of Hadean protocrust, as constrained by detrital zircon grains from the Limpopo Belt (see Zeh *et al.*, 2008). The dotted line marks a two-stage depleted mantle evolution model (for further explanation see text).

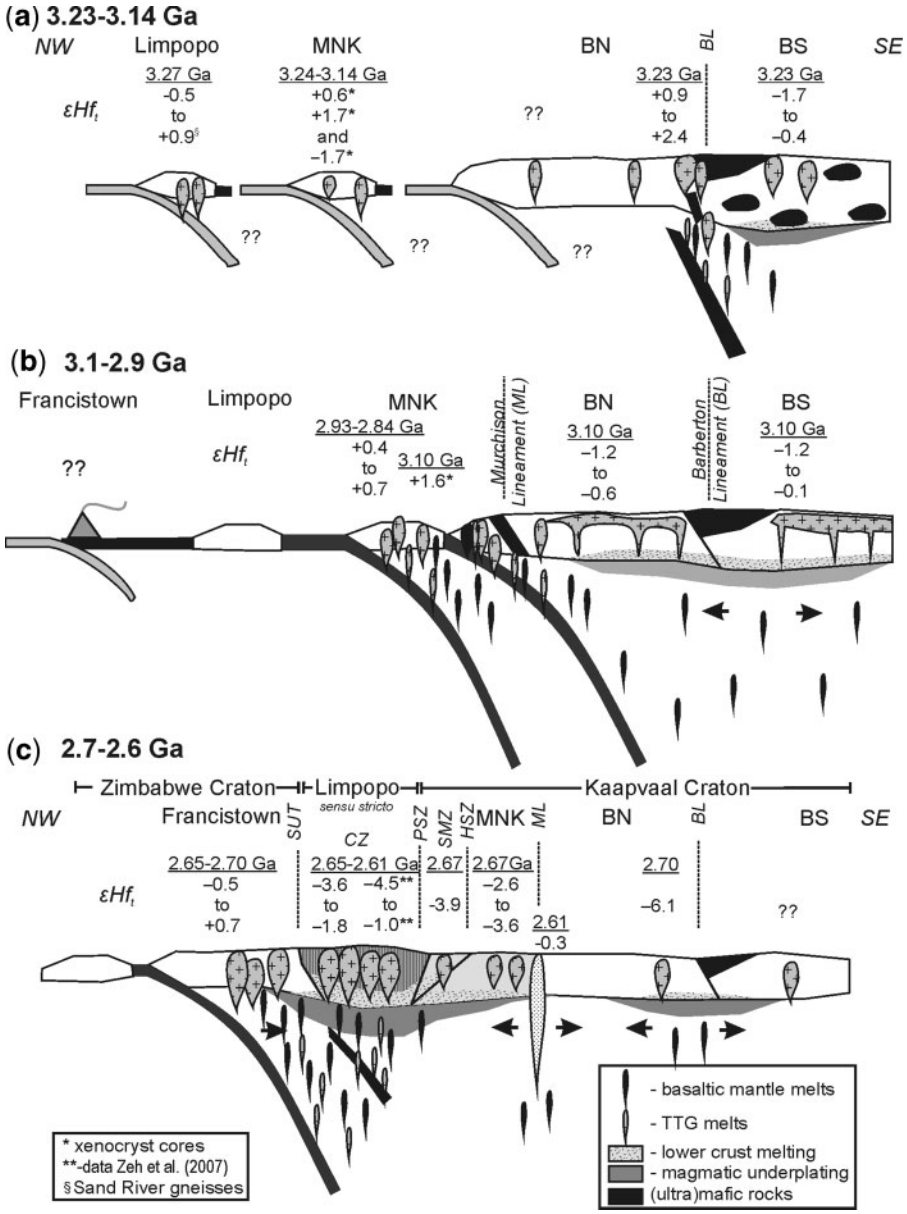

Fig. 13. Synopsis illustrating the accretion and evolution of the distinct terranes of the Kalahari Craton: (a) at 3·23–3·14 Ga; (b) 3·1–2·9 Ga; (c) 2·7–2·6 Ga. BS, Barberton South terrane; BN, Barberton North terrane; MNK, Murchison–Northern Kaapvaal Craton terrane; CZ, Central Zone; SMZ, Southern Marginal Zone; HSZ, Hout River Shear Zone; PSZ, Palala Shear Zone; SUT, Sashwe–Umlali Shear and Thrust Zone; BL, Barberton Lineament; ML, Murchison Lineament (for further explanation see text).

results: Lekkersmaak granite (MB1, 2795 ± 8 Ma; previously published age is 2690 ± 65: Walraven, 1989), the Cunning Moor pluton (GL1, 3049 ± 8 Ma: previously published age is 2784 ± 53 Ma: Barton *et al.*, 1983*a*), and a gabbro sample from the Rooiwater complex (MB3, 2611 ± 10 Ma; previously published age is 2740 ± 4 Ma: Poujol *et al.*, 1996). For samples MB1 and GL1, the published data are very imprecise, and the quoted age for the Cunning Moor pluton results from Rb–Sr whole-rock analyses. Thus, our new age data are more likely to represent the true intrusion ages. The 2740 Ma age of the Cunning Moor pluton perhaps reflects the timing of a final metamorphic overprint. This conclusion is supported by the finding of a few zircon overgrowths with distinct initial $^{176}Hf/^{177}Hf$ in sample GL1, which yielded Pb–Pb ages of 2·7–2·74 Ga (see Fig. 6o and Table S1). The significantly younger U–Pb zircon age for the hornblende gabbro of the Rooiwater complex (2611 ± 10 Ma: concordia age, MSWD = 0·1, $P = 0·98$, $n = 5$) might reflect the fact that this complex consists of magmatic rocks that formed

during distinct intrusion events in the vicinity of the Murchison–Thabazimbi Lineament.

In addition to the samples above, new U–Pb zircon ages are presented for a large number of, so far, undated granitoids (see Tables 3 and S1). These comprise two tonalitic gneiss samples from the Ancient Gneiss Complex, Swaziland (east of Manzini), which yielded within error identical concordant ages of 3245 ± 8 (AGC1) and 3238 ± 8 Ma (AGC2), interpreted as crystallization ages. Both samples also contain a few inherited cores with ages between 3·44 and 3·54 Ga (see Tables 3 and S1). Furthermore, four new samples were dated from the area between the Giyani–Pietersburg and Murchison greenstone belts: sample MB4 (2839 ± 8 Ma: Groot Letaba gneiss, near Tzaneen), sample GB1 (2784 ± 8 Ma: Groot Letaba gneiss, south to Giyani), sample GB2 (2931 ± 8 Ma: Meriri granite gneiss of the Giyani belt), and sample PB1 (2679 ± 8 Ma: Uitloop granite of the Pietersburg greenstone belt). The first age data are presented here for granitoid rocks of the Francistown–Tati greenstone belt: sample FT3 (2649 ± 9 Ma: Hill View tonalite), sample FT5 (2700 ± 8 Ma: Sikukwe TTG Suite), sample FT6 (2662 ± 6 Ma: Sikukwe TTG Suite), sample FT7 (2734 ± 39 Ma: Tati TTG Suite), sample FT10 (2648 ± 12 Ma: airport granite), sample FT11 (2707 ± 7 Ma: Selkirk sanukitoid). Moreover, new geochronological results from the Central Zone of the Limpopo Belt were obtained for samples from the Phikwe terrane (sample SP2, 2658 ± 9 Ma: Selebi–Phikwe granite; sample SP3, 2612 ± 12 Ma; sample SP4, 2610 ± 7 Ma), the Mahalapye terrane (sample Mo5a, 2040 ± 18 Ma: diorite near Radisele), and from the Motloutse terrane (sample SP1, 2645 ± 22 Ma—intrusion age; 2056 ± 12 Ma—metamorphic overprint).

Lu–Hf isotope data

During this study, Lu–Hf isotope analyses were obtained from 559 zircon domains in 37 samples. These data yield a wide spectrum of initial $^{176}Hf/^{177}Hf_{ap}$ from 0·2805 to 0·2815 (see Figs 6–8 and 9a). Most zircon domains, with concordant ages between 3·5 and 2·65 Ga (level of concordance between 95 and 105%), scatter near the evolution trend of the chondritic uniform reservoir (CHUR), whereas discordant analyses plot on horizontal arrays left of the CHUR line (towards lower ages). As mentioned above, these horizontal arrays (and the general shift of the data to the left of the CHUR line) can be interpreted to result from post-zircon growth alteration, which caused single or multiple Pb-loss events but did not change the primary $^{176}Hf/^{177}Hf$ (see Gerdes & Zeh, 2009). Zircon grains with concordant ages of about 2·0 Ga, and some of the 2·6–2·7 Ga age cluster, plot significantly below the CHUR line.

If all Lu–Hf isotope data of the respective samples are calculated back to the time of zircon crystallization ($^{176}Hf/^{177}Hf_{int}$), the overall pattern becomes simpler (Fig. 9b). In general, the reduced dataset reveals a clear increase of initial $^{176}Hf/^{177}Hf_{int}$ with decreasing intrusion age; that is, younger granitoids generally have more radiogenic hafnium than older ones. As shown in Fig. 9b, the average $^{176}Hf/^{177}Hf_{int}$ of most granitoids of the BS, BN, MNK and Francistown terranes or domains plot near CHUR, whereas those from the Limpopo Belt are always subchondritic, in particular those formed at *c.* 2·0 Ga. It should be noted, however, that the Hf isotope evolution trends are more complex in detail, as will be discussed below.

Our results also indicate that the scatter in $^{176}Hf/^{177}Hf_{int}$ is less than ±0·00005 (2 SD) for most samples (see Table 3). For some samples it is even lower (e.g. BB3 ± 0·00002). This is usually based on 7–28 (mostly 15) zircon spot analyses, carefully selected from magmatic zircon domains, and corresponds to variations of ±0·6 to ±2·0 epsilon units (see Tables 3 and S2). The lower range is close to the external reproducibility estimated from the reference zircon grains. More extreme variations in $^{176}Hf/^{177}Hf_{int}$ were obtained for only three samples: KK12 (Boesmanskop syenite: ±0·00007), KA (Gaborone Granite Suite: ±0·00009), and SP2 (Selebi–Phikwe granite: ±0·00013) (see Table 3 and Figs 6h and 8b). The $^{176}Hf/^{177}Hf_{int}$ scatter obtained for samples KK12 and KA is considered to represent natural variations of the protolith magmas, perhaps as a result of incomplete mixing of an older (less radiogenic) and younger (more radiogenic) component. In contrast, the scatter observed for sample SP2 may result from the presence of xenocryst zircon cores, which were masked by subsequent zircon alteration processes and, thus, could not be identified properly by means of CL images and U–Pb spot analyses.

DISCUSSION

Crustal evolution of the distinct terranes

BS terrane

The age data obtained during this study indicate that the BS terrane was affected by four magmatic events (I–IV in Fig. 10): at 3·54–3·51 Ga, ~3·45 Ga, 3·22–3·25 Ga, and ~3·1 Ga. The first magmatic event (3·54–3·51 Ga) is documented by the xenocryst zircon cores found in sample AGC1 (central Swaziland), and in the Theespruit tonalite (sample BB3) of the southern Barberton Mountain Land (sample BB3) (see Tables 3 and S1). In addition, such ages are reported from the Steyndorp pluton of the Barberton Mountain Land (3·51 Ga: Kamo & Davis, 1994; Amelin *et al.*, 2000), from the Ancient Gneiss Complex in NW Swaziland (Compston & Kröner, 1988; Kröner *et al.*, 1989), and from the Ngwane gneiss of the Dwalile granite–greenstone belt of SW Swaziland (3·52 Ga: Kröner & Tegtmeyer, 1994). Hf isotope data obtained from the xenocryst zircon cores yield either chondritic or

slightly subchondritic εHf_{ap} (sample AGC1: $\varepsilon Hf_{3.54Ga} = +0.5$ to $+0.7$; sample BB3: $\varepsilon Hf_{3.53Ga} = -1.0$; see Fig. 10a and b, Table S2). At this point it should be noted that xenocryst zircon grains with ages older than 3·6–3·7 Ga, as reported by Compston & Kröner (1988) and Kröner *et al.* (1989), have not been found during this study.

The second magmatic event (*c.* 3·45 Ga) is documented by the emplacement ages of the Stolzburg granite (BB2) and Theespruit granite (BB3) of the southern Barberton Mountain Land, and by a xenocryst zircon core found in sample AGC2 (Figs 2 and 10, and Table 3). Epsilon Hf data obtained from several zircon domains in these samples scatter around zero (sample BB2: $\varepsilon Hf_{3.45Ga} = +0.3 \pm 1.6$; sample BB3: $\varepsilon Hf_{3.44Ga} = 0.5 \pm 0.6$; zircon core in sample AGC2: $\varepsilon Hf_{3.44Ga} = +0.6$ to $+1.3$; see Tables 3 and S2). It is worth noting that our zircon Hf isotope data for the Stolzburg pluton (sample BB2) are, within error, identical to those previously obtained by Amelin *et al.* (2000; $\varepsilon Hf_{3.45Ga} = -0.1$ to $+2.0$), and overlap with εHf_t values obtained from tholeiitic basalts of the Barberton greenstone belt ($\varepsilon Hf_{3.45Ga} = -0.4$ to $+2.3$) (Blichert-Toft & Arndt, 1999). The εHf_t is, however, significantly lower than that of the Barberton komatiites ($\varepsilon Hf_{3.45Ga} = +2.3$ to $+7.1$). This suggests that the TTGs and tholeiitic basalts originate from a mantle reservoir that was different to that of the komatiites.

The third magmatic event (3·22–3·25 Ga) is documented by the Dalmein monzonite (Barberton Mountain Land), and by tonalitic gneisses west of Manzini/Swaziland (samples AGC1 and AGC2). These tonalitic gneisses occur in an area that is designated as Ngwane gneiss on the geological map (e.g. Jackson, 1984; Robb *et al.*, 2006). However, the Ngwane gneiss *sensu stricto* is older (3521 ± 23 Ma; see Kröner & Tegtmeyer, 1994). This indicates that the ancient gneiss domain of Swaziland, which at present is designated as Ngwane gneiss, is heterogeneous and consists of granitoids emplaced during distinct magmatic events between 3·52 and 3·24 Ga. The finding of xenocryst zircon cores in samples AGC1 and AGC2 (Fig. 10a, Tables 3 and S2) suggests that crustal material (up to 0·3 Ga older) was recycled at *c.* 3·25 Ga. This interpretation is also supported by the fact that the predominant magmatic zircon domains formed at 3·24 Ga show lower εHf_t values (AGC1: $\varepsilon Hf_{3.24Ga} = -0.5 \pm 1.1$; AGC2: $\varepsilon Hf_{3.24Ga} = -1.7 \pm 1.1$; Fig. 10, Table S2) than the xenocryst zircon cores ($\varepsilon Hf_{3.54–3.44Ga} = +0.5$ to $+1.3$; Fig. 10, Table S2). The Hf isotope data, in particular those of the zircon cores and rims of the TTG sample AGC2, allow an interpretation that an older continental crust (>3·45 Ga) component with a $^{176}Lu/^{177}Hf_{today}$ of 0·015 was re-melted at 3·24 Ga (BS trend in Fig. 10); further explanation of the significance of the $^{176}Lu/^{177}Hf_{today}$ is given below. The zircon grains in the Dalmein monzonite yielded nearly chondritic $\varepsilon Hf_{3.20Ga}$ of -0.7 ± 1.4 (see Fig. 10b, Table 3), similar to that of samples AGC1 and AGC2 from Swaziland.

The fourth magmatic event (*c.* 3·1 Ga) is documented by the intrusion of the Pigg's Peak and Mpuluzi batholiths, and the Boesmanskop syenite (see Figs 2 and 10b, and Table 3). Lu–Hf isotope data for the Pigg's Peak granite (sample KK19) and Boesmannskop syenite (sample KK12) scatter around CHUR (KK19: $\varepsilon Hf_{3.10Ga} = -0.1 \pm 1.5$; KK12: $\varepsilon Hf_{3.09Ga} = -0.4 \pm 2.6$; Fig. 10b and Table 3), whereas data obtained from the Mpuluzi batholith are mostly subchondritic (sample KK11: $\varepsilon Hf_{3.08Ga} = -1.7 \pm 2.2$). In general, the data for the 3·1 Ga granites plot significantly above those of the BS trend (see Fig. 10).

BN terrane

For the BN terrane, three magmatic events are documented by the data obtained during this study: at 3·23 Ga, *c.* 3·01 Ga and *c.* 2·7 Ga. From their timing the two oldest events correspond to magmatic events III and IV as described above for the BS terrane. However, the Lu–Hf isotope data reveal some important differences, as shown in Fig. 10. The oldest magmatic event (at 3·23 Ga) of the BN terrane is documented by the intrusion ages of the Kaap Valley (sample KK13), Nelshoogte (sample KK89) and Stentor plutons (sample KK7), which were all emplaced on the northern flank of the Barberton greenstone belt, near the inferred Barberton Lineament (see Anhaeusser, 2006). Zircon grains from these plutons yielded the highest εHf_{int} values (mostly superchondritic) of all granitoids analysed so far from the central Kaapvaal Craton (sample KK13: $\varepsilon Hf_{3.23Ga} = +2.5 \pm 0.8$; KK89: $\varepsilon Hf_{3.24Ga} = +1.4 \pm 0.8$; KK7: $\varepsilon Hf_{3.22Ga} = +0.9 \pm 1.0$; Fig. 10c and Table 3). These εHf_{int} values are generally higher than those estimated for contemperaneous granitoids of the BS terrane (e.g. Dalmein pluton) (see Fig. 10b).

At 3·1 Ga, the BN terrane was intruded by the Salisbury granite (sample KK20), and Nelspruit batholith (sample KK 18). These two granitoids yield subchondritic εHf_{int} (sample KK18: $\varepsilon Hf_{3.11Ga} = -1.0 \pm 1.0$; KK20: $\varepsilon Hf_{3.10Ga} = -0.8 \pm 1.1$; Fig. 10c, Table 3), indicating that these rocks contain older recycled crust. This interpretation is constrained by a few inherited zircon grains found in the Nelspruit granite (samples KK18). Their cores yielded Pb–Pb ages between 3·21 and 3·24 Ga (see Tables 3 and S1), and show negative εHf_{ap} between -1.3 and -2.2. That gives a clear hint that these zircon grains are not derived from the 3·23 Ga granitoids mentioned above (e.g. Kaap Valley granite), but come from a more evolved crustal source.

The youngest granite analysed from the BN terrane is the potassium-rich Mpageni granite (sample KK06), which intruded the Nelspruit batholith north of the Barberton greenstone belt (Fig. 2) at 2698 ± 7 Ma. The zircon analyses for this granite yielded the most negative $\varepsilon Hf_{2.98Ga}$ of the BN terrane, -6.1 ± 1.2, indicating that this

granite was formed by re-melting of a large proportion of older crust. In general, the formation of the Mpageni granite could be explained either by partial crustal anatextis of the 3·23 Ga TTGs of the BN terrane or by melting of a compositionally different crustal source (at least in part). In fact, both scenarios can account for the observation that the 2·7 Ga Mpageni granite shows a distinct composition to the 3·23 Ga TTGs, and that the Archean TTGs and the Mpageni granite plot together on a crustal evolution trend with an average $^{176}Lu/^{177}Hf_{today}$ of 0·095 (see Fig. 10c). It is worth noting that this ratio is too high for Archean TTGs (average value is 0·005: see Kamber *et al.*, 2002; Condie, 2005). In our example an increase of the $^{176}Lu/^{177}Hf_{today}$ from 0·005 (TTG) to 0·0095 (observed) could be achieved if zircon was fractionated in the source of the granitic melts (for further explanation see below).

As shown in Fig. 10d, the zircon Lu–Hf data for the Cunning Moor pluton (sample GL1) plot near to the BN trend ($^{176}Lu/^{177}Hf_{today} = 0·095$). The xenocryst zircon cores of the Cunning Moor pluton show a $\varepsilon Hf_{3·27Ga} = +2·6$ (similar to the Kaap Valley tonalite), the predominant zircon domains $\varepsilon Hf_{3·05Ga} = -0·5 \pm 1·0$ (similar to the Nelspruit batholith), and overgrowths rims $\varepsilon Hf_{2·70Ga} = -4·0 \pm 0·8$ (similar to the Mpageni granite).

MNK terrane, Southern Marginal Zone and Gaborone Suite

The MNK terrane, which is bounded by the Murchison–Thabazimbi–Lineament to the south and the Hout River Shear Zone to the north, contains granitic rocks with ages between 3·3 and 2·65 Ga. Granitoids of the MNK terrane analysed during this study yielded emplacement ages between 2·93 and 2·61 Ga, but some of them contain xenocryst cores as old as 3·22 Ga (Fig. 11a, Table S1). Such cores are found in the Lekkersmaak granite (sample MB1: $\varepsilon Hf_{3·11Ga} = +1·8$), in the Groot Letaba granite gneiss near Tzaneen (sample MB4: $\varepsilon Hf_{3·21Ga} = +1·9$), and in the Meriri granite gneiss of the Giyani greenstone belt (sample GB2: $\varepsilon Hf_{3·24–3·14}$ between −1·6 and +0·7) (Fig. 11a, and Tables 3 and S2). Relics of even older crust (up to 3·3 Ga), as reported by Brandl & Kröner (1993), Kröner *et al.* (2000) and Poujol *et al.* (2003), have not been found during this study.

In general, the εHf_{int} data obtained from the MNK terrane granitoids fit on a trend that is characterized by decreasing εHf_{int} toward younger ages, and plots above the crustal evolution trend as defined by the rocks from the BN terrane (see Fig. 11a). Granitoids of the MNK terrane that were emplaced between 2·9 and 2·78 Ga mostly scatter around CHUR or are slightly subchondritic (GB2, Meriri granite gneiss: $\varepsilon Hf_{2·93Ga} = +0·7 \pm 1·5$; MB4, Groot Letaba gneiss near Tzaneen: $\varepsilon Hf_{2·84Ga} = +0·4 \pm 1·5$; MB1, Lekkersmaak granite: $\varepsilon Hf_{2·80Ga} = -0·7 \pm 1·3$; GB1, Groot Letaba gneiss south to Giyani: $\varepsilon Hf_{2·79Ga} = +0·3 \pm 1·8$; PB2, Turfloop granite: $\varepsilon Hf_{2·78Ga} = -0·2 \pm 2·1$). All younger granitoids plot significantly below CHUR; for example, the Mashishimale granite (sample MB2: $\varepsilon Hf_{2·67Ga} = -3·5 \pm 1·7$), and within the Uitloop granite Pietersburg greenstone belt (sample PB1: $\varepsilon Hf_{2·68Ga} = -2·6 \pm 1·9$). The only exception is the hornblende gabbro of the Rooiwater complex (sample MB3), which shows significantly higher $\varepsilon Hf_{2·61Ga}$ of $-0·6 \pm 1·3$ (Fig. 11b).

It is worth noting that the Matok granite, which intruded the high-grade rocks of the SMZ at 2679 ± 6 Ma, indicates, within error, identical εHf_{int} to the similarly old granitoids of the MNK terrane (sample PB6; see Table 3). This agreement supports previous inferences that the rocks constituting the SMZ represent the high-grade metamorphic equivalent of those exposed to the south of the Hout River Shear Zone, meaning that they are more related to the MNK terrane than to the Central Zone of the Limpopo Belt (Coward *et al.*, 1976; van Reenen *et al.*, 1987, 1992; Kreissig *et al.*, 2000; Barton *et al.*, 2006). As shown in Fig. 11, the analyses of all granitoid rocks of the MNK terrane and the SMZ fit on a single crustal evolution trend. This trend proceeds from 2·93 Ga ($\varepsilon Hf_{2·93Ga} = +0·7$: sample GB2) to 2·02 Ga ($\varepsilon Hf_{2·02Ga} = -12·5$: sample ETG), and requires an average crustal $^{176}Lu/^{177}Hf$ of about 0·012, a value that is similar to modern mature continental crust (Rudnick & Fountain, 1995; Wedepohl, 1995). This trend excludes only the Hf isotope data obtained from xenocryst zircon cores (which plot below the MNK and BN trends), and those of the Rooiwater complex hornblende gabbro (which plots above; Fig. 11a and b). The data from the Rooiwater complex gabbro probably indicate that mantle-derived magmas intruded at 2·61 Ga. The older U–Pb zircon age of 2·74 Ga, as obtained by Poujol *et al.* (1996), either represents an older phase of Rooiwater intrusion, or it was obtained from zircon xenocrysts, perhaps assimilated during mafic magma ascent.

Further evidence for juvenile magma addition to the Kaapvaal Craton crust during the Neoarchean is provided by data from the granites of the Gaborone Suite, which intruded at the western end of the Thabazimbi–Murchison Lineament at 2·77 Ga (see Fig. 1, and Tables 3 and S2). Zircon grains from these granitoids yield the highest εHf_{int} of +4·3 (sample KA) obtained during this study, although the average values are lower (sample GA: $\varepsilon Hf_{2·78Ga} = 2·1 \pm 1·6$; sample KA: $\varepsilon Hf_{2·78Ga} = 1·3 \pm 3·1$, Table 3). Such high values were reported, so far, only from a few Neoarchean xenocryst zircon cores analysed from leucogranitic melts of the Mahalapye complex of the Limpopo Belt (Zeh *et al.*, 2007).

Limpopo Belt (Central Zone)

The samples studied from the Motloutse (SP1) and Phikwe terranes (SP2, SP3, SP4) yield Neoarchean emplacement ages between 2·60 and 2·65 Ga, and the diorite sample Mo5 from the Mahalapye terrane a Paleoproterozoic age

of about 2·03 Ga (see Tables 3 and S1). In addition, there is evidence for the existence of pre-Neoarchean crustal material in the Phikwe and Motloutse terranes, as constrained by xenocryst zircon cores in samples SP1 and SP2 (*c.* 2·85 Ga; also see McCourt *et al.*, 2004), and by the hafnium isotope data for highly discordant zircon domains, which show significantly lower $^{176}Hf/^{177}Hf_{ap}$ than the predominant magmatic domains (see Fig. 8 and Table S2). Such low $^{176}Hf/^{177}Hf_{ap}$ domains were found in sample SP1 ($^{176}Hf/^{177}Hf_{ap} = 0{\cdot}28086–0{\cdot}28060$), and sample SP3 ($^{176}Hf/^{177}Hf_{ap} = 0{\cdot}28091–0{\cdot}28083$) (see Fig. 8a–c and Table S2). Partial recycling or inheritance of pre-Neoarchean crust during magma emplacement at 2·60–2·65 Ga in the Phikwe and Motloutse terranes is also supported by the fact that all Neoarchean zircon domains yield subchondritic εHf_{int}: samples SP1 ($\varepsilon Hf_{2{\cdot}65Ga} = -2{\cdot}7 \pm 2{\cdot}1$), SP2 ($\varepsilon Hf_{2{\cdot}66Ga} = -3{\cdot}7 \pm 1{\cdot}6$), SP3 ($\varepsilon Hf_{2{\cdot}65Ga} = -1{\cdot}6 \pm 1{\cdot}0$), and SP4 ($\varepsilon Hf_{2{\cdot}61Ga} = -2{\cdot}5 \pm 1{\cdot}9$). In fact, these values are within error identical to those previously obtained from Neoarchean granitoids of the Beit Bridge and Phikwe terranes of the Limpopo Belt, comprising the Bulai granite ($\varepsilon Hf_{2{\cdot}61Ga} = -3{\cdot}1 \pm 1{\cdot}2$), Regina gneisses ($\varepsilon Hf_{2{\cdot}65Ga} = -4{\cdot}5 \pm 1{\cdot}3$), and Zanzibar gneisses ($\varepsilon Hf_{2{\cdot}61Ga} = -1{\cdot}3 \pm 1{\cdot}4$) (see Table 3 and Zeh *et al.*, 2007).

In addition to the predominant magmatic zircon domains, Paleoproterozoic metamorphic zircon overgrowths were found in samples SP1 (U–Pb age = 2·056 Ga, $^{176}Hf/^{177}Hf$ up to 0·28148) and SP4 (U–Pb age *c.* 2·0 Ga, $^{176}Hf/^{177}Hf$ up to 0·28133) (see Fig. 8a and d). These Paleoproterozoic overgrowths formed most probably during a high-grade metamorphic overprint of the Phikwe and Motloutse terranes. At nearly the same time the Mahalapye terrane was intruded by granites and diorites. The Mokgware diorite (sample Mo5) of the Mahalapye terrane has $\varepsilon Hf_{2{\cdot}03Ga} = -3{\cdot}6 \pm 1{\cdot}3$, which is much higher than the values obtained from the nearby Mokgware granite ($\varepsilon Hf_{2{\cdot}02Ga} = -10{\cdot}6 \pm 2{\cdot}5$), but lower than those obtained from the Lose quarry diorite ($\varepsilon Hf_{2{\cdot}06Ga} = -0{\cdot}8 \pm 0{\cdot}6$) [the last two values are from Zeh *et al.* (2007), recalculated for CHUR constants of Bouvier *et al.* (2008)]. The observed range of $\varepsilon Hf_{2{\cdot}0Ga}$ from −10·6 to −0·8 in the diorites and granites gives a clue that depleted(?) mantle-derived melts were mixed with different portions of much older crust during the evolution of the Mahalapye terrane at *c.* 2·0 Ga. This feature is unique throughout the Limpopo Belt (and even the Kalahari Craton). Finally, it should be noted that most of the granitoid rocks of the LCZ (Beit Bridge, Phikwe and Motloutse terranes) fit on the same crustal evolution trend as the granitoids from the MNK terrane (see Fig. 11c).

Francistown arc complex

The granitoid rocks of the Francistown arc complex yielded Neoarchean ages of about 2·65 Ga and 2·70 Ga: sample FT3 (Hill view tonalite: 2649 ± 9 Ma), sample FT6 (Sikukwe TTG: 2662 ± 6 Ma), sample FT10 (airport granite: 2648 ± 12 Ma), sample FT5 (Sikukwe TTG: 2700 ± 8 Ma), sample FT7 (Tati-TTG: 2734 ± 39 Ma), sample FT11 (Selkirk sanukitoid: 2707 ± 7 Ma). The younger emplacement ages are, within error, identical to those obtained from many granitoid rocks from the LCZ, whereas the three older samples are more similar to the U–Pb age data obtained from the granitoids of the NMZ (Berger *et al.*, 1995; Blenkinsop *et al.*, 2004).

It is worth noting that the Neoarchean granitoid rocks of the Francistown arc complex show, in contrast to those of the LCZ, higher εHf_{int}, which scatters around CHUR (Fig. 11d): sample FT3 ($\varepsilon Hf_{2{\cdot}65Ga} = +0{\cdot}1 \pm 0{\cdot}9$), FT5 ($\varepsilon Hf_{2{\cdot}70Ga} = +0{\cdot}7 \pm 1{\cdot}1$), FT6 ($\varepsilon Hf_{2{\cdot}66Ga} = +1{\cdot}1 \pm 1{\cdot}1$), FT7 ($\varepsilon Hf_{2{\cdot}73Ga} = -0{\cdot}2 \pm 1{\cdot}9$), FT10 ($\varepsilon Hf_{2{\cdot}65Ga} = -0{\cdot}1 \pm 1{\cdot}6$), and FT11 ($\varepsilon Hf_{2{\cdot}65Ga} = -0{\cdot}1 \pm 1{\cdot}7$). This near-CHUR composition of all the Francistown terrane samples could be interpreted in at least three different ways. First, it could reflect the possibility that all the magmas were derived by melting of a mantle source that had a chondritic composition at about 2·65–2·70 Ga. Second, the parental melts could have been derived from a depleted mantle source (mantle wedge below the Francistown arc), but assimilated at least some portions of older crust during their ascent [as suggested by Zhai *et al.* (2006)]. Third, the TTGs formed by remelting of a mafic lower crust, which was derived from a depleted mantle source some 300 Ma prior to granitoid emplacement (for further explanation see below).

Crust–mantle Lu–Hf compositions and evolutionary trends

The U–Pb and Lu–Hf isotope datasets obtained during this study indicate that the granitoids of the distinct terranes fit on different crustal evolution trends, which start with chondritic or superchondritic εHf_t at different times (BS-terrane at 3·44 Ga, BN-terrane at 3·23 Ga, MNK-terrane and SMZ at 2·92 Ga, Francistown terrane at 2·7 Ga), and require $^{176}Lu/^{177}Hf_{today}$ between 0·004 and 0·015 (Figs 10–12). These trends give a clear indication that the crustal evolution of the various terranes occurred independently from each other. However, it is worth noting that the $^{176}Lu/^{177}Hf_{today}$ values constrained by the U–Pb and Lu–Hf isotope data for the distinct terranes have large uncertainties, and do not necessarily reflect the true average crustal Lu–Hf composition. These uncertainties result from at least two of the following causes, as described below.

Composition of the 'depleted' mantle reservoir of the Kalahari domain

It is not clear whether or not the starting point of the crustal evolution trend for each terrane (see arrows in Figs 10–12) represents the most primitive end-member; that is, a granitoid that was derived from a mantle source at the

time of emplacement without being modified by assimilation of older crust. In addition, there is some uncertainty about the Lu–Hf isotope composition of the 'depleted' mantle reservoir of the Kalahari domain (part of the Archean Earth from which the various terranes of the Kalahari Craton were derived). For instance, the Hf isotope data for zircon grains from the oldest TTGs of the BS terrane [3·44–3·53 Ga: analysed during this study, and by Amelin *et al.* (2000)] yielded $\varepsilon Hf_{3.53Ga}$ from −0·8 to +2·1 (similar to tholeiitic basalts with $\varepsilon Hf_{3.53Ga} = -0.4$ to +2·3), whereas komatiites formed at the same time show higher $\varepsilon Hf_{3.45Ga}$ of +2·3 to +7·1 (Blichert-Toft & Arndt, 1999). Thus, if the Barberton komatiites represent the early Archean depleted mantle composition underneath the BS terrane, both the tholeiitic basalts and the TTGs must contain older crust; such an interpretation agrees with that of Blichert-Toft & Arndt (1999). Those workers argued that the Barberton basalts and komatiites result from melting of distinct (perhaps heterogeneous) mantle sources. The Barberton komatiites (low Al_2O_3/TiO_2, high $\varepsilon Hf_{3.53Ga}$) are interpreted to be derived from a deep-seated, garnet-enriched mantle source at 3·5 Ga, whereas the tholeiitic basalts (chondritic Al_2O_3/TiO_2, lower $\varepsilon Hf_{3.53Ga}$) formed by melting of a shallower, garnet-free mantle source at the same time. The similarity of the εHf_t suggests that the 3·53–3·44 Ga Barberton TTGs were generated by melting of the tholeiitic basalts shortly after the latter were formed; either by slab-melting during subduction or during lower mafic crust foundering. Involvement of older crust (>3·53 Ga) during the formation of the early Archean Barberton TTGs at 3·55–3·44 Ga is highly likely, and supported by local observations and some global analogies. Direct evidence for crust >3·53 Ga in the BS terrane is revealed by 3·6–3·7 Ga U–Pb zircon ages from TTGs of the Ancient Gneiss Complex (Compston & Kröner, 1988), and indirectly by 3·7–3·9 Ga Nd model-ages, and by the negative Eu anomalies of metasediments (Kröner & Tegtmeyer, 1994). Furthermore, the inheritance of older crust appears likely, if we consider that an early Hadean mafic protocrust with TTG constituents (Blichert-Toft & Albarède, 2008; Harrison *et al.*, 2008; Zeh *et al.*, 2008) was cannibalized, and at least partly recycled at the Hadean to Early Archean transition between 3·9 and 3·3 Ga. Such a scenario was recently proposed on the basis of detrital zircon U–Pb and Lu–Hf data from the Limpopo Belt (Zeh *et al.*, 2008) (see Fig. 12b), and is supported by various data from Greenland, and Canada [see discussions by Kamber *et al.* (2003, 2005), Kramers (2007) and Zeh *et al.* (2008)]. Furthermore, the idea of recycling of older crust at 3·5 Ga is in agreement with the fact that most εHf_t data from the BS terrane plot well below the assumed depleted mantle array deduced from the present-day MORB data of Chauvel & Blichert-Toft (2001) (see Fig. 12). It is, however, unclear whether or not this can be extrapolated as linear array to Archean rocks or requires another model. As shown in Fig. 12b, the linear array fits some of the Lu–Hf isotope data for crustal rocks from Greenland (3·9–3·6 Ga), Australia (3·1–2·5 Ga) and North America (3·0–2·7 Ga). However, apart from a few 'outliers', the dataset could also be explained by a non-linear or by a two-stage evolution model, characterized by a slightly increasing εHf_t (from +1·0 to +3·0) between 4·5 and 3·1 Ga, and a steeper increase between 3·1 Ga and today (Fig. 12). In any case, the existing datasets indicate that a depleted mantle source (with respect to hafnium) that was distinctly different from CHUR existed at or even prior to 3·1–3·5 Ga. Thus, the nearly chondritic εHf_{int} data obtained from the 3·44–2·0 Ga granitoids of the Kalahari Craton (Fig. 12) most probably reflects successive recycling of older crust in concert with juvenile mantle addition, rather than sampling of a chondritic mantle reservoir over a period of 1·5 Gyr.

Successive alteration of the crust

Another source of uncertainty in the $^{176}Lu/^{177}Hf_{today}$ value derived for the respective terranes (Figs 10 and 11) could result from processes that caused a change in the crustal Lu–Hf composition with time. Such processes could have been (1) zircon fractionation during anatectic melting of an existing lower continental crust (zircon and non-radiogenic hafnium remained in the restitic lower crust), and/or (2) admixing of depleted mantle-derived magmas to existing older crust. Based on the available datasets, it seems likely that such processes played an important role during the intrusion of the youngest granitoids of the BN terrane (Mpageni granite), and the 3·10–3·23 Ga granitoids of the BS terrane. As shown in Fig. 10c, the Mpageni granite and the 3·23 Ga TTGs (Kaap Valley, Nelshoogte, and Stentor plutons) fit on a crustal evolution trend that requires $^{176}Lu/^{177}Hf_{today} = 0.0095$, whereas the 3·23 Ga TTGs and 3·10 Ga granites (Nelspruit and Salisbury granite) lie on a different trend with a lower $^{176}Lu/^{177}Hf$ of 0·004. For the BS terrane, the 3·1 Ga granitoids (Pigg's Peak, Boesmannskop and Mpuluzi granites) plot well above the trend defined by the 3·44 and 3·23 Ga granitoids (see Fig. 10a and b).

Terrane accretion and geotectonic implications

The results from this study clearly indicate that the terranes of the Kalahari Craton (BS, BN, MNK and Francistown) lie on distinct crustal evolution trends with little or no overlap (Figs 10, 11 and 12a). This requires that the continental crust that constitutes these terranes formed at different times, and subsequently evolved differently. Furthermore, it requires that the terranes of the Kalahari Craton were successively accreted.

BS and BN terrane accretion

A striking feature is that the TTGs of the BN terrane, which intruded the northern flank of the Barberton greenstone belt (near the Barberton Lineament) at about 3·23 Ga, show much higher $\varepsilon Hf_{3\cdot23Ga}$ (+0·9 to +2·4: Kaap Valley, Nelshoogte and Stentor tonalite) than the coevally emplaced granitoids of the BS terrane (−1·7 to −0·4: Dalmein granite, Ngwane gneisses, samples AGC1 and AGC2) (Fig. 12a). This suggests that the BS terrane underwent crustal recycling, whereas new granitic crust was formed in the BN terrane. Furthermore, it supports the idea that the Barberton Lineament represents a real suture zone, along which two distinct terranes became accreted during the closure of an oceanic basin, and that the BN terrane formed the lower, subducted plate (see below). In general, this interpretation agrees with previous models, which are mainly based on field observations and geochronological data (e.g. de Ronde & de Wit, 1994; Lowe, 1994; de Ronde & Kamo, 2000; Poujol *et al.*, 2003; Anhaeusser, 2006). The positive εHf_t of the 3·23 Ga TTGs of the BN terrane suggest two possibilities. Either these TTGs were formed by melting of relatively young subducted oceanic crust (MORB), which was derived from the depleted mantle immediately prior to the subduction process, and/or by melting processes within the mantle wedge above the subduction zone (Martin *et al.*, 2005). For the BN TTGs slab melting seems highly likel, as the Kaap Valley tonalite exhibits many similarities to Cenozoic adakites (e.g. Smithies, 2000).

In contrast to the BN TTGs the much lower $\varepsilon Hf_{3\cdot23Ga}$ of the BS TTGs (e.g. trondjhemite west of Manzini: samples AGC1 and AGC2) could result from melting of a thick pile of older basaltic crust with some older granite–greenstone components (Fig. 13a). This interpretation is supported by the presence of xenocryst zircon cores in samples AGC1 and AGC2 (3·4–3·5 Ga), and by field relationships, indicating that the TTGs west of Manzini contain abundant mafic xenoliths (metabasalts). The intrusion of the Dalmein monzonite and of some porphyry dykes (at 3·21 Ga) in the southern Barberton Mountain Land might indicate that their parental melts were derived from the mantle wedge above the 3·23 Ga subduction zone, and that these melts underwent differentiation and assimilation of older crustal material (3·45–3·53 Ga) during their ascent. A purely crustal origin for the Dalmein monzonite, perhaps as a result of melting of older (3·45–3·55 Ga) TTGs can be excluded because of its relatively high $\varepsilon Hf_{3\cdot21Ga}$ of −0·4 (above the BS trend: Fig. 10b).

At *c.* 3·1 Ga, the amalgamated Barberton terranes (BS and BN) were intruded by potassium-rich granitoids (Pigg's Peak, Mpuluzi and Nelspruit batholiths) and some smaller granite bodies (e.g. the Boesmanskop syenite, and Salisbury monzogranite). Based on combined field work and geochronological data, Schoene *et al.* (2008) concluded that the emplacement of these batholiths or granitoids was related to transtensional movements that affected the Barberton greenstone belt and adjacent areas in Mesoarchean times. Those workers also suggested that the batholiths resulted from the fractionation of a thickened continental crust that was formed during terrane collision (BS and BN) between 3·30 and 3·23 Ga (together with the formation of a thick and rigid mantle lithosphere underneath the eastern Kaapvaal Craton). Schoene *et al.* (2008) preferred a model in which subsequently the crustal differentiation process was solely driven by 'incubational' heating, accompanied by the migration of granitic melts and heat-producing elements (U–Th–K) from the lower into the upper crust between 3·2 and 3·1 Ga. Although this model may be sound from a mechanical point of view it is, at least in parts, inconsistent with the data obtained during this and some previous studies. First at all, the emplacement of the Mesoarchean granitoids occurred within a relatively short time span between 3·14 and 3·08 Ga (this study; Kamo & Davis, 1994; Schoene *et al.*, 2008), which contradicts a long-lasting crustal differentiation and migration model. Second, the hafnium isotope data for the potassium-rich granitoids, in particular for those from the BS terrane (Pigg's Peak granite, Mpuluzi granite, and Boesmanskop syenite) clearly point to the addition of a depleted mantle component at 3·1 Ga. In fact, the εHf_{int} compositions of these granitoids plot well above the BS terrane crustal evolution trend (Fig. 10b). Some zircon grains even yield super-chondritic $\varepsilon Hf_{3\cdot1Ga}$ of up to +1·0 (e.g. Pigg's Peak granite and Boesmanskop syenite). In this context it is worth noting that the relatively large scatter in the εHf_{int} of zircon from the Boesmanskop syenite (Fig. 6h and Table 3) could be interpreted to reflect incomplete mixing of older crust and a depleted mantle component during syenite formation and magma ascent at 3·1 Ga.

In contrast to the granitoids of the BS terrane, those of the BN terrane (Nelspruit batholith and Salisbury granite) are consistent with a simple crust recycling model, if just the Lu–Hf isotope data are considered. As shown in Fig. 10c, the TTGs and potassic granitoids plot on a crustal trend with an average $^{176}Lu/^{177}Hf_{today}$ of 0·004, a ratio that is typical for Archean TTGs (see Condie, 2005). However, if the 3·23 Ga TTGs were the direct source for the 3·1 Ga potassium-rich granites they must have undergone important fractionation processes during partial anatexis and magma ascent [consistent with the model of Schoene *et al.* (2008)]. Furthermore, any zircon in the melt source must have been completely removed, otherwise the resulting granitic melts would have been enriched in radiogenic hafnium (^{176}Hf), with the consequence that the 3·1 Ga granitoids would plot significantly above the inferred $^{176}Lu/^{177}Hf_{today}$ trend of 0·004 (Fig. 10c). In our opinion, both assumptions are unrealistic; in particular if we take

into account results from other high-grade gneiss terranes, such as from the Central Zone of the Limpopo Belt, where the Sand River TTG gneisses were partially remelted twice (Gerdes & Zeh, 2008). Despite this multiple high-grade metamorphic overprint only small volumes of potassic granite melts (leucosomes) were formed. Furthermore, these TTGs contain abundant magmatic zircon grains or domains (Zeh *et al.*, 2007; Gerdes & Zeh, 2009). Thus, in our opinion it seems more likely that the potassium-rich granitoids of the BN terrane, like those of the BS terrane, formed by anatexis of a crust older than 3·23 Ga (perhaps underrepresented in this study), in concert with the addition of K-rich melts from a mantle source at 3·1 Ga. The existence of older crust is supported by the identification of xenocryst zircon cores (3·21–3·3 Ga) with subcondritic $\varepsilon Hf_{3\cdot21Ga}$ of −2·5 in the Nelspruit batholith (Figs 6l and 10c; also see Kamo & Davies, 1994).

The formation of mantle melts underneath the eastern Kaapvaal Craton may provide an effective heat source (alternative or additional to the incubational crustal heating) needed to form the voluminous potassic batholiths at 3·1 Ga (Fig. 13b). In principle, it seems possible that mafic melts could have accumulated at the crust–mantle boundary, and that these melts homogenized with lower crustal melts, prior to their ascent. In general, such mafic mantle melts could have been formed by processes involving the ascent of asthenospheric mantle, either as a result of the foundering of lower mafic crust and the subcontinental lithospheric mantle and/or by mantle plume activity. They could also be formed in response to subduction processes beneath the eastern Kaapvaal Craton (BS–BN terranes). In fact, it is a striking feature that the formation of the 3·1 Ga Kaapvaal batholiths occurred at the same time as the start of accretion of new terranes at the northern and northwestern margins of the early Kaapvaal Craton (Poujol *et al.*, 2002, 2003) (see Fig. 13b).

Nevertheless, all three processes mentioned above (foundering, mantle plumes, subduction) are problematic, in particular if we consider that the Kaapvaal Craton has a very old and thick subcontinental mantle keel. The question, however, is when this thick (and relatively cold) mantle keel was formed: prior to or after 3·1 Ga? So far, there is only limited evidence for the existence of a thick subcontinental lithosphere older than 3·2–3·3 Ga (Richardson *et al.*, 1984). Currently, such old ages have been obtained only from silicate inclusion in diamonds from the Kimberley block (part of the Kaapvaal Craton to the west of the Colesburg lineament; Fig. 1), which according to Schmitz *et al.* (2004) accreted to the Witwatersrand block (comprising the BS and BN terranes) not before 2·9 Ga. Furthermore, the geological significance of these ages is debatable, and is strongly based on the assumption that the silicate inclusions analysed from a large number of diamonds are syngenetic [see review by Richardson *et al.* (2004) and Shirey *et al.* (2004)]. In contrast, most data provide evidence that the thick subcontinental mantle root beneath the Kaapvaal Craton formed later than 3·1–2·9 Ga. This is supported by Re-depletion ages obtained from peridotitic and eclogitic mantle xenoliths from several kimberlite pipes (Pearson, 1995), and by the study of lower crustal rocks (Moser *et al.*, 2000; Schmitz *et al.*, 2004). Thus, complex mantle activity beneath the proto Kaapvaal Craton (BS and BN terranes) at 3·1 Ga, comprising lithospheric foundering, mantle plumes and even subduction, cannot be excluded. Any of these processes could also be responsible for the lithospheric rifting that caused the formation of basins filled with Dominion Supergroup rocks (Poujol *et al.*, 2003).

BN and MNK terrane accretion and evolution

As shown in Fig. 11a and b, all the granitoid rocks from the MNK terrane fit on an evolutionary trend that is parallel to that of the BN terrane but shifted to younger ages. This offset indicates that the Murchison lineament represents an important crustal suture zone along which distinct terranes were accreted (Vearncombe *et al.*, 1992; Poujol *et al.*, 2003; Anhaeusser, 2006). The granitoids with the most isotopic primitive signatures, analysed during this study, yield near-chondritic hafnium isotope compositions between $\varepsilon Hf_{2\cdot79–2\cdot93Ga}$ of $+0\cdot3 \pm 1\cdot8$ and $+0\cdot7 \pm 1\cdot8$ (samples GB1, GB2 and MB4, Table 3). These values indicate either that these granitoid rocks (TTGs) were derived from a near-chondritic mantle source at 2·9–2·8 Ga, or that abundant amounts of even older crust were recycled during their formation. Recycling seems to be most likely, and is supported by the finding of zircon xenocrysts in the Mac Kop conglomerate (3·36 Ga: Poujol *et al.*, 1996), the Goudplaats–Hout River gneisses to the north of the Giyani greenstone belt (3·23–3·27 Ga: Brandl & Kröner, 1993; Kröner *et al.*, 2000), the meta-andesites of the Gyani greenstone belt (3·2 Ga: Brandl & Kröner, 1993) and the TTGs of the French Bob mine (3·23 Ga: Poujol *et al.*, 1996). Furthermore, it is supported by the finding of xenocryst zircon grains in the Meriri granite gneiss (3·22–3·14 Ga), Lekkersmaak granite (3·11–2·99 Ga), and in the Groot Letaba gneiss near Tzaneen (3·21–2·95 Ga) (this study; see Table 3). As shown in Fig. 11a and b, these xenocryst zircons show a wide scatter in εHf_{ap} from −1·6 to +1·9, and do not plot on the crustal trend derived for the MNK terrane. This also confirms that the MNK terrane contains older crust that was recycled during magma formation at 2·9–2·8 Ga. It is worth noting that our data provide no evidence for the existence of any juvenile island arc in the MNK terrane at 2·9–2·8 Ga. This finding is different from that for the Superior province of Canada, where numerous primitive island arcs were accreted at nearly the same time (2·95–2·70 Ga), as constrained by the hafnium isotope data of Polat & Münker (1994) and Davis *et al.* (2005) ($\varepsilon Hf_{2\cdot7Ga} = +2\cdot8$ to $+6\cdot8$). In summary,

our data for the MNK terrane indicate that pre-existing Archean crust was recycled during the formation of new continental crust at 2·9–2·8 Ga, and that this recycling process took place during the accretion of the MNK with the BN terrane.

Following the accretion process the crust of the MNK terrane was re-melted (with melt fractionation) without any significant new mantle influence. This is supported by the negative εHf_{int} of the 2·67 Ga granitoids (samples PBl and MB2: $\varepsilon Hf_{int} = -2{\cdot}6$ to $-3{\cdot}5$), and reflected by the successive decrease in εHf_{int} between 2·9 and 2·02 Ga (Fig. 11a). The only exception is presented by the hornblende gabbro of the Rooiwater complex, whose εHf_{int} requires the addition of new mantle-derived magma at 2·61 Ga, perhaps caused by local mantle melting underneath the Murchison–Thabazimbi suture zone (Fig. 13c). Thus far, the reason for the formation of the 2·67 Ga granitoids in the MNK terrane is not entirely clear. However, it is likely that their emplacement occurred in response to the first phase of the 'Limpopo orogeny' at 2·67 Ga, during which the rocks of the LCZ (i.e. Limpopo Belt *sensu stricto*) were accreted to the northern edge of the Kaapvaal Craton, comprising the MNK terrane and the SMZ (see Fig. 13c). This interpretation is supported by geochronological data for granulites from the SMZ (2·67 Ga), and from kyanite–staurolite-bearing metapelites in the vicinity of the Hout River Shear Zone (2·67–2·69 Ga; Kreissig *et al.*, 2001). It is also indicated by data for the Matok granite, which was emplaced in the high-grade gneisses of the SMZ at 2·68 Ga (immediately after thrusting of the Hout River Shear Zone) and has the same $\varepsilon Hf_{2\cdot68Ga}$ of −3·9 as the equivalent age granitoids of the MNK terrane (see Table 3 and Fig. 13c). Thus, the combined U–Pb and Lu–Hf isotope datasets are consistent with previous interpretations (based on field relationships, geochronological and Pb isotope data), suggesting that the SMZ is genetically related to the Kaapvaal Craton, and not to the Limpopo Belt *sensu stricto* (e.g. Coward *et al.*, 1976; van Reenen *et al.*, 1987, 1992; Kreissig *et al.*, 2000; Barton *et al.*, 2006). At this point, however, it is worth noting that the Hf isotope data alone do not allow such a discrimination (see Fig. 11a–c). Furthermore, it should be emphasized that the tectono-metamorphic–magmatic evolution of the northern edge of the Kaapvaal Craton (MNK + SMZ) and the LCZ was not absolutely synchronous during the Neoarchean. Magmatism and high-grade metamorphism in the SMZ took place between 2·69 and 2·67 Ga, and in the LCZ between 2·65 and 2·61 Ga (e.g. Kröner *et al.*, 1998; Zeh *et al.*, 2007; Millonig *et al.*, 2008; Van Reenen *et al.*, 2008; Gerdes & Zeh 2009; and below).

Finally, it should be noted that the 2·77 Ga Gaborone Granite Suite, which was intruded slightly earlier than the first phase of the Limpopo Orogeny, does not fit on the crustal evolution trends of the MNK and LCZ terranes, but is characterized by higher εHf_{int} (Fig. 11b). These data indicate that the western part of the MNK terrane was intruded by important amounts of depleted mantle-derived magmas at 2·77 Ga. The reason for this is still enigmatic, and perhaps results from the special position of the Gaborone Magmatic Complex at the intersection of two major crustal lineaments, the ENE–WSW-trending Murchison–Thabazimi and the north–south-trending Colesburg lineaments (Fig. 1).

Accretion of the LCZ and the Francistown arc complex

As shown in Fig. 11d and Table 3, the granitoids of the Francistown arc complex intruded between 2·7 and 2·65 Ga, whereas most granitoids of the LCZ were emplaced later (2·65–2·61 Ga). Furthermore, the granitoids of the Francistown arc complex have higher $\varepsilon Hf_{2\cdot70-2\cdot65Ga}$ (−0·5 to +0·7) compared with those of the LCZ (Motloutse and Phikwe terrane: $\varepsilon Hf_{2\cdot65-2\cdot60Ga} = -3{\cdot}6$ to $-1{\cdot}8$; Beit Bridge terrane: $\varepsilon Hf_{2\cdot65-2\cdot60Ga} = -4{\cdot}5$ to $-1{\cdot}0$). These data suggest that during the Neoarchean magmatism older crust was recycled in both units, but that the degree of recycling was higher in the LCZ. For the LCZ, older crust relics are revealed by xenocryst zircon ages between 2·8 and 3·9 Ga, obtained from felsic and mafic orthogneisses (Kröner *et al.*, 1998, 1999; Zeh *et al.*, 2007; Chudy *et al.*, 2008), and from metasediments throughout the Central Zone (Barton *et al.*, 2003; McCourt *et al.*, 2004; Zeh *et al.*, 2008). In contrast, there is no direct evidence for the crustal source that 'contaminated' the Francistown arc complex. According to McCourt *et al.* (2004) and Zhai *et al.* (2006) the Francistown terrane represents a continental magmatic arc that resulted from northeastward subduction of juvenile oceanic crust underneath the Zimbabwe Craton, and ceased with the accretion of the Motloutse terrane (= Limpopo Belt) at about 2·65 Ga. This model, however, cannot account in an easy way for the voluminous TTG magmatism, which affected all complexes of the LCZ (Motloutse, Phikwe, Beit Bridge) between 2·65 and 2·60 Ga. To explain their formation, it would be easier to accrete the Zimbabwe terranes by southeastward-directed subduction underneath the Limpopo Belt (Fig. 13c), as previously suggested by Dirks & Jelsma (2002). In such a case, the variable $\varepsilon Hf_{2\cdot65-2\cdot60Ga}$ from −4·5 to −1·0 of the Limpopo granitoids could be explained as a result of variable mixing of older crust (>2·7 Ga) either with slab-melts or with mafic melts (perhaps underplated; see Fig. 13c) formed by partial melting of the mantle wedge above a subduction zone. Southeastward-directed subduction could account for enrichment of the mantle wedge, as required by geochemical and geochronological data for lamprophyres from the LCZ (Watkeys & Armstrong, 1985). Furthermore, it could provide an explanation for the high-temperature, medium-pressure metamorphic overprint (850°C and 7 kbar) that affected some parts of

the LCZ at 2·64 Ga (see Millonig *et al.*, 2008; Gerdes & Zeh, 2009).

SUMMARY AND CONCLUSIONS

U–Pb and Lu–Hf isotope data, obtained by LA-SF-ICP-MS on zircon grains from 37 granitoid samples, in combination with field relationships, provide evidence that the Kalahari Craton consists of at least five distinct terranes—Barberton South (BS), Barberton North (BN), Murchison–Northern Kaapvaal (MNK), Limpopo Central Zone (LCZ) and Francistown—which underwent different crustal evolutions and were successively accreted at *c.* 3·23 Ga, 2·9 Ga and 2·65–2·7 Ga.

The data reveal that most of the granitoids of the Kalahari Craton have near-chondritic to subchondritic εHf_t (BS: $\varepsilon Hf_{3.4–3.1Ga} = -1.7$ to $+0.5$; MNK: $\varepsilon Hf_{2.9–2.7Ga} = -3.4$ to $+0.7$; Francistown: $\varepsilon Hf_{2.71–2.65Ga} = -0.5$ to $+1.1$; LCZ: $\varepsilon Hf_{2.65–2.0Ga} = -12.4$ to -1.8), suggesting that crustal recycling—perhaps by mixing of older crust with a depleted mantle reservoir—played an important role in their petrogenesis. Recycling of crustal material is supported by the presence of xenocryst zircon domains in all terranes, except the Francistown arc. Super-chondritic εHf_t values, indicative of a significant depleted mantle influence, were obtained only from the oldest granitoids of the BN terrane ($\varepsilon Hf_{3.23Ga} = +2.4 \pm 0.8$), the Gaborone Granite Suite ($\varepsilon Hf_{2.77Ga} = +2.0 \pm 1.6$), and from a few detrital zircon from the Mahalapye complex of the Limpopo Belt ($\varepsilon Hf_{2.71Ga}$ up to $+7.1$; Zeh *et al.*, 2007). Most of the data, however, plot below the assumed depleted mantle array deduced from present-day MORB data (Fig. 12). This suggests that the depleted mantle beneath the Archean Kalahari domain, and the Archean mantle array in general, evolved differently than currently assumed.

Furthermore, the data show that the Hf isotope variation of magmatic zircon domains (excluding xenocryst cores and metamorphic overgrowths) of the Archean granitoids is commonly less than ± 1.5 ε-units (2 SD), and only in few cases reaches ± 3.1 ε-units. Such occasional large εHf_t variations can be ascribed to incomplete isotope equilibration during magma generation and crystallization, probably caused by mixing of magmas of contrasting isotope composition. Finally, this study demonstrates that the combined usage of CL imaging with *in situ* U–Pb and Lu–Hf isotope spot analyses provides a powerful tool to distinguish zircon domains formed and/or altered at different times.

ACKNOWLEDGEMENTS

We thank the Deutsche Forschungsgemeinschaft (DFG) for financial support (grant KL692/16-1/2), Heidi Höfer (University of Frankfurt) for her help with the BSE and CL images, and Janina Schastok (University of Frankfurt) and Peter Späthe (University of Würzburg) for their help with sample preparation. Furthermore, we are indebted to Charles Byron, who assisted us during field work in the Francistown–Tati area. This work benefited from the helpful and constructive reviews of Randall Parrish, Jan Kramers and Tom Andersen.

SUPPLEMENTARY DATA

Supplementary data for this paper are available at *Journal of Petrology* online.

REFERENCES

Aldiss, D. T. (1991). The Motloutse Complex and the Zimbabwe Craton/Limpopo Belt transition in Botswana. *Precambrian Research* **50**, 89–109.

Amelin, Y., Lee, D., Halliday, A. N. & Pidgeon, R. T. (1999). Nature of the Earth. *Nature* **399**, 252–255.

Amelin, Y., Lee, D.-C. & Halliday, A. N. (2000). Early–middle Archean crustal evolution deduced from Lu–Hf and U–Pb isotopic studies of single zircon grains. *Geochimica et Cosmochimica Acta* **64**, 4205–4225.

Andersen, T., Griffin, W. L. & Pearson, N. J. (2002). Crustal evolution in the SW part of the Baltic Shield: the Hf isotope evidence. *Journal of Petrology* **43**, 1725–1747.

Anhaeusser, C. R. (2006). A reevaluation of Archean intracratonic terrane boundaries on the Kaapvaal Craton, South Africa: Collisional suture zones? In: Reimold, W. U. & Gibbson, R. (eds) *Processes on the Early Earth Geological Society of America, Special Publications* **405**, 315–332.

Armstrong, R. A., Compston, W., De Wit, M. J. & Williams, I. S. (1990). The stratigraphy of the 3·5–3·2 Ga Barberton greenstone belt revisited: a single zircon ion microprobe study. *Earth and Planetary Science Letters* **101**, 90–106.

Armstrong, R. A., Compston, W., Retief, E. A. & Welke, H. J. (1991). Zircon ion microprobe studies bearing on the age and evolution of the Witwatersrand triad. *Precambrian Research* **53**, 243–266.

Bagai, Z., Armstrong, R. & Kampunzu, A. B. (2002). U–Pb single zircon geochronology of granitoids in the Vumba granite–greenstone terrain (NE Botswana): implication for the Archaean Zimbabwe craton. *Precambrian Research* **118**, 149–168.

Barton, J. M., Jr (1983). Pb-isotopic evidence for the age of the Messina Layered Intrusion, Central Zone, Limpopo Mobile Belt. In: van Biljon, W. J. & Legg, J. H. (eds) *The Limpopo Belt. Geological Society of South Africa, Special Publications* **8**, 43–44.

Barton, J. M., Jr (1996). The Messina layered intrusion, Limpopo belt, South Africa, an example on the in-situ contamination of an Archean anorthosite complex by continental crust. *Precambrian Research* **78**, 139–150.

Barton, J. M., Jr & Sergeev, S. (1997). High precision, U–Pb analyses of single grains of zircon from quartzite in the Beit Bridge Group yield a discordia. *South African Journal of Geology* **100**, 37–41.

Barton, J. M., Jr, Robb, L. J., Anhaeusser, C. R. & Van Nierop, D. A. (1983*a*). Geochronologic and Sr-isotopic studies of certain units in the Barberton granite–greenstone terrane, South Africa. In: Anhaeusser, C. R. (ed.) *Contributions to the Geology of the Barberton Mountain Land. Geological Society of South Africa, Special Publications* **9**, 63–72.

Barton, J. M., Jr, Du-Toit, M. C., Van Reenen, D. D. & Ryan, B. (1983*b*). Geochronologic studies in the Southern Marginal Zone of

the Limpopo Mobile Belt, southern Africa. In: van Biljon, W. J. & Legg, J. H. (eds) *The Limpopo Belt. Special Publication, Geological Society of South Africa* **8**, 55–64.

Barton, J. M., Jr, Doig, R., Smith, C. B., Bohlender, F. & Van Reenen, D. D. (1992). Isotopic and REE characteristics of the intrusive charnoenderbite and enderbite geographically associated with the Matok Pluton, Limpopo Belt, southern Africa. *Precambrian Research* **55**, 451–467.

Barton, J. M., Jr, Barnett, W. P., Barton, E. S., Barnett, M., Doorgapershad, A., Twiggs, C., Klemd, R., Martin, J., Millonig, L. & Zenglein, R. (2003). The geology of the area surrounding the Venetia kimberlite pipes, Limpopo Belt, South Africa. A complex interplay of nappe tectonics and granitoid magmatism. *South African Journal of Geology* **106**, 109–128.

Barton, J.M., Jr, Klemd, R. & Zeh, A. (2006). The Limpopo Belt: A result of Archean to Proterozoic, Turkic-type orogenesis? In: Reimold, W. U. & Gibbson, R. (eds) *Processes on the Early Earth. Geological Society of America, Special Publications* **405**, 315–332.

Berger, M. & Rollinson, H. (1997). Isotopic and geochemical evidence for crust–mantle interaction during late Archean crustal growth. *Geochimica et Cosmochimica Acta* **61**, 4809–4829.

Berger, M., Kramers, J. D. & Nägler, T. F. (1995). An Archaean high grade province adjacent to a granite greenstone terrain: geochemistry and geochronology of charnoenderbites in the Northern Marginal Zone of the Limpopo Belt, Southern Africa and genetic models. *Schweizerische Mineralogische und Petrographische Mitteilungen* **75**, 17–42.

Blenkinsop, T. G., Kröner, A. & Chiwara, V. (2004). Single stage, late Archean exhumation of granulites in the Northern Marginal Zone, Limpopo Belt, Zimbabwe, and relevance to gold mineralization at Renco Mine. *South African Journal of Geology* **107**, 377–396.

Blichert-Toft, J. & Albarède, F. (1997). The Lu–Hf isotope geochemistry of chondrites and the evolution of the mantle–crust system. *Earth and Planetary Science Letters* **148**, 243–258.

Blichert-Toft, J. & Albarède, F. (2008). Hafnium isotopes in Jack Hills zircons and the formation of the Hadean crust. *Earth and Planetary Science Letters* **265**, 686–702.

Blichert-Toft, J. & Arndt, N. T. (1999). Hf isotope compositions of komatiites. *Earth and Planetary Science Letters* **171**, 439–451.

Boshoff, R., van Reenen, D. D., Smit, C. A., Perchuk, L. L., Kramers, J. D. & Armstrong, R. (2006). Geologic history of the Central Zone of the Limpopo Complex: the West Alldays area. *Journal of Geology* **114**, 699–716.

Bouvier, A., Vervoort, J. D. & Patchett, P. J. (2008). The Lu–Hf and Sm–Nd isotopic composition of CHUR: constraints from unequilibrated chondrites and implications for the bulk composition of terrestrial planets. *Earth and Planetary Science Letters* **273**, 48–57.

Brandl, G. & Kröner, A. (1993). Preliminary results of single zircon studies from various Archaean rocks of the north-eastern Transvaal. *Abstracts, 16th Colloquium on African Geology, Mbabane, Swaziland, Vol. 2*, 54–56.

Brandl, G., Jaeckel, P. & Kröner, A. (1996). Single zircon age for the felsic Rubbervale Formation, Murchison greenstone belt, South Africa. *South African Journal of Geology* **99**, 229–234.

Brandl, G., Cloete, M. & Anhaeusser, C. R. (2006). Archaean greenstone belts. In: Johnson, M. R., Anhaeusser, C. R. & Thomas, R. J. (eds) *The Geology of South Africa.* Pretoria: Geological Society of South Africa, Johannesburg/Council of Geosciences, pp. 9–57.

Buick, I. S., Williams, I. S., Gibbson, R. L., Cartwright, I. & Miller, J. A. (2003). Carbon and U–Pb evidence for a Palaeoproterozoic crustal component in the Central Zone of the Limpopo Belt, South Africa. *Journal of the Geological Society, London* **160**, 601–612.

Carney, J. N., Aldiss, D. T. & Lock, N. P. (1994). *The geology of Botswana*, Garborone: Geological Survey Department.

Chauvel, C. & Blichert-Toft, J. (2001). A hafnium isotope and trace element perspective on melting of the depleted mantle. *Earth and Planetary Science Letters* **190**, 137–151.

Chavagnac, V., Kramers, J. D., Nägler, T. F. & Holzer, L. (2001). The behaviour of Nd and Pb isotopes during 2·0 Ga migmatization in paragneisses of the Central Zone of the Limpopo Belt (South Africa and Botswana). *Precambrian Research* **112**, 51–86.

Chudy, T., Zeh, A., Gerdes, A., Klemd, R. & Barton, J. M., Jr (2008). Paleoarchean (3·3 Ga) mafic magmatism and Paleoproterozoic (2·02 Ga) amphibolite-facies metamorphism in the Central Zone of the Limpopo Belt: New geochronological, petrological and geochemical constraints from metabasic and metapelitic rocks from the Venetia area. *South African Journal of Geology* **111**, 387–408.

Cloete, M. (1999). *Aspects of volcanism and metamorphism of the Onverwacht Group lavas in the south-western portion of the Barberton greenstone belt. Memoirs of the Geological Survey of South Africa*, **84**, 232 pp.

Compston, W. & Kröner, A. (1988). Multiple zircon growth within early Archean tonalitic gneiss from the Ancient Gneiss Complex, Swaziland. *Earth and Planetary Science Letters* **87**, 13–28.

Condie, K. C. (2005). TTGs and adakites: are they both slab melts? *Lithos* **80**, 33–44.

Condie, K. C., Beyer, E., Belousova, E., Griffin, W. L. & O'Reilly, S. Y. (2005). U–Pb isotopic ages and Hf isotopic composition of single zircons: The search for juvenile Precambrian continental crust. *Precambrian Research* **139**, 42–100.

Coward, M. P., James, P. R. & Wright, L. (1976). Northern margin of the Limpopo mobile belt, southern Africa. *Geological Society of America Bulletin* **87**, 601–611.

Davis, D. W., Amelin, Y., Nowell, G. M. & Parrish, R. R. (2005). Hf isotopes in zircon from the western Superior province, Canada: Implications for Archean crustal development and evolution of the depleted mantle reservoir. *Precambrian Research* **114**, 295–325.

De Ronde, C. E. J. & de Wit, M. J. (1994). Tectonic history of the Barberton greenstone belt, Southern Africa: 490 million years of Archean crustal evolution. *Tectonics* **13**, 983–1005.

De Ronde, C. E. J. & Kamo, S. L. (2000). An Archean arc–arc collision event: a short-lived (ca 3 Myr) episode, Weltevreden area, Barberton greenstone belt, South Africa. *Journal of African Earth Sciences* **30**, 219–248.

De Ronde, C. E. J., Kamo, S., Davis, D. W., de Wit, M. J. & Spooner, E. T. C. (1991). Field geochemical and U–Pb isotopic constraints from hypabyssal felsic intrusions within the Barberton greenstone belt, South Africa: implications for tectonics and the timing of gold mineralization. *Precambrian Research* **49**, 261–280.

De Wit, M. J., Armstrong, R. A., Hart, R. J. & Wilson, A. H. (1987). Felsic igneous rocks within the 3·3 to 3·5 Ga Barberton greenstone belt: high crustal level equivalents of the surrounding tonalite–trondhjemite terrain, emplaced during thrusting. *Tectonics* **6**, 529–562.

De Wit, M. J., Roering, C., Hart, R. J., Armstrong, R. A., De Ronde, C. E. J., Green, R. W. E., Tredoux, M., Peberdy, E. & Hart, R. A. (1992). Formation of an Archaean continent. *Nature* **357**, 553–562.

De Wit, M. J., Armstrong, R. A., Kamo, S. L. & Erlank, A. J. (1993). Gold-bearing sediments in the Pietersburg greenstone belt: age equivalents of the Witwatersrand Supergroup sediments, South Africa. *Economic Geology* **88**, 1242–1252.

Dirks, P. H. G. M. & Jelsma, H. A. (2002). Crust–mantle decoupling and the growth of the Archaean Zimbabwe craton. *Journal of African Earth Science* **34**, 157–166.

Dodson, M. H., Compston, W., Williams, I. S. & Wilson, J. F. (1988). A search for ancient detrital zircons in Zimbabwean sediments. *Journal of the Geological Society, London* **145**, 977–983.

Dorland, H. C., Beukes, N. J., Gutzmer, J., Evans, D. A. D. & Armstrong, R. A. (2006). Precise SHRIMP U–Pb age constraints on the lower Watersberg and Soutpansberg Groups, South Africa. *South African Journal of Geology* **109**, 139–156.

Dziggel, A., Stevens, G., Poujol, M., Anhaeusser, C. R. & Armstrong, R. A. (2002). Metamorphism of the granite–greenstone terrane south of the Barberton greenstone belt, South Africa: An insight into the tectono-thermal evolution of the lower portions of the Onverwacht Group. *Precambrian Research* **114**, 221–247.

Eglington, B. M. & Armstrong, R. A. (2004). The Kaapvaal Craton and adjacent orogens, southern Africa: a geochronological database and overview of the geological development of the craton. *South African Journal of Petrology* **107**, 13–32.

Frei, D. & Gerdes, A. (2009). Accurate and precise *in situ* zircon U–Pb age dating with high spatial resolution and high sample throughput by automated LA-SF-ICP-MS. *Chemical Geology* **261**, 261–270.

Gerdes, A. & Zeh, A. (2006). Combined U–Pb and Hf isotope LA-(MC)ICP-MS analyses of detrital zircons: Comparison with SHRIMP and new constraints for the provenance and age of an Armorican metasediment in Central Germany. *Earth and Planetary Science Letters* **249**, 47–61.

Gerdes, A. & Zeh, A. (2009). Zircon formation versus zircon alteration—new insights from combined U–Pb and Lu–Hf *in-situ* LA-ICP-MS analyses, and consequences for the interpretation of Archean zircon from the Central Zone of the Limpopo Belt. *Chemical Geology* **261**, 230–243.

Griffin, W. L., O'Reilly, S. Y., Natapov, L. M. & Ryan, C. G. (2003). The evolution of lithospheric mantle beneath the Kalahari Craton and its margins. *Lithos* **71**, 215–241.

Griffin, W. L., Belousova, E. A., Shee, S. R., Pearson, N. J. & O'Reilly, S. Y. (2004). Archean crustal evolution in the northern Yilgarn Craton: U–Pb and Hf-isotope evidence from detrital zircons. *Precambrian Research* **131**, 231–282.

Grobler, D. F. & Walraven, F. (1993). Geochronology of Gaborone Granite Complex extensions in the area north of Mafikeng, South Africa. *Chemical Geology* **105**, 319–337.

Gruau, G., Chauvel, C., Arndt, N. T. & Cornichet, J. (1990). Aluminium depletion in komatiites and garnet fractionation in the early Archean mantle: hafnium isotope constraints. *Geochimica et Cosmochimica Acta* **54**, 3095–3101.

Halpin, J. A., Gerakiteys, C. L., Clarke, G. L., Belousova, E. A. & Griffin, W. L. (2005). In-situ U–Pb geochronology and Hf isotope analyses of the Rayner Complex, east Antarctica. *Contributions to Mineralogy and Petrology* **148**, 689–706.

Harrison, T. M., Blichert-Toft, J., Müller, W., Albarède, F., Holden, P. & Mojzsis, S. J. (2005). Heterogeneous Hadean hafnium: Evidence of continental crust by 4·4–4·5 Ga. *Science* **310**, 1947–1950.

Harrison, T. M., Schmitt, A. K., McCulloch, M. T. & Lovera, O. M. (2008). Early (≥4·5 Ga) formation of terrestrial crust: Lu–Hf, $\delta^{18}O$, and Ti thermometry results for Hadean zircons. *Earth and Planetary Science Letters* **268**, 476–486.

Hartlaub, R. P., Heaman, L. M., Simonetti, A. & Böhm, C. O. (2006). Relics of Earth' earliest crust: U–Pb, Lu-Hf, and morphological characteristics of >3·7 Ga detrital zircon of the western Canadian Shield. In: Reimold, W. U. & Gibbson, R. (eds) *Processes on the Early Earth. Geological Society of America, Special Publications* **405**, 315–332.

Hawkesworth, C. J. & Kemp, A. I. S. (2006). Using hafnium and oxygen isotopes in zircons to unravel the record of crustal evolution. *Chemical Geology* **226**, 144–162.

Henderson, D. R., Long, L. E. & Barton, J. M. (2000). Isotopic ages and chemical and isotopic compositions of the Archean Turfloop batholith, Pietersburg granite–greenstone terrane, Kaapvaal Craton, South Africa. *South African Journal of Geology* **103**, 38–46.

Hisada, K. & Miyano, T. (1996). Petrology and microthermometry of aluminous rocks in the Botswanan Limpopo Central Zone: evidence for isothermal decompression and isobaric cooling. *Journal of Metamorphic Geology* **14**, 183–197.

Holzer, L., Frei, R., Barton, J. M., Jr & Kramers, J. D. (1998). Unraveling the record of successive high grade events in the Central Zone of the Limpopo Belt using Pb single phase dating of metamorphic minerals. *Precambrian Research* **87**, 87–115.

Holzer, L., Barton, J. M., Jr, Paya, B. K. & Kramers, J. D. (1999). Tectonothermal history in the western part of the Limpopo Belt: test of tectonic models and new perspectives. *Journal of African Earth Sciences* **28**, 383–402.

Horstwood, M. S. A., Nesbitt, R. W., Noble, S. R. & Wilson, J. F. (1999). U–Pb zircon evidence for an extensive early Archean craton in Zimbabwe: a reassessment of the timing of craton formation, stabilization and growth. *Geology* **27**, 707–710.

Iizuka, T. & Hirata, T. (2005). Improvements of precision and accuracy in in-situ Hf isotope microanalysis of zircon using laser ablation-MC-ICPMS technique. *Chemical Geology* **220**, 121–137.

Jackson, M. P. A. (1984). Archean structural styles in the Ancient Gneiss Complex of Swaziland, southern Africa. In: Kröner, A. & Greiling, R. (eds) *Precambrian Tectonics Illustrated*. Stuttgart: Schweitzerbart, pp. 1–18.

Jaeckel, P., Kröner, A., Kamo, S. L, Brandl, G. & Wendt, J. I. (1997). Late Archaean to early Proterozoic granitoid magmatism and high-grade metamorphism in the central Limpopo belt, South Africa. *Journal of the Geological Society, London* **154**, 25–44.

James, D. E. & Fouch, M. J. (2002). Formation and evolution of Archean cratons: insights from Southern Africa. In: Ebinger, C., Fowler, M. & Hawkesworth, C. J. (eds) *The Early Earth: Physical, Chemical and Biological Development. Geological Society, London, Special Publications* **199**, 1–26.

James, D. E., Fouch, M. J., VanDecar, J. C., van der Lee, S. & Group, K. S. (2001). Tectospheric structure beneath southern Africa. *Geophysical Research Letters* **28**, 2485–2488.

Jelsma, H. A. & Dirks, P. H. G. M. (2002). Neoarchean tectonic evolution of the Zimbabwe Craton. In: Fowler, C. M. R., Ebinger, C. B. & Hawkesworth, C. J. (eds) *The Early Earth: Physical, Chemical and Biological Development. Geological Society, London, Special Publications* **199**, 183–211.

Jelsma, H. A., Vinyu, M. L., Valbracht, P. J., Davies, G. R., Wijbrans, J. R. & Verdurmen, E. A. T. (1996). Constraints on Archean crustal evolution of the Zimbabwe craton: a U–Pb zircon, Sm–Nd and Pb–Pb whole rock isotope study. *Contributions to Mineralogy and Petrology* **124**, 55–70.

Kamber, B. & Biino, G. G. (1995). The evolution of high *T*–low *P* granulites in the Northern Marginal Zone sensu stricto, Limpopo Belt, Zimbabwe—The case for petrography. *Schweizerische Mineralogische Petrographische Mitteilungen* **75**, 427–454.

Kamber, B., Blenkinsop, T. G., Villa, I. M. & Dahl, P. S. (1995*a*). Proterozoic transpressive deformation in the Northern Marginal Zone, Limpopo Belt, Zimbabwe. *Journal of Geology* **103**, 493–508.

Kamber, B., Kramers, J. D., Napier, R., Cliff, R. A. & Rollinson, H. R. (1995*b*). The Triangle Shearzone, Zimbabwe, revisited: New data document an important event at 2·0 Ga in the Limpopo Belt. *Precambrian Research* **70**, 191–213.

Kamber, B. S., Ewart, A., Collerson, K. D., Bruce, M. C. & McDonalds, G. D. (2002). Fluid-mobile trace element constraints on the role of slab melting and implications for Archean crustal growth models. *Contributions to Mineralogy and Petrology* **144**, 38–56.

Kamber, B. S., Collerson, K. D., Moorbath, S. & Whitehouse, M. J. (2003). Inheritance of early Archean Pb-isotope variability from long-lived Hadean protocrust. *Contributions to Mineralogy and Petrology* **145**, 25–46.

Kamber, B. S., Whitehouse, M. J., Bolhar, R. & Moorbath, S. (2005). Volcanic resurfacing and the early terrestrial crust: Zircon U–Pb and REE constraints from the Isua Greenstone Belt, southern Greenland. *Earth and Planetary Science Letters* **240**, 276–290.

Kamo, S. L. & Davis, D. W. (1994). Reassesment of Archean crustal development in the Barberton Mountain Land, South Africa, based on U–Pb dating. *Tectonics* **13**, 167–192.

Kemp, A. I. S., Foster, G. L., Schersten, A., Whitehouse, M. J., Darling, J. & Storey, C. (2009). Concurrent Pb–Hf isotope analysis of zircon by laser ablation multi-collector ICP-MS, with implications for the crustal evolution of Greenland and the Himalayas. *Chemical Geology* **261**, 244–260.

Key, R. M. (1976). The geology of the area around Francistown and Phikwe, Northeast and Central Districts, Botswana. Geological Survey of Botswana District Memoir 3, 121 pp.

Key, R. M., Mapeo, R. B. M., Van Zyl, H. E. M., Hargreaves, R. L. & Holmes, H. (1994). *The geology of the Topisi area. Bulletin Geological Survey Botswana* **38**, 84.

Kramers, J. D. (2007). Hierarchical Earth accretion and the Hadean Eon. *Journal of the Geological Society, London* **164**, 3–17.

Kreissig, K., Nägler, T. F., Kramers, J. D., Van Reenen, D. D. & Smit, C. A. (2000). An isotopic and geochemical study of the northern Kaapvaal Craton and the Southern Marginal Zone of the Limpopo Belt: are they juxtaposed terranes? *Lithos* **50**, 1–25.

Kreissig, K., Holzer, L., Frei, R., Villa, I. M., Kramers, J. D., Kröner, A., Smit, C. A. & Van Reenen, D. D. (2001). Chronology of the Hout River Shear Zone and the metamorphism in the Southern Marginal Zone of the Limpopo Belt, South Africa. *Precambrian Research* **109**, 145–173.

Kröner, A. & Tegtmeyer, A. (1994). Gneiss–greenstone reltionships in the Ancient Gneiss Complex of southwestern Swaziland, southern Africa, and implications for early crustal evolution. *Precambrian Research* **67**, 109–139.

Kröner, A., Compston, W. & Williams, I. S. (1989). Growth of early Archean crust in the Ancient Gneiss Complex of Swaziland as revealed by single zircon dating. *Tectonophysics* **161**, 271–298.

Kröner, A., Hegner, E., Wendt, J. I. & Byerly, G. R. (1996). The oldest part of the Barberton granitoid–greenstone terrain, South Africa: evidence for crust formation at 3·5 and 3·7 Ga. *Precambrian Research* **78**, 105–124.

Kröner, A., Jaeckel, P., Hofmann, A., Nemchin, A. A. & Brandl, G. (1998). Field relationships and age of supracrustal Beit Bridge Complex and associated granitoid gneisses in the Central Zone of the Limpopo Belt, South Africa. *South African Journal of Geology* **101**, 201–213.

Kröner, A., Jaeckel, P., Brandl, G., Nemchin, A. A. & Pidgeon, R. T. (1999). Single zircon ages for granitoid gneisses in the Central Zone of the Limpopo Belt, Southern Africa and geodynamic significance. *Precambrian Research* **93**, 299–337.

Kröner, A., Jaeckel, P. & Brandl, G. (2000). Single zircon ages for felsic to intermediate rocks from the Pietersburg and Giyani greenstone belts and bordering granitoid orthogneisses, northern Kaapvaal Craton, South Africa. *Journal of African Earth Sciences* **30**, 773–793.

Layer, P. W., Kröner, A. & York, D. (1992). Pre-3000 Ma thermal history of the Archean Kaap Valley pluton, South Africa. *Geology* **22**, 1099–1102.

Lowe, D. R. (1994). Accretionary history of the Archean Barberton greenstone belt (3·55–3·22 Ga) southern Africa. *Geology* **22**, 1099–1102.

Ludwig, K. (2001). Isoplot/Ex, rev. 2.49. A Geochronological Toolkit for Microsoft Excel. Berkeley Geochronology Center, Special Publications **1a**.

Maphalala, R. M. & Kröner, A. (1993). Pb–Pb single zircon ages for the younger Archean granitoids of Swaziland, southern Africa. In: *Abstracts, 16th Colloquium on African Geology, Mbabane, Swaziland Vol. 2*, pp. 201–206.

Martin, H., Smithies, R. H., Rapp, R., Moyen, J.-F. & Champion, D. (2005). An overview of adakite, tonalite–trondhjemite–granodiorite (TTG) and sanukitoid relationships and some implications for crustal evolution. *Lithos* **79**, 1–24.

Mason, R. (1973). The Limpopo mobile belt—Southern Africa. *Philosophical Transactions of the Royal Society of London, Series A* **273**, 463–485.

McCourt, S. & Armstrong, R. A. (1998). SHRIMP U–Pb geochronology of granites from the Central Zone, Limpopo Belt, southern Africa: Implications for the age of the Limpopo Orogeny. *South African Journal of Geology* **101**, 329–338.

McCourt, S. & Vearncombe, J. R. (1987). Shear zones bounding the central zone of the Limpopo mobile belt, southern Africa. *Journal of Structural Geology* **9**, 127–137.

McCourt, S. & Vearncombe, J. R. (1992). Shear Zones of the Limpopo Belt and adjacent granitoid–greenstone terranes, implications for late Archaean collision tectonics in Southern Africa. *Precambrian Research* **55**, 553–570.

McCourt, S., Kampunzu, A. B., Armstrong, R. A. & Bagai, Z. (2004). The crustal architecture of Archaean terranes in Northeastern Botswana. *South African Journal of Geology* **107**, 147–158.

Meyer, F. M., Robb, L. J., Reimold, W. U. & de Bruin, H. (1994). Contrasting low and high Ca granites in the Archean Barberton Mountain Land, southern Africa. *Lithos* **32**, 63–76.

Millonig, L., Zeh, A., Gerdes, A. & Klemd, R. (2008). Neoarchaean high-grade metamorphism in the Central Zone of the Limpopo Belt (South Africa): Combined petrological and geochronological evidence from the Bulai pluton. *Lithos* **103**, 333–351.

Mkweli, S., Kamber, B. & Berger, M. (1995). Westward continuation of the craton–Limpopo Belt tectonic break in Zimbabwe and new age constraints on the timing of the thrusting. *Journal of the Geological Society, London* **152**, 77–83.

Moore, M., Davis, D. W., Robb, L. J., Jackson, M. C. & Grobler, D. F. (1993). Archean rapakivi granite–anorthosite–rhyolite complex in the Witwatersrand Basin hinterland, southern Africa. *Geology* **21**, 1031–103.

Moser, D. E., Flowers, R. & Hart, R. J. (2000). Birth of the Kaapvaal lithosphere at 3·08 Ga: implications for the growth of ancient continents. *Science* **291**, 465–468.

Nägler, T. F., Kramers, J. D., Kamber, B. S., Frei, R. & Prendergast, M. D. A. (1997). Growth of subcontinental lithospheric mantle beneath Zimbabwe started at of before 3·8 Ga; Re–Os study on chromites. *Geology* **25**, 983–986.

Parman, S. W., Dann, J. C., Grove, T. L. & de Wit, M. J. (1997). Emplacement conditions of komatiite magmas from the 3·49 Ga Komati Formation, Barberton Greenstone Belt, South Africa. *Earth and Planetary Science Letters* **150**, 303–323.

Parman, S. W., Grove, T. L., Dann, J. C. & De Wit, J. M. (2004). A subduction origin for komatiites and cratonic lithospheric mantle. *South African Journal of Geology* **107**, 107–118.

Patchett, P. J., Kouvo, O., Hedge, C. E. & Tatsumoto, M. (1981). Evolution of continental crust and mantle heterogeneity: evidence from Hf isotopes. *Contributions to Mineralogy and Petrology* **78**, 279–297.

Pearson, D. G. (1999). The age of continental roots. *Lithos* **48**, 171–194.

Pearson, N. J., Griffin, W. L. & O'Reilly, S. Y. (2008). Mass fractionation correction in laser ablation multiple-collector ICP–MS: implications for overlap corrections and precise and accurate in situ isotope ratio measurement. In: Sylvester, P. (ed.) *Laser Ablation ICP–MS in the Earth Sciences: Current Practices and Outstanding Issues. Mineralogical Association of Canada, Short Course Series* **40**, 93–116.

Pettingill, H. S. & Patchett, P. J. (1981). Lu–Hf total-rock age for the Amîtsoq gneisses, West Greenland. *Earth and Planetary Science Letters* **55**, 150–156.

Polat, A. & Münker, C. (2004). Hf–Nd isotope evidence for contemporaneous subduction processes in the source of late Archean arc lavas from the Superior Province, Canada. *Chemical Geology* **213**, 403–429.

Poujol, M. (2001). U–Pb isotopic evidence for episodic granitoid emplacement in the Murchison greentone belt, South Africa. *Journal of African Earth Sciences* **33**, 155–163.

Poujol, M. & Robb, L. J. (1999). New U–Pb zircon ages on gneisses and pegmtites from south of the Murchison greenstone belt, South Africa. *South African Journal of Geology* **102**, 93–97.

Poujol, M., Robb, L. J., Respaut, J. P. & Anhaeusser, C. R. (1996). 3·07–2·97 Ga greenstone belt formation in the northeastern Kaapvaal Craton: implications for the origin of the Witwatersrand Basin. *Economic Geology* **91**, 1455–1461.

Poujol, M., Anhaeusser, C. R. & Armstrong, R. A. (2002). Episodic granitoid emplacement in the Archaean Amalian–Kraaipan terrane, South Africa: confirmation from single zircon U–Pb geochronology. *Journal of African Earth Sciences* **35**, 147–161.

Poujol, M., Robb, L. J., Anhaeusser, C. R. & Gericke, B. (2003). A review of the geochronolgical constraints on the evolution of the Kaapvaal Craton, South Africa. *Precambrian Research* **127**, 181–213.

Ranganai, R. T., Kampunzu, A. B., Atekwana, E. A., Paya, B. K., King, J. G., Koosimile, D. I. & Stettler, E. H. (2002). Gravity evidence for a larger Limpopo Belt in southern Africa and geodynamic implications. *Geophysical Journal International* **149**, 9–14.

Richardson, S. H., Gurney, J. J., Erlank, A. J. & Harris, J. W. (1984). Origin of diamonds in old enriched mantle. *Nature* **310**, 198–202.

Richardson, S. H., Shirey, S. B. & Harris, J. W. (2004). Episodic diamond genesis at Jwaneng, Botswana, and implications for Kaapvaal craton evolution. *Lithos* **77**, 143–154.

Rino, S., Komiya, T., Windley, B. F., Katayama, I., Motoki, A. & Hirata, T. (2004). Major episodic increase of continental crustal growth determined from zircon ages of river sands; implications for mantle overturns in the Early Precambrian. *Physics of the Earth and Planetary Interiors* **146**, 369–394.

Robb, L. J., Brandl, G., Anhaeusser, C. R. & Poujol, M. (2006). Archean granitoid intrusions. In: Johnson, M. R., Anhaeusser, C. R. & Thomas, R. J. (eds) *The Geology of South Africa*. Pretoria: Geological Society of South Africa: Johannesburg/Council of Geosciences, pp. 57–94.

Roering, C., Van Reenen, D. D., Smit, C. A., Barton, J. M., Jr, De Beer, J. H., De Wit, M. J., Stettler, E. H., Van Schalkwyk, J. F., Stevens, G. & Pretorius, S. (1992). Tectonic model for the evolution of the Limpopo Belt. *Precambrian Research* **55**, 539–552.

Rollinson, H. R. & Blenkinsop, T. (1995). The magmatic, metamorphic and tectonic evolution of the Northern Marginal Zone of the Limpopo Belt in Zimbabwe. *Journal of the Geological Society, London* **152**, 66–75.

Rudnick, R. L. & Fontain, D. M. (1995). Nature and composition of the continental crust: a lower crustal perspective. *Reviews of Geophysics* **33**, 267–309.

Schaller, M., Steiner, O., Studer, I., Holzer, L., Herwegh, M. & Kramers, J. D. (1999). Exhumation of the Limpopo Central Zone granulites and dextral continent-scale transcurrent movement at 2·0 Ga along the Palala Shear Zone, Northern Province, South Africa. *Precambrian Research* **96**, 263–288.

Scherer, E., Münker, C. & Mezger, K. (2001). Calibration of the lutetium–hafnium clock. *Science* **293**, 683–687.

Scherer, E., Whitehouse, M. J. & Münker, C. (2007). Zircon as a monitor of crustal growth. *Elements* **3**, 19–24.

Schmitz, M. D., Bowring, S. A., de Wit, M. J. & Gartz, V. (2004). Subduction and terrane collision stabilize the west Kaapvaal craton tectosphere 2·9 billion years ago. *Earth and Planetary Science Letters* **222**, 363–376.

Schoene, B., de Wit, M. J. & Bowring, S. A. (2008). Mesoarchean assembly and stabilization of the eastern Kaapvaal craton: A structural–thermochronological perspective. *Tectonics* **27**, TC5010, doi:10.1029/2008TC002267.

Shirey, S. B., Richardson, S. H. & Harris, J. W. (2004). Integrated models of diamond formation and craton evolution. *Lithos* **77**, 923–944.

Smithies, R. H. (2000). The Archean tonalite–trondhjemite–granodiorite (TTG) series is not an analogue of Cenozoic adakite. *Earth and Planetary Science Letters* **182**, 115–125.

Söderlund, U., Patchett, J. P., Vervoort, J. D. & Isachsen, C. E. (2004). The ^{176}Lu decay constant determined by Lu–Hf and U–Pb isotope systematics of Precambrian mafic intrusions. *Earth and Planetary Science Letters* **219**, 311–324.

Stacey, J. S. & Kramers, J. D. (1975). Approximation of terrestrial lead isotope evolution by a two-stage model. *Earth and Planetary Science Letters* **26**, 207–221.

Stevenson, R. K. & Patchett, P. J. (1990). Implications for the evolution of continental crust from Hf isotope systematics of Archean detrital zircons. *Geochimica et Cosmochimica Acta* **54**, 1683–1697.

Taylor, P. N., Kramers, J. D., Moorbath, S., Wilson, J. F., Orpen, J. L. & Martin, A. (1991). Pb/Pb, Sm–Nd and Rb–Sr geochronology in the Archean Craton of Zimbabwe. *Chemical Geology* **87**, 175–196.

Tegtmeyer, A. R. & Kröner, A. (1987). U–Pb zircon ages bearing on the nature of early Archean greenstone belt evolution, Barberton Mountain Land, southern Africa. *Precambrian Research* **36**, 1–20.

Van Reenen, D. D., Barton, J. M., Jr, Roering, C., Smit, C. A. & Van Schalkwyk, J. F. (1987). Deep crustal response to continental collision: The Limpopo belt of southern Africa. *Geology* **15**, 11–14.

Van Reenen, D. D., Roering, C., Ashwal, L. D. & de Wit, M. L. (1992). Regional geological setting of the Limpopo Belt. *Precambrian Research* **55**, 1–5.

Van Reenen, D. D., Perchuk, L. L., Smit, C. A., Varlamov, D. A., Boshoff, R., Huizenga, J. M. & Gerya, T. V. (2004). Structural and *P–T* evolution of a major cross fold in the Central Zone of the Limpopo high-grade terrain, South Africa. *Journal of Petrology* **45**, 1413–1439.

Vearncombe, J. R. (1991). A possible Archaean island arc in the Murchison Belt, Kaapvaal Craton, South Africa. *Journal of African Earth Sciences* **13**, 299–304.

Vearncombe, J. R., Barton, J. M., Cheshire, P. E., De Beer, J. H., Stettler, E. H. & Brandl, G. (1992). *Geology, geophysics and mineralisation of the Murchison schist belt, Rooiwater Complex and surrounding granitoids. Memoirs of the Geological Survey of South Africa* **81**, 139 pp.

Vervoort, J. D. & Blichert-Toft, J. (1999). Evolution of the depleted mantle: Hf isotope evidence from juvenile rocks through time. *Geochimica et Cosmochimica Acta* **63**, 533–556.

Vervoort, J. D., Patchett, P. J., Gehrels, G. E. & Nutman, A. P. (1996). Constraints on early Earth differentiation from hafnium and neodymium isotopes. *Nature* **379**, 624–627.

Walraven, F. (1989). The Geology of the Pilgrim's Rest area. Explanations Sheet 2430 (1:250–000) Geological Series). Pretoria: Geological Survey of South Africa.

Watkeys, M. K. & Armstrong, R. A. (1985). The importance of being alkaline—deformed late Archean lamprophyric dykes, Central Zone, Limpopo Belt. *Transactions of the Geological Society of South Africa* **88**, 195–206.

Wedepohl, K. H. (1995). The compositions of the continental crust. *Geochimica et Cosmochimica Acta* **59**, 1217–1232.

Westerlund, K. J., Gurney, J. J., Carlson, R. W., Shirey, S. B., Hauri, E. H. & Richardson, S. H. (2004). A metasomatic origin for late Archean eclogitic diamonds: Implications from internal morphology of diamonds and Re–Os and S isotope characteristics of their sulphide inclusions from the late Jurassic Klipspringer kimberlites. *South African Journal of Geology* **107**, 119–130.

Wilson, J. F., Bickle, M. J., Hawkesworth, C. J., Martin, A., Nisbet, E. G. & Orpen, J. L. (1978). Granite–greenstone terrains of the Rhodesian Archean Craton. *Nature* **271**, 23–27.

Wilson, J. F., Nesbitt, R. W. & Fanning, C. M. (1995). Zircon geochronology of Archaean felsic sequences in the Zimbabwe craton: a revison of greenstone stratigraphy and a model for crustal growth. In: Coward, M. P. & Ries, A. C. (eds) *Early Precambrian Processes. Geological Society, London, Special Publications* **95**, 109–126.

Woodhead, J., Hergt, J., Shelley, M., Eggins, S. & Kemp, R. (2004). Zircon Hf-isotope analysis with an excimer laser, depth profiling, ablation of complex geometries, and concomitant age estimation. *Chemical Geology* **209**, 121–135.

Wu, F. Y., Yang, Y. H., Xie, L. W., Yang, J. H. & Xu, P. (2006). Hf isotopic compositions of the standard zircons and baddeleyites in U–Pb geochronology. *Chemical Geology* **234**, 105–126.

Zeh, A., Klemd, R., Buhlmann, S. & Barton, J. M. (2004). Pro- and retrograde *P–T* evolution of granulites of the Beit Bridge Complex (Limpopo Belt, South Africa): constraints from quantitative phase diagrams and geotectonic implications. *Journal of Metamorphic Geology* **22**, 79–95.

Zeh, A., Klemd, R. & Barton, J. M., Jr (2005*a*). Petrological evolution in the roof of the high-grade metamorphic Central Zone of the Limpopo Belt, South Africa. *Geological Magazine* **142**, 229–240.

Zeh, A., Holland, T. J. B. & Klemd, R. (2005*b*). Phase relationships in grunerite–garnet-bearing amphibolites in the system CFMASH, with applications to metamorphic rocks from the Central Zone of the Limpopo Belt, South Africa. *Journal of Metamorphic Geology* **23**, 1–17.

Zeh, A., Gerdes, A., Klemd, R. & Barton, J. M., Jr (2007). Archean to Proterozoic crustal evolution in the Central Zone of the Limpopo Belt (South Africa/Botswana): Constraints from combined U–Pb and Lu–Hf isotope analyses of zircon. *Journal of Petrology* **48**, 1605–1639.

Zeh, A., Gerdes, A., Klemd, R. & Barton, J. M., Jr (2008). U–Pb and Lu–Hf isotope record of detrital zircon grains from the Limpopo Belt—evidence for crustal recycling at the Hadean to early-Archean transition. *Geochimica et Cosmochimica Acta* **72**, 5304–5329.

Zhai, M., Kampunzu, A. B., Modisi, M. P. & Bagai, Z. (2006). Sr and Nd isotope systematics of the Francistown plutonic rocks, Botswana: implications for Neoarchean crustal evolution of the Zimbabwe craton. *International Journal of Earth Sciences (Geologische Rundschau)* **95**, 355–369.

Zheng, J., Griffin, W. L., O'Reilly, S. Y., Lu, F., Wang, C., Zhang, M., Wang, F. & Li, H. (2004). 3·6 Ga lower crust in central China: new evidence on the assembly of the North China craton. *Geology* **32**, 229–232.